2016

Evaluation Of Concrete Degradation Using Acoustic Emission: Data Filtering And Damage Detection

Marwa A. Abdelrahman
University of South Carolina

EVALUATION OF CONCRETE DEGRADATION USING ACOUSTIC EMISSION: DATA FILTERING AND DAMAGE DETECTION

by

Marwa A. Abdelrahman

Bachelor of Science
Helwan University, 2010

Master of Science
University of South Carolina, 2013

Submitted in Partial Fulfillment of the Requirements

For the Degree of Doctor of Philosophy in

Civil Engineering

College of Engineering and Computing

University of South Carolina

2016

Accepted by:

Paul Ziehl, Major Professor

Juan Caicedo, Committee Member

Fabio Matta, Committee Member

John Rose, Committee Member

Cheryl L. Addy, Vice Provost and Dean of the Graduate School

DEDICATION

To my parents, my husband, and my precious daughter.

ACKNOWLEDGEMENTS

I would like to express the deepest gratitude to my advisor, Dr. Paul Ziehl for his invaluable advice, guidance and support throughout this work. His guidance and patience were always there during all times of difficulties.

I would like to thank my committee members, Dr. Fabio Matta, Dr. Juan Caicedo and Dr. John Rose for their guidance and feedback during my research. Special thanks to my fellow graduate students and friends at the University of South Carolina, especially Rafal Anay who helped me during the experimental work included in this dissertation.

I owe my deepest gratitude to my husband, Mohamed for his endless love, support, and encouragement. No words can describe my infinite love to you and our precious daughter, Dana. I would like to express my deepest thanks to my father who always has faith in me and continually supported me through my life and my sincere appreciation to my mother for her inspiration and support that motivated me throughout the difficult times. I am eternally grateful to both of you.

First and last, great thanks are due to God "ALLAH", without his will nothing can be achieved.

ABSTRACT

The prevalence of aging and deteriorating infrastructure in the U.S. has raised concerns regarding its level of serviceability, reliability, and vulnerability to natural disasters. This issue has gained attention recently and efforts are being conducted to accelerate the delivery of enhanced nondestructive testing (NDT) and structural health monitoring (SHM) methods. Acoustic emission (AE) is a strong candidate for these applications due to its high sensitivity and potential for damage detection in different materials. However, several challenges associated with the technique hinder the development of automated, reliable, real-time SHM using AE.

This study aims to advance the use of AE for condition assessment of concrete structures by addressing two main challenges. The first is AE data filtering to exclude irrelevant noise and wave reflections. Effective filtering and data reduction enhances the quality of the data and lowers the cost of its transfer and analysis; ultimately increasing the reliability of the method. The second issue is detecting slow rate material degradation mechanisms in concrete. For example, alkali-silica reaction (ASR) affects civil infrastructure around the nation, and available condition assessment methods for this type of damage are either invasive or not feasible for field conditions. Despite the awareness of ASR concrete deterioration; there is lack of research investigating the ability of AE to detect and assess it. In addition, recent laboratory investigations have shown promising results in detecting and evaluating damage related to corrosion of steel in concrete using AE. However, the results have not been extended to field applications.

This dissertation includes three studies that address the aforementioned issues. In the first study, wavelet analysis was used to study the distribution of energy in AE signals in the time-frequency domain. Criteria to differentiate between AE signals from artificial sources (pencil lead breaks) and wave reflections were developed. The results were tested and validated by applying the developed filters on data collected from actual cracking during load testing of a prestressed concrete beam. The second study presents a laboratory test conducted to assess the feasibility of using AE to detect ASR damage in concrete. Accelerated ASR testing was undertaken with a total of fifteen specimens tested; twelve ASR and three control specimens. The results of this study showed that AE has the potential to detect and classify ASR damage. Relatively good agreement was obtained with standard ASR measurements of length change and petrographic examination. The third study discusses a field application for long-term, remote monitoring of damage due to corrosion of reinforcing steel and potential thermal cracking in a decommissioned nuclear facility. The structure was monitored for approximately one year and AE damage detection and classification methods were successfully applied to assess the damage at the monitored regions. This study also included an accelerated corrosion test conducted on a concrete block cut from a representative structure.

The studies included in this dissertation provide: 1) an innovative approach for filtering AE data collected during cracking of concrete, 2) a proof of concept study on detecting ASR damage using AE, and 3) field application on AE monitoring of corrosion damage in aging structure. The outcomes of this research demonstrate the ability of AE for condition assessment, structural health monitoring, and damage prognosis for in-service structures.

TABLE OF CONTENTS

LIST OF TABLES

LIST OF FIGURES

CHAPTER 1

INTRODUCTION

1.1 BACKGROUND

The state of infrastructure has a significant impact on the quality of life, economic prosperity, and development of communities. Existing infrastructure is subjected to growing burdens due to increasing populations and limited resources, which can affect both safety and reliability. An approach to address this issue is through the promotion of resilience and sustainability for newly constructed systems and implementing effective structural health monitoring and maintenance strategies for existing structures.

Aging of infrastructure is an emerging problem in the U.S. as the majority of structures are either approaching, or have been used in excess of, their design service life. The American Society of Civil Engineers (ASCE) described the performance of the nation's infrastructure as nearly failing with an assigned grade of D+ in its latest report card. Thus, there is a pressing need for investment to upgrade our infrastructure to avoid catastrophic failures such as the I-35W Bridge collapse in Minneapolis, MN in 2007. Educated decisions regarding funding prioritization and maintenance scheduling require reliable condition assessment and structural health monitoring techniques to evaluate the state of existing structures.

Structural health monitoring (SHM) is the process of tracking the condition of a structure over time using arrays of sensors to collect data on parameters involved in the evaluation of the integrity of the structure. SHM provides several structural

diagnostic approaches. These include detection, localization, and assessment of the extent of damage. In addition, the temporal aspect of monitoring gives a historical database which enables structural prognosis (evolution of damage and remaining service life estimation). The later characteristic is the main advantage of modern SHM over traditional nondestructive testing (NDT) methods. Long term SHM can be used to periodically update information related to the reliability of a structure considering inevitable aging and related degradation arising by environmental conditions or extreme events. It can also alert the owner when certain parameters have reached preset values. The structural condition insight provided by SHM can greatly enhance maintenance and mitigation activities and potentially mitigate future failures of civil infrastructure.

There are two approaches involved in SHM: a) global monitoring which provides information about the behavior of the structure as a whole, and b) local monitoring which provides information about behavior at critical locations in the structure. Depending on the objective of the SHM system and the information of interest, the decision on the best approach is made. There are multiple SHM systems and sensors that have been developed and applied; however, further investigations are needed to achieve reliable and cost effective SHM practices.

Acoustic emission (AE) is a promising SHM technique due its passive nature and real time monitoring capability. Acoustic emission is defined as transient stress waves generated by a localized release of energy (active damage progression). The stress waves are detected and converted to electrical signals by means of piezoelectric sensors attached to the surface of, or embedded within, the structure. The signals are then analyzed for damage detection and classification. Technological advances have allowed the

development of wireless, low power AE systems which adds an advantage to the technique for field investigations. One of the main challenges associated with AE monitoring is data filtering as the high sensitivity of the sensors results in the collection of noise due to wave reflections and other spurious sources that are not directly related to damage propagation.

As one of the main materials used in building infrastructure, damage detection in concrete has been previously investigated (Ziehl et al., 2008; Xu et al., 2013; Schumacher, 2008; Nair and Cai, 2010). The high sensitivity of the method enables it to detect active cracks long before they become visible (micro-cracking). In addition to cracking due to excessive loading, concrete is susceptible to damage due to material degradation mechanisms including corrosion of reinforcing steel, freeze-thaw damage, chemical attack and alkali-silica reaction. Recently, the feasibility of using AE to detect and classify corrosion of reinforcing steel has been demonstrated through laboratory testing (Zdunek et al., 1995; Ohtsu and Tomoda, 2008; Mangual et al., 2013a; b; ElBatanouny et al., 2014a; Appalla et al., 2015). While research efforts are progressing in this area, the reliability of AE for real time monitoring of corrosion damage in field structures has not been established. Furthermore, there is a lack in research investigating the feasibility of using AE to detect damage due to other material degradation mechanisms such as alkali-silica reaction. This document aims to address these gaps as described in the following sections.

1.2 RESEARCH SIGNIFICANCE

The research in this study targets two of the main challenges associated with AE as a structural health monitoring and damage evaluation method. The first challenge is data reduction (rejection of noise) which is usually existent in AE data due to the high sensitivity of the method. Most available approaches for filtering irrelevant data are empirical and

subjective which increases the opportunity for deceptive results when operated by unexperienced users. Signal processing methods have the potential for uncovering the different signatures present in signals from different sources. This study implements wavelet analysis to develop an algorithm that can be used to differentiate target AE signals, due to cracking of prestressed concrete, from signals due to spurious sources such as waves due to reflections from cracked surfaces or boundaries.

The second challenge is detecting slow rate (sometimes referred to as low-level) concrete degradation mechanisms such as damage due to corrosion of reinforcing steel and alkali-silica reaction (ASR) which affect numerous structures including bridges, buildings, and nuclear power plants. These degradation mechanisms have significant effects on durability, safety, and serviceability. There is very limited information available in the published literature related to monitoring of ASR damage with AE. The second study in this research shows the results of accelerated ASR testing using small scale specimens. The results highlight the potential of AE to detect and classify ASR damage, which could broaden field applications of AE.

Recent research efforts have established the potential of AE to detect and classify corrosion damage. However, the developed AE methods for corrosion damage evaluation are limited to well-controlled laboratory experiments and have not been extended to field conditions. The third study focuses on long term AE monitoring of critical locations in a decommissioned nuclear facility known to have corrosion damage. This application demonstrates the appropriateness of AE monitoring for field conditions and provides further insight for potential complications.

An important outcome of this research is that it demonstrates the potential of AE data reduction and damage assessment algorithms for assessing the condition of in-service structures. This addresses one of the main challenges associated with modern SHM techniques where large amounts of data are collected. Significant effort is usually needed to interpret and analyze this data. The data reduction and damage assessment methods developed through the course of this work can be easily programmed, thereby providing meaningful information to facility managers without the need for rigorous assessment of large data sets. This can subsequently help in maintenance planning and prioritization especially in large scale and complex infrastructure systems.

1.3 OBJECTIVES

The main objective of this work is to address some of the existing gaps in the research related to SHM and condition assessment of damage in concrete structures using AE. This can be summarized in two main topics: 1) developing a reliable filtering approach for AE data that can differentiate between damage related signals and signals due irrelevant sources, and 2) investigating the feasibility of using AE to detect slow rate damage related to concrete material degradation and assessing the use of AE for long-term structural health monitoring of in-service structures.

Three independent studies were performed to target these topics; each study has its own sub-objectives as summarized below.

1.3.1 Signal processing method for AE data filtering

Wavelet analysis was employed to study the distribution of energy in AE signals generated from different sources in the time-frequency domain. The objectives of this study were to:

1. Investigate the use of wavelet analysis to develop filtering criteria to differentiate between induced target signals and noise.
2. Verify the efficiency of the filters using data generated from cracking of a prestressed concrete beam and compare the results to those obtained with customary AE data filtering approaches.

1.3.2 Detection and classification of alkali-silica reaction damage

AE sensors were used to monitor small-scale concrete specimens during an accelerated ASR test. The objectives of this study were to:

1. Investigate the use of AE for detection of ASR induced damage while comparing AE activity results to standard ASR diagnostic measurements.
2. Develop ASR damage classification methods based on AE parameters; through correlating AE with ASR petrographic examination results.

1.3.3 Remote monitoring of damage at a decommissioned nuclear facility

Two AE systems were used to monitor different locations at a decommissioned nuclear facility. In addition, a block was cut from a representative aged concrete structure and tested under accelerated corrosion in laboratory. The objectives of this study were to:

1. Validate the applicability of AE to remotely monitor damage related to corrosion of reinforcement and thermal cracking at an in-service structure.
2. Examine the effect of environmental conditions such as rain and temperature on AE activity.
3. Investigate the correlation between AE results and electrochemical measurements during an accelerated corrosion test of the concrete block.

4. Demonstrate possible approaches for estimating the sectional loss of reinforcing steel and remaining service life.

1.4 LAYOUT OF DISSERTATION

The dissertation consists of six chapters. Chapter 2 provides background information on the acoustic emission (AE) technique and review of available literature related to detection and quantification of damage related to corrosion of reinforcing steel and alkali-silica reaction. Background on commonly used AE data filtering methods as well as available research studies related to implementing signal processing for filtering AE data from concrete members is also discussed.

Chapters 3 through 5 were written in paper format and submitted for publication as journal articles. Therefore, some AE basics and background information may be repeated in these chapters.

Chapter 3 is titled "Signal Processing Techniques for Filtering Acoustic Emission Data in Prestressed Concrete" where wavelet analysis was used to develop four AE data filtering criteria based on data generated from artificial sources. The filtering criteria yielded improved results, in comparison to conventional methods, when applied to AE data from cracking of a prestressed concrete beam during load testing.

Chapter 4 is titled "Classification of Alkali-Silica Reaction Damage Using Acoustic Emission: A Proof-of-Concept Study". This chapter provides a proof of concept study that demonstrates the feasibility of using AE for monitoring ASR damage in concrete. The results showed the potential for the AE based method for quantification of the extent of damage caused by this degradation mechanism.

The title of chapter 5 is “Remote Monitoring and Evaluation of Damage at a Decommissioned Nuclear Facility”. This chapter demonstrates the feasibility of using AE for remote monitoring of in-service structures. The study extends the AE corrosion damage assessment methods developed in the laboratory to monitor damaged zones in a decommissioned nuclear facility. A complementary study of an accelerated corrosion test was performed on a block taken from a representative structure to provide deeper insight into the corrosion process.

Chapter 6 summarizes the research conducted in this dissertation and provides the conclusions drawn. Recommendations for future research are also described.

CHAPTER 2

LITERATURE REVIEW

2.1 INTRODUCTION

Acoustic emission (AE) is an emerging nondestructive evaluation (NDE) method that is suitable for long term real-time monitoring. AE is defined by the American Society of Testing and Materials (ASTM E1316-16) as 'the class of phenomena whereby transient elastic waves are generated by the rapid release of energy from localized sources within a material'. AE sensors can detect transient stress waves emitted from deformations and fractures such as crack formation or growth and convert them to electrical signals that can be recorded and analyzed by data acquisition systems. Several parameters can be measured from the signal waveform which can later be used in data filtering and analysis. Figure 2.1 shows a typical waveform with some of the parameters that are usually measured; followed by the definition of these parameters. Many studies have investigated the feasibility of using acoustic emission technique for condition assessment and structural health monitoring of concrete structures in the last two decades. The method can be used for detecting micro-cracks during load tests and/or due to concrete material degradation such as corrosion of steel in concrete (Ono, 2012; Abdelrahman, 2013).

Signal amplitude: is the magnitude of the peak voltage of the largest excursion attained by the signal wave form from a single emission event, usually reported in dB.

Duration: is the time between AE signal start and the signal end (the time between the first threshold crossing and the last threshold crossing of the signal).

Rise-time: is the time between AE signal start and the peak amplitude of that AE signal (measured in microseconds).

Signal strength: is the measured area of the rectified AE signal, with units proportional to volt-sec.

Signal energy: is the energy contained in a detected acoustic emission burst signal with units usually reported in joules or values that can be expressed in logarithmic form (dB, decibels).

Count: is the number of times the acoustic emission signal exceeds a preset threshold during any selected portion of a test, and the *count rate* is the number of counts during a fixed period of time.

Frequency: is the number of cycles per second of the pressure variation in a wave.

A detailed literature review of the main topics of this dissertation is presented in the following sections.

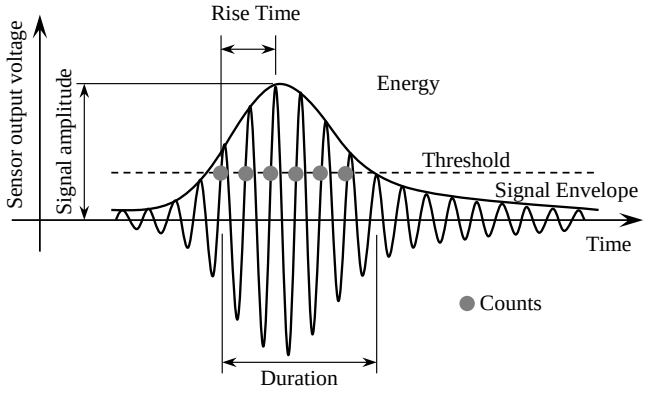

Figure 2.1 AE signal features (Xu, 2008).

2.2 AE DATA FILTERING

Due to the high sensitivity of the method, AE datasets usually include noise resulting from wave reflections, mechanical rubbing, electromagnetic interference, moving traffic and environmental sources such as rain, wind-born debris, and hail. The high

presence of noise can result in large amounts of data that are hard to handle. Effective data filtering can help reduce the size of the data without losing any key information targeted through the monitoring process. The basic level of filtering is usually achieved through setting a threshold for data acquisition which gets rid of low amplitude signals and helps in noise reduction. Values for band-pass frequency filter, peak definition time (PDT), hit definition time (HDT) and hit lockout time (HLT) can be adjusted in the data acquisition system to define the collected signals and reduce signals due to wave reflections. Even with these data acquisition setup, the percentage of signals due to spurious sources is usually high in most datasets. These settings have been implemented solely in different studies related to investigating or developing damage detection algorithms for concrete structures (Xu, 2008; Schumacher, 2008; ElBatanouny et al., 2014b). However, further filtering is needed for: a) accurate source location, and b) data reduction to decrease the cost of data handling and analysis.

2.2.1 Parameter-Based Filters

Parameter-based filters are easy to apply using data acquisition software. However, filtering limits need to be decided on by experienced user as the limits are usually empirical. Noise due to electromagnetic interference can result from ground loops of AE cables or poorly connected ground power which may affect the quality of the data. These signals usually have very short duration with a single spike waveform. Duration filters are used in that situation by discarding all signal with very short duration (may be less than 10 micro-seconds). Signal strength filter can also be used to filter electric noise with dramatically high signal strength. Some researchers also define frequency filter to discard signals with very low frequency (less than 20 kHz) as they are often associated with background noise,

vibration and machine noises (Beattie, 2013; Martinez-Gonzalez et al., 2013). A filtering criteria based on Root Mean Square (RMS) of AE waveforms was proposed by Sagasta et al. (2013) to distinguish between signals due to concrete cracking and signals due to mechanical friction collected during a dynamic test of concrete slab.

The Swansong II filter (also referred to as duration-amplitude filter, D-A) is a commonly used filter to reduce noise related to reflections and external sources such as leaks or mechanical rubbing in the collected AE data (Tinkey et al., 2002). The hypothesis of this filter is that signals with low amplitude and long duration are associated with noise. Thus, this filter can be developed by plotting amplitude versus log duration and visually investigating the waveforms of the signals, as shown in Figure 2.2, to develop the filtering limits (Tinkey et al., 2002). Similar procedure was used in research studies to develop rise time-amplitude (R-A) filters to be used with the D-A filters to further improve the quality of the data (Abdelrahman et al., 2014; ElBatanouny et al., 2014b). Swansong II filters have generated good results in different studies for filtering AE data collected from cracking of concrete during load tests (Abdelrahman et al., 2014; ElBatanouny et al., 2014b; 2014d; Anay et al., 2015), damage related to corrosion of steel in concrete (ElBatanouny et al., 2014), damage due to ASR deterioration in concrete (Abdelrahman et al., 2015) and fatigue crack growth in steel (Yu et al., 2011; Nemati et al., 2015; Hossain, 2013). Source location results of concrete cracking events were significantly enhanced using these filters and showed good agreement with visually detected cracks (ElBatanouny et al., 2014b; 2014d). However, this filtering technique is a post processing procedure and different limits are used depending on the researcher and the type of damage monitored.

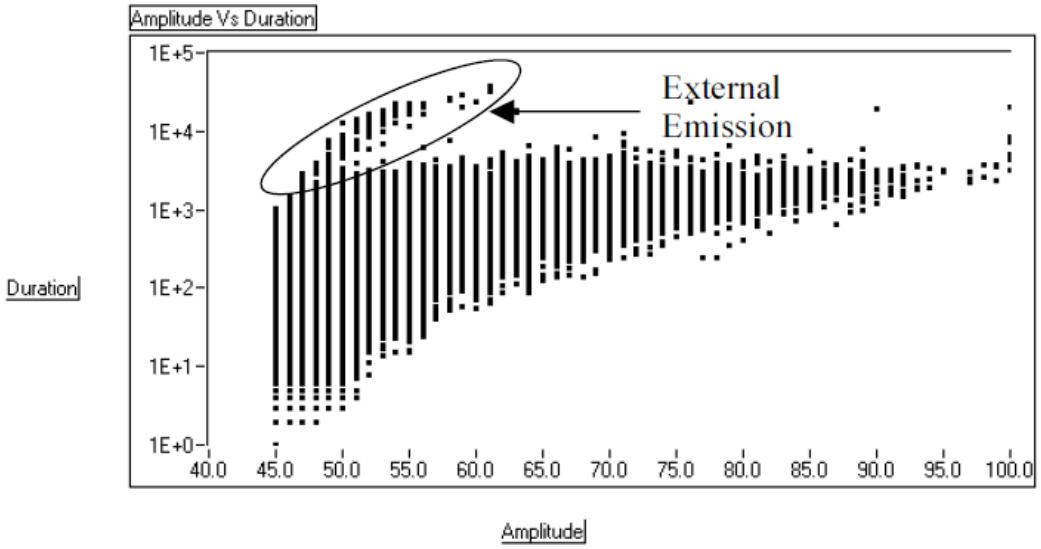

Figure 2.2 AE amplitude versus log duration plot for developing Swansong II filters (Tinkey et al., 2002).

2.2.2 Pattern Recognition Techniques

Pattern recognition is the process by which patterns, regularities or significant features in the data are recognized to be used in categorizing the data into identifiable classes (source characterization). Thus, three steps are involved in the analysis: data perception, feature extraction, and classification (Sharma et al., 2015). The features, which are used in classifier design, can be readily measured parameters from the waveform (amplitude, rise time, RMS, etc.) or obtained through signal processing of the waveform (Fourier transform, wavelet analysis, etc.). Once features are extracted, the classification process is performed to assign each input to a class.

There are two classification methodologies:

1. Supervised pattern recognition where each new unknown pattern is classified to a predefined class. This involves a learning process where a training dataset of representative AE hits for each signal class (AE source) is used in the classifier design. This method is suitable when the type of

damage is known in advance. Different Supervised classifier algorithms can be used for AE data including K-nearest neighbors method (K-NN method) (Godin et al., 2004), the linear classifier and the Back Propagation Neural Network (Anastasopoulos, 2005).

2. Unsupervised pattern recognition where data is classified into groups (number of clusters) depending on their features and similarities and these groups are defined as classes afterwards. This procedure does not implicate any prior knowledge or labeled database. However, it involves significant trialing by the user to achieve satisfactory results and the number of classes has to be defined. Popular unsupervised clustering methods include principal component analysis (PCA) (Jolliffe, 2002) and the k-means algorithm (Likas et al., 2003).

The implementation of these methodologies on AE data have been mainly investigated for: a) classification of micro-failure mechanisms in composites such as fiber fracture, matrix cracking, splitting and delamination (Ono and Huang, 1997; Marec et al., 2008; Hamdi et al., 2013; McCrory et al., 2015), b) identifying the progression of damage in concrete beams during load tests (Gołaski et al., 2006; Calabrese et al., 2010), and c) classification of damage due to corrosion of steel in a post-tensioned concrete beam (Calabrese et al., 2013). Kappatos and Dermatas (2009) utilized Neural Networks (NNs) to differentiate between two sources of AE signals, simulated cracking and drop signals, generated in steel plate. The presence of white-Gaussian noise with zero mean has been also investigated. The classification accuracy was high in the presence of low to medium

level of noise (higher than 90%). However, with higher level of noise the classification rate approaches the random selection rate (50%).

Few research efforts have utilized clustering methods to identify data due to noise. Ercolino et al. (2015) used k-means method via PCA of AE features to detect wire breaking of prestressed strand during accelerated corrosion test. Swansong II filters were applied as an initial filtering process before pattern recognition analysis. The results of k-means method showed three clusters of data; one of them was associated with spurious AE data that created false alarms (includes signals with high amplitude that did not correspond to damage progression evidenced by the inspection of the strand). The separation of such data can help in eliminating false alarms regarding the monitored damage.

Doan et al. (2014) investigated AE data collected during fatigue test on a carbon fiber reinforced polymer (CFRP) composite specimen. A noise model was developed from AE data collected before application of load using multivariate statistical approach. The model was used to delete AE events detected during the test and have similar characteristics to the modeled noise. A progressive feature selection and a clustering approach based on Gustafson-Kessel algorithm (GK) (Placet et al., 2013) was used for data classification. This resulted in defining five AE data clusters; one of them was linked to noise related to internal friction or fretting between faces of developed matrix cracking.

Hinton (1999) investigated statistical pattern recognition approach to separate data due to crack extension and data due to noise generated from a 2024-T4 aluminum specimen with a straight-through notch tested under fatigue loading. Ma and Chen (2015) proposed a method based on wavelet transform and a pattern recognition method (RPF neural network) to differentiate between simulated AE signals for metal plate crack, corrosion,

and condensation (interference signals) data. However, the method was developed based only on small size datasets from simulated sources.

2.2.3 Signal Processing Techniques

Signal processing is usually used to develop a representation of the signal that makes certain characteristics more explicit. Since it is a waveform based analysis it is not affected by the threshold setting. Frequency analysis (Fourier transform) and time-frequency analysis (such as Short Time Fourier Transform (STFT), Wavelet analysis and Hilbert-Huang Transform (HHT) are the most common signal processing approaches utilized for AE data. These tools have been utilized in the classifier design for the pattern recognition analysis of AE data as described in the previous section (Hamdi et al., 2013; Marec et al., 2008; Zitto et al., 2012).

Kaphle (2012) studied the distribution of energy in AE signals in different frequency bands using Short Time Fourier Transform (STFT) to discriminate between AE signals generated from pencil lead breaks (PLB) and AE signals from dropping steel balls (BD) on a steel beam. R15α sensors with resonant frequency of 150 kHz were used. High threshold value (60 dB) for data recording was used to minimize lower amplitude noise signals. It was observed that most of the energy resides around two peaks of 70 kHz and 170 kHz for PLB signals and around 70 kHz only for the BD signals; which provides a guide to distinguish between different sources. In the same study, a three point bending load test was performed on a steel specimen and AE signals were collected from crack formation and extension. Same sensor type and acquisition threshold were used for that application. Ten representative AE signals were chosen by the researcher for each of three different AE sources during the test; cracking, impact and rubbing. It was observed from

STFT results of the thirty investigated signals that energy is distributed differently in the time-frequency domain for the different sources. This indicates that the energy distribution in the signals reveals information about the nature of the source.

Background on wavelet transform, its advantage over STFT and related research are described in this section as the method has been investigated in the research presented in Chapter 3.

2.2.3.1 Wavelet Analysis of AE data

To analyze signals in the frequency domain, Fourier transform is usually applied by comparing the signal with complex sinusoidal functions that are spread over the entire time domain. However, this method was developed assuming that signals are stationary and it only describes the global frequency content of the signal. In an effort to overcome these drawbacks, the Short Time Fourier Transform (STFT) is employed to describe the signal's local frequency properties by segmenting the signal and comparing each segment (assuming it is stationary) with a sliding window function using conventional Fourier transform; which is why STFT is also referred to as 'windowed' Fourier transform.

The resolution in time and frequency are related by the uncertainty principle which lower bounds their product as shown in the equation $\Delta t \Delta f \geq \frac{1}{4\pi}$, which means that short time duration frequency bandwidth cannot be attained simultaneously. STFT uses single window width in terms of time and frequency which results in resolution deficiencies in the time-frequency representation especially in the case of short duration high frequencies. Wavelet analysis offers better resolution by using short windows (high time resolution) at high frequencies and long windows (low time resolution) at low frequencies (Rioul and Vetterli, 1991). This makes the method suitable for analyzing transient signals such as

acoustic emission signals. As shown in Figure 2.3 the frequency bandwidth in STFT is constant while it changes logarithmically in the wavelet decomposition analysis.

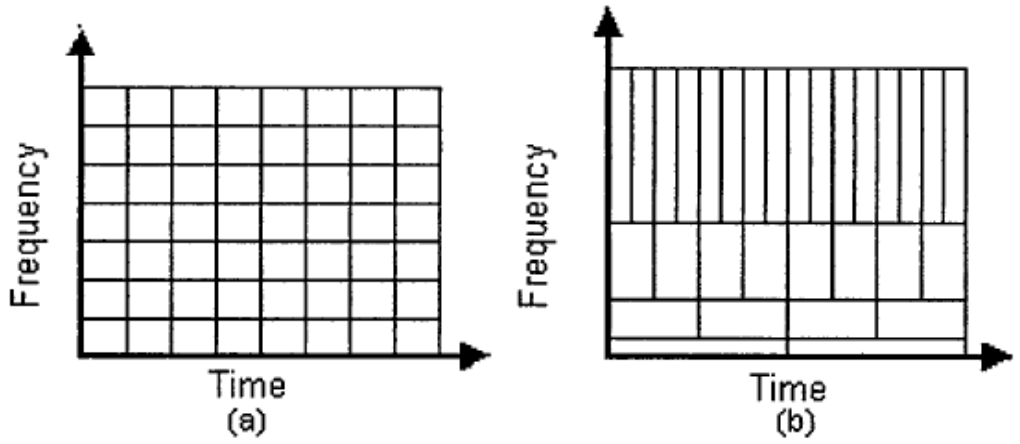

Figure 2.3 (a) Time-frequency resolution in Short Time Fourier Transform, and (b) Wavelet Transform (Ganesan et al., 2004).

Wavelet transformation is a linear decomposition which is attained by comparing the signal with a set of elementary functions that are obtained by the time scaling and shifting of a mother function. Let the mother function be *ψ(t)* with a mean frequency of ω_0, then the scaled and shifted function is $\psi\left(a^{-1}(t-b)\right)$ with a frequency = ω_0/a where *a* is the scale index and *b* is the time shifting. Then the wavelet transform can be obtained as the inner product of the signal *s(t)* and $\psi\left(a^{-1}(t-b)\right)$ as shown in Equation 2.1:

$$CWT(a,b) = \frac{1}{\sqrt{|a|}} \int s(t)\psi\left(\frac{(t-b)}{a}\right) dt \qquad a \neq 0 \qquad (2.1)$$

As seen in Equation 2.1, the wavelet transform is a function of time *(b)* and frequency (ω_0/a). Thus, it can be used to define how the signal's frequency content evolves in time which makes it ideal for analyzing non-stationary signals.

Wavelet transform has been previously investigated for damage detection and classification in concrete (Yoon et al., 2000) and composite materials (Ni and Iwamoto,

2004; Loutas et al., 2006; Marec et al., 2008; Lu et al., 2011; Arumugam et al., 2013; Hamdi et al., 2013). Hamstad et al. (2002) implemented wavelet analysis to study the wave propagation properties of AE signals for source identification in aluminum plates. Grosse et al. (2004) indicated that wavelet transform can be used for denoising AE signals by extracting coefficients related to the low frequency noise (caused by loading devices) imposed in the signals. Denoising AE signals would enable accurate detection of signal arrival time which would improve AE source location. Wijaya and Kencanawati (2014) investigated discrete wavelet transform (DWT) to find the best wavelet base decomposition level for denoising AE signals for enhanced source location of micro-cracking events in concrete. However, the study did not provide enough evidence for the improvement achieved by denoising of AE signals. Kharrat et al. (2015) deployed DWT for denoising continuous AE signals collected during fatigue test of CFRP specimen (before sweeping the signals for potential hits). Continuous wavelet transform was employed by Zitto et al. (2012) for denoising AE signals generated during dynamic test on a concrete slab. The frequency band associated with concrete fracture (cracking) was statistically identified, and then the denoised signals were reconstructed using only the assigned scales for cracking.

Since signal processing is a waveform-based approach, it involves large volumes of data (as waveforms have to be recorded not only signal parameters). However, as indicated previously, this gives it the advantage of being threshold independent approach. The studies found in literature for filtering AE data using wavelet analysis are mainly dedicated to denoising of AE signals. In other words the signal is decomposed by wavelet analysis at a selected decomposition level (N) and the detail coefficients are attained. Then a threshold method, based on noise modeling, is applied on the signal details and afterwards

the signal is reconstructed using the original approximation coefficients of the Nth level and the modified detail coefficients of all levels (Kharrat et al., 2015).

Wavelet analysis has the potential to provide information about the nature of the signal source. The development of wavelet-based filters that enable the complete elimination of signals attributed to spurious sources, rather than denoising the signals, could allow effective data reduction without losing any key targeted information. This would significantly lower the cost of data handling and data analysis for damage evaluation. Data reduction is valuable for field applications where spurious signals (signals that have no correlation to the damage state), sometimes account for the majority of the collected data.

It is noted that there are additional research efforts for filtering AE data that does not belong to the main three approaches (parameter-based filtering, pattern recognition and signal processing) described above. Niri et al. (2013) proposed a probabilistic approach based on nonlinear Kalman Filtering method for AE source location. The proposed method yield confidence interval for AE source location instead of a single point as it considers the uncertainty involved in the estimated time of flight. Martinez-Gonzalez et al. (2013) proposed a filtering approach based on the characteristics of the initial segment of the recorded AE signals. The filtering technique improved the damage evaluation of small steel specimens subjected to three point bending test; as verified by the inspection of the specimen using Confocal Microscope.

2.3 EVALUATING ALKALI-SILICA REACTION DETERIORATION IN CONCRETE

Alkali-silica reaction (ASR) is a chemical reaction that occurs in concrete between alkali hydroxides in the pore solution and reactive siliceous minerals in certain aggregates. The reaction product is an expansive gel that swells with the absorption of moisture which leads to concrete cracking and ultimately affects the durability and serviceability of the structure. The extent of this deterioration is affected by the reactivity of the aggregate, alkali concentration, availability of moisture, and temperature (Williams et al., 2009). Research investigating ASR mechanism and subsequent damage has been conducted since the late 1930s (Stanton, 1940). Procedures to prevent its occurrence in new construction have been developed; including standard practice for determining the reactivity of aggregates (ASTM C1260; Thomas, 2009; AASHTO, 2011). However, ASR is currently affecting numerous concrete structures around the nation (Stark et al., 1993) and only few mitigation techniques are permitted for slowing the reaction in in-service structures. ASR damage has gained further attention for research after it has been detected in the Seabrook Station, nuclear power plant in New Hampshire, in 2010 almost 25 years after plant construction. Although considerable research has been performed to investigate possible mitigation measures for ASR deterioration, this section is limited to studies discussing the current practice and research related to detecting and monitoring of ASR damage.

2.3.1 Current Practice for Evaluating ASR Damage

ASR damage is currently assessed in field structures by visual inspection of cracks (crack mapping), length change measurements, and/or concrete coring with subsequent petrographic examination. A detailed protocol for detecting and evaluating ASR damage

in structures was described in FHWA report in 2010 (Fournier et al., 2010). First, condition survey (visual inspection) was performed to assess the nature and the extent of the apparent signs of deterioration, exposure conditions, and the probability of ASR deterioration. Common visual signs of ASR include concrete expansion, cracking, surface discoloration and gel exudations. However, these symptoms can result from other degradation mechanisms and are not exclusively related to ASR. Classification system based on the visual condition survey is shown in Table 2.1 (after Fournier et al., 2009). Exposure conditions were used in conjunction with Table 2.1 to estimate the probability of ASR damage; as the potential for ASR is low in dry sheltered environments and high in concrete members with frequent exposure to moisture. In case of medium to high potential of ASR, further levels of investigation were carried on. The second level of investigation included gathering any available information regarding the age of the structure, concrete mixes and materials (including type and source of cement and aggregate and their proportions), building plans and drawings, previous inspections or testing, and other structures in the area constructed using same material. In addition, crack mapping was performed and the extent of cracks is estimated using the Cracking Index (CI) which involves measuring the crack widths. In cases where the cracking index exceeded certain criteria, more detailed investigations were warranted. Additional investigation included taking cores from the structure and performing expansion tests and petrographic examination to confirm the presence of alkali-silica reaction and quantify its damage using Damage Rating Index (DRI). Sometimes additional cores were taken to perform stiffness damage testing (SDT) which estimate the physical damage caused from ASR-induced cracks. Structures diagnosed with ASR damage were then instrumented for length change (expansion),

temperature, humidity and surface cracking measurements. Then decisions for mitigation/remediation measures were made based on the collective assessment of in-situ and laboratory investigations. Field applications for evaluating ASR damage using the aforementioned methods, on structures across the United States, can be found in a later report published by FHWA (Thomas et al., 2013a; 2013b).

Length change measurement and petrographic examination are further discussed in this section; as these methods have been used as benchmarks for ASR damage detection in the study described in Chapter 4.

Table 2.1 Classification system for the condition survey (after Fournier et al. 2010)

Feature	Potential for ASR		
	Low	Medium	High
Expansion and/or displacement of elements	None	Some evidence (e.g., closure of joints in pavements, jersey barriers, spalls, misalignments between structural members)	Fair to extensive signs of volume increase leading to spalling at joints, displacement and/or misalignment of structural members
Cracking and crack pattern	None	Some cracking pattern typical of ASR (e.g., map cracking or cracks aligned with major reinforcement or stress)	Extensive map cracking or cracking aligned with major stress or reinforcement
Surface discoloration	None	Slight surface discoloration associated with some cracks	Many cracks with dark discoloration and adjacent zone of light colored concrete
Exudations	None	White exudations around some cracks; possibility of colorless, jelly-like exudations	Colorless, jelly-like exudations readily identifiable as ASR gel associated with several cracks

2.3.1.1 Length Change Measurements

Field length change measurements are usually performed using demountable mechanical strain gauges (DEMEC) which consists of a standard or a digital dial gauge attached to an Invar bar. The DEMEC points, between which measurements are taken, are fixed or drilled into the surface of concrete members showing signs of ASR damage (Figure 2.4) (Fournier et al., 2010). Initial length measurements can be taken 12 to 24 hours after installation of DEMEC points and the weather condition (temperature and humidity) should be documented. The measurements should be repeated periodically (2-3 times a year) (Fournier et al., 2010). However, there is inherent variability associated with length change measurements as well as vulnerability to weather conditions.

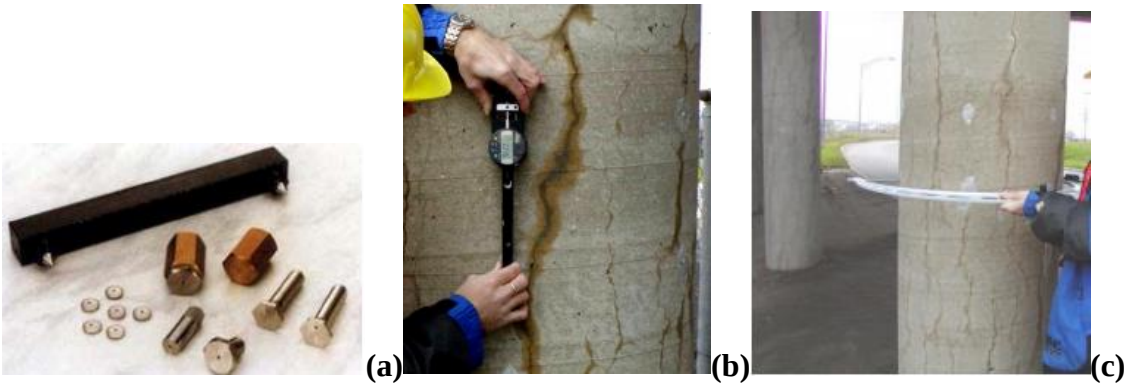

(a) (b) (c)

Figure 2.4 (a) Example of accessories used as DEMEC points, (b) and (c) Length-change measurements in reinforced concrete columns affected by ASR (Fournier et al., 2010).

Length change measurements are also performed in laboratory on cores taken from the structures to evaluate the potential for further expansion due to ASR (Expansion tests). These cores are kept at high temperature (38^{o}C [100°F]) and humidity (> 95% RH), similar to testing conditions of ASTM C1293. Length change measurements are taken periodically for a period of 6-12 months in order to attain sufficient data for investigating the expansion rates (Fournier et al., 2010). However, the results of the expansion tests are not necessarily

representative to the behavior of structure due to the different environmental and stress conditions.

2.3.1.2 Petrographic Examination (Damage Rating Index)

The basics of petrographic examination for ASR were introduced in the early 1980's by Blight et al. (1981) where polished concrete sections from drilled cores, from the affected members of structures, are examined visually and a scoring system is used to evaluate the condition of concrete. The petrographic score depends on the number of ASR features observed in the examined sections. Petrographic examination was advanced to be more damage quantifiable and the damage rating index (DRI) method was described by Grattan-Bellew and Danay (1992) in the 1990's and applied on cores from different structures in Canada (Grattan-Bellew, 1995; Rivard et al., 2000) and the United States (Thomas et al., 2013a; 2013b). The process of petrographic assessment is performed by drawing a grid on the polished concrete sections and counting the number of ASR petrographic features observed under microscope (16x magnification). Each feature is counted and multiplied by weighing factor, as shown in Table 2.2, to account for its probable contribution to the concrete deterioration. The weighted values for each feature are then summed and the total value is normalized to a 100 cm^2 (15.5 $in.^2$) surface area to obtain the damage rating index (DRI). It is noted that researchers (Grattan-Bellew and Mitchell, 2006; Shrimer, 2006) have revised the weighing factors in an effort to correlate the relative importance of each feature to the measured expansion due to ASR, which is variable for different types of aggregates (Rivard et al., 2002). The DRI method provides a measure to the amount of deterioration of a given specimen such that the higher values of DRI indicate higher values of deterioration. However, the method is subjective,

dependent on the experience of the operator, and it is not currently standardized. In addition, there are no DRI limits for ASR damage classification to identify low, moderate or severe ASR damage. Thus, the method is considered semi-quantitative which is suitable for obtaining relative information when applied to a set of cores examined by the same petrographer.

Table 2.2 DRI Weighing factors for each petrographic feature (Grattan-Bellew, 1995)

Petrographic feature	Weighing factor
Coarse aggregate with crack (CA)	0.25
Coarse aggregate with crack and gel (CAG)	2.0
Coarse aggregate debonded (D)	3.0
Reaction rim around aggregate (R)	0.5
Cement paste with crack (CP)	2.0
Cement paste with crack and gel (CPG)	4.0
Air void lined with gel (AV)	0.5

2.3.2 Research Related to Detecting ASR Aamage using NDE Methods

Several NDE methods have been recently investigated for detecting ASR damage. The potential for using diffuse ultrasound to detect micro-cracks related to ASR was demonstrated in a previous study (Deroo et al., 2010). Microwave method has been used to differentiate between mortars containing alkali–silica reactive (ASR) aggregate and non-reactive aggregate (Donnell et al., 2013; Hashemi et al., 2014). Distiguishing between ASR and non-ASR specimens was also achieved using ultrasonic method where frequency dependent attenuation was observed for ASR specimens (Gong et al., 2014a). Also a stretching factor method was able to detect the progress of ASR damage (Gong et al.,

2014b). A systematic study using a series of ultrasonic techniques demonstrated that acoustic nonlinearity parameter can track ASR damage with higher sensitivity than wave speed and attenuation parameters. The results also showed a correlation between measured acoustic nonlinearity parameter and the reduction of compressive strength due to ASR damage (Qu et al., 2015). Nondestructive testing techniques: ultrasonic pulse-velocity (UPV), impact-echo, spectral analysis of surface waves (SASW) and surface wave transmission (SWT), were investigated on exposure site specimens for ASR detection. UPV and impact-echo tests were able to detect low levels of expansion from ASR (expansions less than 0.10%) but they showed poor results with higher levels of expansion. On the other hand, the results from surface wave methods, SASW and SWT, failed to show a clear indication of ASR damage presence.

For acoustic emission, to the best of the writer's knowledge, only one study is available for investigating its feasibility to monitor ASR damage. Pour-Ghaz et al. (2012) cast concrete specimens using reactive aggregates and placed the specimens in water for 24 hours, after de-molding, then placed the specimens in 1N NaOH solution at a temperature of 38 ±1 °C (100±1.8°F). The specimens were monitored using acoustic emission broadband sensors (375 kHz) and LVDTs for length change measurements. The results showed the possibility of using AE for early detection of ASR-induced damage (detected at five days of conditioning) as compared to length change measurements where the threshold of 0.1% expansion was reached after 18-20 days. It is noted that these measurements were collected from different specimens. However, AE activity plateaued after 22 days of conditioning. That observation was interpreted by the researcher to be a possible result of high signal attenuation caused by excessive cracking and/or gel formation

due to loss of surface contact between the sensor and the specimen. More research is, therefore, needed to investigate the feasibility of using AE for ASR damage detection and also to examine any hindrances to the method sensitivity caused by the gel formation.

2.4 EVALUATING DAMAGE RELATED TO CORROSION OF STEEL IN CONCRETE

Corrosion of steel reinforcement can significantly affect the durability of concrete structures which may lead to severe damage and catastrophic failures. This damage mechanism can be initiated due to exposure to moisture, high chloride content in concrete, insufficient cover, deicing salts, highly permeable mortar or poor grout quality; among other factors. Visual inspection is a commonly used method for assessment of infrastructure. However, corrosion of steel in concrete cannot be visually detected in its early stages. Electrochemical methods such as half-cell potential (HCP) and polarization resistance are established techniques for corrosion assessment and they have been implemented in field when corrosion damage is suspected (Flis et al., 1992; Videm, 1997). HCP method is invasive as it requires direct connection with the steel for reliable measurements which may be prohibited in nuclear facilities. Additionally, it only provides an estimate for the probability of corrosion at local positions and does not offer quantitative assessment. Linear polarization resistance (LPR) method is commonly used for estimating the corrosion rate (Andrade et al., 1990; Broomfield et al., 1994). However, this method assumes uniform corrosion and does not account for the presence of pitting corrosion. Also it yields sometimes unstable readings. A description on how these electrochemical measurements are performed is given below, followed by a review on the current literature for evaluating steel corrosion in concrete using acoustic emission.

2.4.1 Electrochemical Measurements

2.4.1.1 Half-cell potential

Half-cell potential (HCP) is a measure of the potential of a metal against a reference electrode. Copper/copper sulphate (CSE) and silver/silver chloride in potassium chloride solution are commonly used reference electrodes. This method is described in ASTM C876 (ASTM C876-09) and is traditionally employed to determine the likelihood of corrosion activity as described in Table 2.3 (for a copper-copper sulfate reference electrode). Half-cell potential is measured by connecting the steel reinforcement to the positive terminal of a voltmeter while connecting a reference electrode to the negative terminal as shown in Figure 2.5. The reference electrode must be in contact with dampened concrete at the position where the potential is measured.

2.4.1.2 Linear Polarization Resistance

Linear polarization resistance (LPR) is a method used to measure polarization resistance (R_p) which can be used to calculate corrosion current (I_{corr}), and corrosion current density (i_{corr}). These parameters can give insight to the corrosion process by determining the corrosion rate (CR). Linear polarization resistance measurements may be performed using a potentiostat system which is connected through three cables to the steel reinforcement, copper plate, and copper-copper sulfate probe as the working, counter, and reference electrode (Figure 2.5). The reference electrode must maintain contact with the concrete surface adjacent to the targeted reinforcement, throughout the duration of the linear polarization resistance test, after dampening the concrete surface with a wet sponge.

The potentiostat applies a linear voltage sweep by polarizing the working electrode ±20 mV from the equilibrium potential (E_{corr}) at a rate of 0.166 mV/s and measuring the

current response (ASTM G59-97 2014). While recording the readings, the system plots a graph of the measured current on the x-axis and applied potential on the y-axis. The user selects a portion of the curve in the linear region and passes through the point of zero relative potential to equilibrium potential (approximately in the center of the region), and then the system estimates the corresponding slope ($\Delta E/\Delta I$); which is the R_p value (Equation 2.2). ΔE and ΔI in Equation 2.2 are the range of the potential and the corresponding current, respectively, in the linear portion of the graph. The measured R_p value has the unit of Ohms (as the potential is expressed in Volt and the current in Amperes). If the comparison of results with others from different specimens is needed, R_p values can be expressed in Ohm.cm^2 by dividing the potential by the current density (current expressed per unit area). As R_p is an instantaneous measure of concrete resistivity, some fluctuations are to be expected in the readings.

The corrosion current (I_{corr}) can be calculated from Equation 2.2 which can be applied to calculate the corrosion rate (CR) using Equation 2.3.

$$R_p = \frac{\Delta E}{\Delta i} = \frac{b_a \times b_c}{2.303 \times I_{corr}(b_a + b_c)} \quad (2.2)$$

$$CR = \frac{0.13 \times I_{corr} \times EW}{A \times d} \quad (2.3)$$

where R_p is the polarization resistance, Ω; ΔE is the change in applied potential relative to corrosion potential E_{corr}, mV; Δi is the current response to applied potential spectrum, mA; I_{corr} is the corrosion current, µA; b_a, b_c are the anodic and cathodic Tafel slopes respectively, mV; CR is the corrosion rate in milli-inch per year (mpy); EW is the equivalent weight of iron, 27.92 g; A is the surface area of the anode, cm^2; and d is the density of iron, 7.8 g/cm^3.

Table 2.3 ASTM corrosion for Cu-$CuSO_4$ reference electrode (ASTM C876-09)

Potential Against Cu-CuSO4 Electrode	Corrosion Condition
> – 200 mV	Low Risk (10% probability of corrosion)
– 200 to – 350 mV	Intermediate corrosion risk
< – 350 mV	High corrosion risk (90% probability)
< – 500 mV	Severe corrosion damage

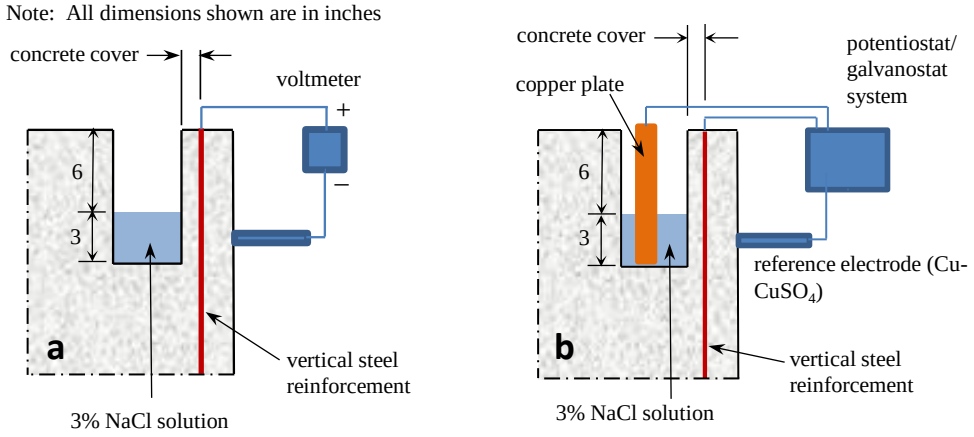

Figure 2.5 Schematic representations: (a) HCP test setup, and (b) LPR test setup.

2.4.2 Acoustic Emission Monitoring

The expansion associated with corrosion products creates stresses which result in concrete cracking. The high sensitivity of AE to crack formation makes it a well-suited method for detecting the micro-cracks related to corrosion initiation. Investigating the feasibility of detecting corrosion using AE dates back to 1980s (Dunn et al., 1983; Weng et al., 1982). Early studies have investigated measured AE parameters collected from accelerated corrosion tests of small reinforced concrete (RC) specimens and their correlation with the results of electrochemical measurements or physical examination of

test specimens (Dunn et al., 1983; Weng et al., 1982; Zdunek et al., 1995; Li et al., 1998; Idrissi and Limam, 2003; Assouli et al., 2005). The results of these studies indicated the feasibility of using AE for early corrosion detection.

AE was used to monitor stress corrosion cracking (SCC) of steel strand in a simulated concrete pore (SCP) solution contaminated by sulphate, chloride, and thiocyanate ions (Ramadan et al., 2008). Three stages of damage were identified by investigating the accumulated AE hits; crack initiation, cracks growth and propagation, and steel failure. Deep pits and crevices associated with local corrosion were detected near the fracture using scanning electron microscope (SEM).

Pattern recognition analysis (principal component analysis (PCA) and K-means method) of AE data was investigated to evaluate damage during an accelerated corrosion test of a prestressing strand under axial tensile load. The onset of wire breakage of the strand was identified using AE data clusters (Ercolino et al., 2015). Djeddi et al. (2013) utilized "Visual ClassTM" program which is a frequency domain pattern recognition system to classify signals due to possible AE sources occurred during SCC test of prestressing strand. Three signal groups were identified and the researcher inferred that they are due to hydrogen penetration, hydrogen gas evolution and crack propagation and rupture. AE data collected during SCC of a post-tensioned concrete beam was analyzed in another study using PCA and self-organizing map algorithms to monitor the evolution of the corrosion damage of steel wires. Three stages; initiation, propagation and rupture were identified and correlated to specific characteristics of the AE events.

Ohtsu and Tomoda (2008) performed two corrosion tests; impressed current accelerated test and a cyclic wet/dry test on RC specimen while being continuously

monitored using AE and the number of AE events per hour was recorded. AE results of both tests indicated two high activity periods correlated to onset of corrosion and cracking initiation. For the cyclic corrosion test *b*-value parameter was also utilized to identify these two periods. HCP measurements indicated the high probability of corrosion after the second period was observed in both tests; which demonstrates the feasibility of using AE for early corrosion detection. The plots of RA (rise time/amplitude) versus average frequency (counts/duration) designated other-type cracks and tensile cracks occurred at the first and second high AE activity periods, respectively. These results were also verified through SEM observations of the reinforcing bar. Kawasaki et al. (2013) achieved similar AE trends as Ohtsu and Tomoda (2008), in terms of number of AE events per hour, RA and average frequency results, in a cyclic wet/dry test of RC beams. Lower *Ib*-values were also observed at the second stage which indicates large-scale cracks. SiGMA analysis showed shear cracks and mixed-mode cracks near the rebar in stage 1 (corrosion initiation) and mostly tensile cracks (corrosion-induced cracks) at stage 2. Results were verified by inspecting a specimen at the end of each stage using SEM and electron probe micro analyzer (EPMA).

Two stages of depassivation of concrete (corrosion initiation) and cracking were also recognized by Patil et al. (2014) during impressed current accelerated corrosion test of RC cylinders. These stages were defined by sudden rises in AE cumulative signal strength (CSS). The CSS was found to have similar trend to the phenomenological model of corrosion of steel in sea water described by Ohtsu and Tomoda (2008). The effect of concrete cracks on corrosion initiation was investigated by Di Benedetti et al. (2013) by testing pre-cracked small scale RC specimens past the steel bar with two different crack

widths and subjecting them to accelerated corrosion test. The specimens with the wider crack exhibited corrosion initiation earlier than specimens with finer crack, as evidenced by AE CSS and HCP results, which was attributed to the higher chloride penetration and chemical aggression. Similar results for corrosion initiation were obtained using AE average signal level (ASL) and absolute energy (AbE) parameters (time driven parameters) where sharp knee was observed for each parameter at the time of corrosion initiation. AE source location of corrosion events was performed by Mangual et al. (2013a; 2013b) from data collected during accelerated corrosion test on two sets of small scale concrete specimens with steel strands to investigate uniform and localized corrosion damage.

The use of Intensity Analysis to detect and classify corrosion damage was proposed by ElBatanouny et al. (2012). Intensity analysis (IA) classification limits were developed by Mangual et al. (2013b) using results of accelerated corrosion test of pre-cracked small scale specimens with embedded strands. The chart was developed by plotting historic index ($H(t)$) versus severity (S_r) and classification limits were formed to divide the chart area into different regions that corresponds to different levels of damage. Historic index a form of trend analysis that compares the signal strength of the most recent hits to the average value of all hits (Equation 2.4). Severity is defined as the average signal strength for the 50 events having the largest numerical value of signal strength (Equation 2.5).

$$H(t) = \frac{N}{N-K} \frac{\sum_{i=K+1}^{N} S_{oi}}{\sum_{i=1}^{N} S_{oi}} \tag{2.4}$$

$$S_r = \frac{1}{50} \sum_{i=1}^{i=50} S_{oi} \tag{2.5}$$

The maximum values of historic index and severity calculated from the results of each specimen was plotted and the chart was divided into different damage regions based on the physical damage state as determined through visual inspection, HCP, and section

loss of the prestressing strands (Figure 2.6). The classification limits were performed such that Region A for the passive condition, region B for depassivated steel (early corrosion) where measured sectional losses were less than 15%, region C for thin cracked specimens with steel sectional loss ranging to 21%, and region D for severely cracked specimens with sectional losses between 23 and 28%.

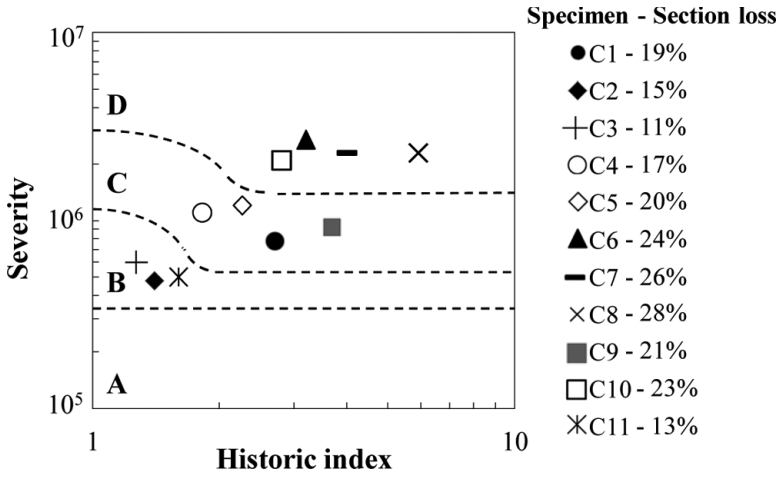

Figure 2.6 Intensity Analysis corrosion classification chart (Mangual et al., 2013a).

The developed IA chart was investigated by ElBatanouny et al. (2014) using data collected during accelerated corrosion test (wet/dry cycles) on medium scale prestressed concrete beams. Two of the three conditioned specimens were pre-cracked to different crack widths to facilitate chloride ingress and achieve different corrosion levels. This study used the same type of sensors as Mangual et al. (2013b), R6I resonant sensors, and the same limits of the IA chart were used to classify the damage. The classification results were in agreement with the actual damage occurred in the specimens as indicated by SEM analysis of the corroded strands. This shows the ability of the developed IA chart to classify damage independent of the scale of the specimens and the duration of the test. The same IA chart was also used to qualify corrosion damage in post-tensioned (PT) concrete

specimens (Appalla et al., 2015). Two sets of specimens were cast to simulate internal and external PT structures. The sensors were placed on the external surface of the specimens; ducts for the external PT and concrete for the internal PT. The results of the damage classification using AE agreed with electrochemical measurements collected during the test.

Velez et al. (2015) qualified corrosion damage in specimens representative of prestressed concrete piles subjected to wet/dry cycles. The results reported after approximately one year of monitoring showed that corrosion initiated in two of the specimens. The same approach using IA was used to analyze the collected AE data. A parametric analysis was conducted to modify the constants used to calculate the historic index and severity parameters. A modification to the proposed IA chart limits was also proposed based on historic index results.

Jagasivamani (2014) deployed AE sensors on reinforced concrete columns in a bridge in Virginia to investigate the applicability of acoustic emission to detect damage in regions with known corrosion deterioration in a setting with high ambient noise. The data was collected for short periods (4 hours each). It was found that RA value (rise time/amplitude) could help in differentiating between signals from ambient noise and corrosion related signals. The study did not include monitoring of ongoing damage using acoustic emission.

The available literature indicates that acoustic emission monitoring for assessment of corrosion damage in general, and early corrosion damage in particular, is promising. Field applications, such as the one presented in Chapter 5 of this dissertation, are needed

to validate and further the development of the method as a real time monitoring and classification technique for corrosion damage in concrete structures.

CHAPTER 3

SIGNAL PROCESSING TECHNIQUES FOR FILTERING ACOUSTIC EMISSION DATA IN PRESTRESSED CONCRETE[1]

[1]Abdelrahman, M., M. ElBatanouny, J. Rose, and P. Ziehl. Submitted to *Research in Nondestructive Evaluation (RNDE)*, 10/21/2016

3.1 ABSTRACT

The current state of infrastructure in the United States and worldwide has raised the need for reliable structural health monitoring techniques. Piezoelectric sensing, such as acoustic emission, has recently gained attention due to its high sensitivity and associated capability for early detection of damage. The high sensitivity of this method, however, also results in the collection of data not directly related to damage growth. Current filtering procedures focus primarily on parametric analysis of the collected signals. This study focuses on developing more robust filtering techniques for acoustic emission data collected from a prestressed concrete specimen. Simulated data was generated to enable proper identification of the source of the collected signals. Filtering criteria were developed through characterization of the energy content using a wavelet transform. The developed filters were capable of separating the induced target signals from other signals with reasonable accuracy and the results were verified through source location. The developed filters were validated using acoustic emission data collected during a load test.

3.2 INTRODUCTION

Aging of infrastructure in the United States and worldwide has been the main drive for research in the area of structural health monitoring/nondestructive evaluation (SHM/NDE). This has resulted in the development or technology transfer of several SHM/NDE methods to assess damage in passively reinforced and prestressed/post-tensioned concrete structures. Current SHM/NDE methods include: vibration measurement and modal analysis,[1] radiography,[2] magnetic flux leakage,[3] impact-echo,[4] ultrasonics,[5] and acoustic emission.[6,7] Acoustic emission is the main focus of this study.

Acoustic emission (AE) monitoring is based on the detection of transient stress waves generated by rapid release of energy within a material, such as that due to crack initiation or growth.[8] The passive nature of sensing with acoustic emission monitoring allows for the development of low-power data acquisition systems that can be used to continuously monitor in-service structures. AE sensors operate in the kHz range which allows for the early detection of damage, but also leads to the generation of large data sets with false signals (or 'noise') from wave reflections and other sources. The main challenges associated with acoustic emission are: 1) development of filters to minimize the size of the data set while simultaneously improving its quality, and 2) developing correlations between AE data and the condition of the structural member under investigation.

Previous research efforts have focused on development of damage assessment algorithms such as: Intensity Analysis,[9-12] load ratio and calm ratio,[13-15] *b*-value and *Ib*-value analysis,[16-18] and pattern recognition.[19,20] However, most of these studies used data from controlled experiments and/or utilized guard sensors which minimized the noise. The current state of the art for AE data reduction (referred to herein as 'data filtering') includes: 1) filters based on detection of AE events and source location (i.e. the same AE wave is detected by more than one sensor and can be located),[21,22] 2) parameter-based filters such as Swansong II filters [11,23-25] and root mean square filters developed for seismic loading,[26,27] and c) pattern recognition based filters.[28] These filters are empirically based and, therefore, are applicable to specific materials and specimen geometries.

A signal processing approach is proposed in this study to filter AE data gathered from a prestressed concrete beam specimen. Similar to voice recognition, acoustic signatures of actual cracking events should be different than those associated with wave

reflections or other noise. The wavelet transform can be used to better understand the characteristics of AE signals in the time-frequency domain.

In this study an artificial acoustic emission source (*Hsu-Nielsen source)*[29] was used to generate AE signals on a prestressed concrete beam instrumented with ten AE sensors. The artificial signals were generated at different horizontal and vertical locations to examine the effect of source-to-sensor distance on the data. Following each artificial signal, the data acquisition system continued monitoring to collect wave reflections. The signals generated from the application of the artificial source itself are hereafter referred to as "induced target signals" and signals due other sources including reflections and other signals not directly related to the source are referred to as "degraded signals". AE signals collected during the test were analyzed using a wavelet transform. Four different filtering criteria are proposed based on the spatial characteristics of the AE signals in the time-frequency domain. The reliability of the filters was assessed based on prior knowledge of the AE source. A parameter-based filter, similar to filters used in previous studies, was also developed to enable comparisons with the wavelet based filters. The data collected during load testing of a similar beam specimen was then used to test and verify the proposed filtering technique.

3.3 RESEARCH SIGNIFICANCE

Noise is present in AE data sets due to wave reflections, mechanical rubbing, and environmental sources such as rain, wind-born debris, and hail. Most approaches for excluding these signals are empirical and require the involvement of an AE expert. The current lack of reliable filtering techniques to reject noise in AE data may lead to deceptive results in source location and damage assessment. This realization raises the need for robust

data filters with predetermined filtering criteria that can be utilized by less experienced users with acceptable accuracy. This paper investigates the use of wavelet analysis of AE signals to develop algorithms for differentiation between induced target AE signals and degraded signals. The establishment of such an approach has the potential to broaden the use of acoustic emission monitoring and to enhance its reliability as a NDE/SHM technique.

3.4 EXPERIMENTAL PROCEDURE

3.4.1 Methodology: Wavelet transform

Signal processing is usually used to develop a representation of the signal that makes certain characteristics more explicit. The Fourier transform and Short Time Fourier Transform (STFT) are common tools to express a signal as a function of frequency. Wavelet analysis offers better resolution than the aforementioned techniques as it uses short time windows (high time resolution) at high frequencies and long time windows (low time resolution) at low frequencies.[30] This property makes it suitable for analyzing transient signals such as acoustic emission signals.

The concept of continuous wavelet analysis was introduced in the 1980s by Grossman and Morlet,[31] followed by the work of Mallat and Meyer of using the multi-resolution analysis (varying the time and frequency resolutions on the time-frequency representation) for orthonormal wavelet bases.[32-34] Daubechies's research later promoted the use of wavelets in mathematics and engineering and developed the basis for the discrete wavelet transform.[35-37]

Wavelet transformation is a linear decomposition which is attained by comparing the signal with a set of elementary functions obtained by the time scaling and shifting of a

mother function. Let the mother function be *ψ(t)* with a mean frequency of ω_0, then the scaled and shifted function is $\psi\left(a^{-1}(t-b)\right)$ with a frequency = ω_0/a where *a* is the scale index and *b* is the time shifting. The wavelet transform can be obtained as the inner product of the signal *s(t)* and $\psi\left(a^{-1}(t-b)\right)$ as follows:

$$CWT(a,b) = \frac{1}{\sqrt{|a|}} \int s(t)\psi\left(\frac{(t-b)}{a}\right)dt \qquad a \neq 0$$

As seen in the above equation, the continuous wavelet transform (CWT) is a function of time *(b)* and frequency (ω_0/a). It can be used to define how frequency content of a signal evolves in time, making it ideal for the analysis of non-stationary signals.

The mother wavelet used in the analysis described in this paper is the "Morlet wavelet" which is a sine wave multiplied by a Gaussian envelope. The Morlet wavelet is a commonly used mother wavelet that satisfies the conditions of localized time and frequency and zero mean.

Wavelet transform has been previously investigated for AE data analysis for damage monitoring and classification in concrete,[38] composite materials[39-43] and galvanized steel coating.[44] Wavelet analysis has also been implemented for de-noising of AE signals to improve the quality of the data.[45,46] De-noising of AE signals generated during dynamic test on a concrete slab was investigated in a previous study by applying continuous wavelet transform and statistically identifying the frequency band associated with concrete fracture (cracking). The filtered data set can then be formed by reconstructing the signals using only the assigned scales for cracking.[47,48] This paper focuses on applying the wavelet transform for filtering AE data through the elimination of signals related to reflections and other spurious sources rather than de-noising the signals. Data reduction is

valuable for field applications where spurious signals (signals that have no correlation to the damage state), sometimes account for the majority of the collected data.

3.4.2 Test specimen and instrumentation

A prestressed concrete T-beam with the cross section shown in Figure 3.1, similar to the specimens described in ElBatanouny et al.[11], was used in this study. The specimen had two 13 mm (0.5 in.) low relaxation prestressing strands prestressed to 68% of the strand ultimate stress [f_{pu} = 1,860 MPa (270 ksi)] and a span of 4.98 m (16 ft. 4in.). It was instrumented with ten R6I AE sensors with the layout shown in Figure 3.2 to enable investigation of different source-to-sensor distances. This sensor type includes a 40 dB preamplifier and has operating frequency of 40-100 kHz and resonant frequency of 55 kHz. The higher sensitivity of the resonant sensors makes them a more suitable choice for monitoring and detection of damage in concrete than wideband sensors. This can be attributed to high signal attenuation associated with the material since waves with higher frequency components propagate in concrete with higher attenuation.[49] In addition, due to concrete heterogeneity and presence of aggregates (typically 20 mm or greater in size), AE waves with frequency higher than 100 kHz may be scattered due to the relation between the wavelength and the size of heterogeneity; 40 mm wavelength at 100 kHz assuming P-wave speed of 4,000 m/s in concrete.[50] The use of resonant sensors will affect the energy distribution in the frequency domain; however, the objective of this paper is to develop effective filters adapted to the commonly used sensor type for concrete. Filters that work effectively on resonant sensor data can be widely implemented considering the popularity of that type of AE sensors.

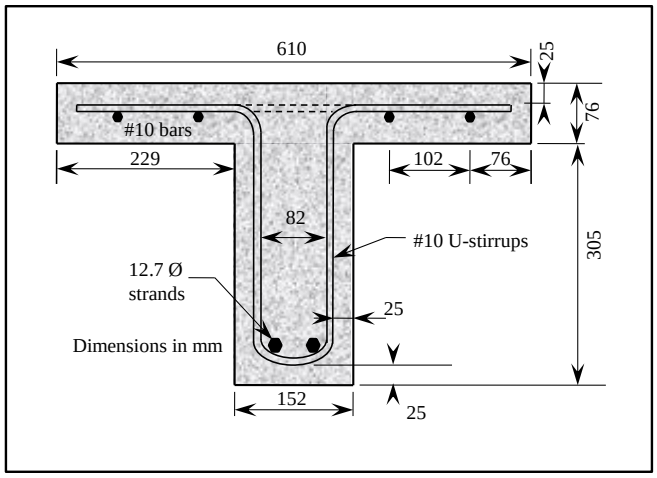

Figure 3.1 Schematic of geometric properties and reinforcement, dimensions in mm (1 inch = 25.4 mm).

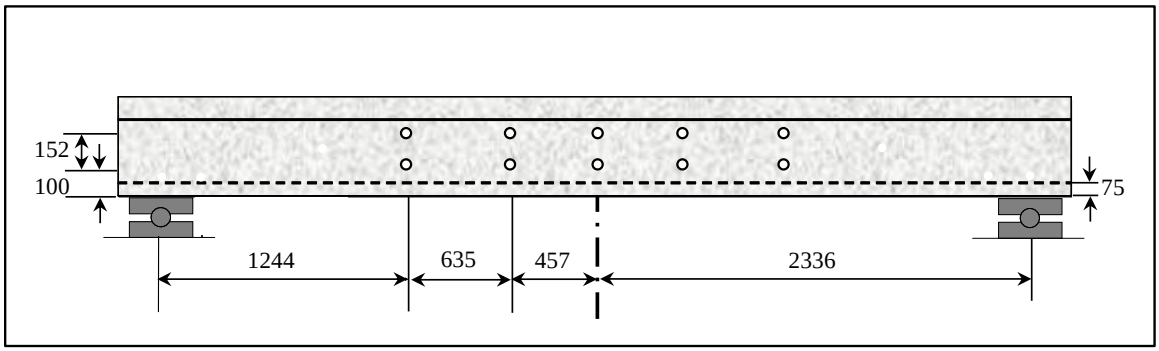

Figure 3.2 AE sensor layout, dimensions in mm (1 inch = 25.4 mm).

The sensors were attached to the specimen using specialized two part epoxy to ensure appropriate acoustic coupling. The data acquisition system, a 16 channel Sensor Highway II system manufactured by Mistras Group Inc., was set with a fixed threshold of 40 dB for all the channels, sampling rate of one million samples per second, pre-trigger of 256 µs, and waveform length of 1024 sample points. Values for peak definition time (PDT), Hit definition time (HDT) and Hit lockout time (HLT) of 200 µs, 400 µs, and 800 µs, respectively, were used to define the collected hits and reduce reflections. All the channels were set to trigger independently from each other during the data collection period. The

described sensor layout and data acquisition setup was chosen to be similar to that described in ElBatanouny et al.[11]

3.4.3 Generation of simulated data

To minimize uncertainty regarding the source and nature of the data sets, simulated data sets with known sources and locations were generated. One conventional artificial source to simulate acoustic emission is the pencil lead break (PLB), also known as the AE Hsu-Nielsen source, as described in ASTM E976.[29,51] PLBs were carefully conducted in the vicinity of the mid-span; six PLBs at each red dot with a total of 630 PLBs, as shown in Figure 3.3. For each PLB, one signal at each sensor for a total of 10 signals were separated from the data set based on time of arrival and these signals were retained in the target signal data set. Other signals resulting from reflections of the AE wave on the boundaries of the specimen and associated with this PLB were retained in the degraded signal data set. The degraded signals represent wave reflections or data that is not associated with the first wave emission from the pencil lead break event, such as the lead sleeve inadvertently impacting the concrete surface after the pencil lead break event has occurred.

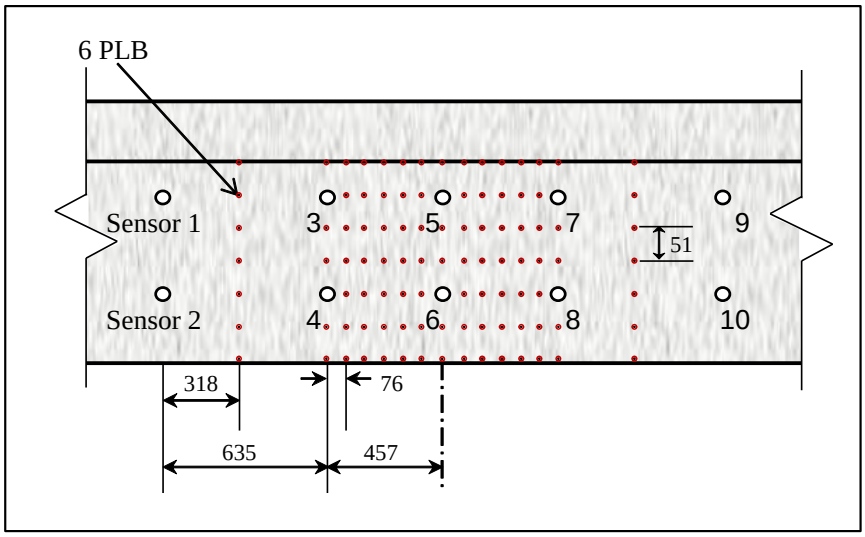

Figure 3.3 Locations of artificial sources (pencil lead breaks), dimensions in mm (1 inch = 25.4 mm).

3.5 DESCRIPTION OF DATA REDUCTION STRATEGY

Data collected due to PLBs at the beam centerline (42 PLBs; 420 target signals and 2,787 degraded signals) was designated as the 'training data set' and was used to develop the data reduction strategy, referred to as 'data filtering' or more simply 'filters'. The developed filters were then investigated for appropriateness using data collected due to PLBs between sensors 1, 2, 3, and 4 (at a distance of 318 mm [12.5 in.] from sensors 1 and 2), which are 42 PLBs (420 target signals and 1,651 degraded signals). This data was designated as the 'testing data set'. Each data set was divided into two groups; 'target signal data' and 'degraded signal data' and wavelet analysis was performed on each group. Figure 3.4 shows an example of the wavelet results for the target signal and the degraded signal data. The wavelet transform, as seen in this figure, provides the distribution of energy (mapped in color contours) in the time-frequency domain. The Y-axis represents the scale which is inversely proportional to the frequency as shown in Figure 3.5.

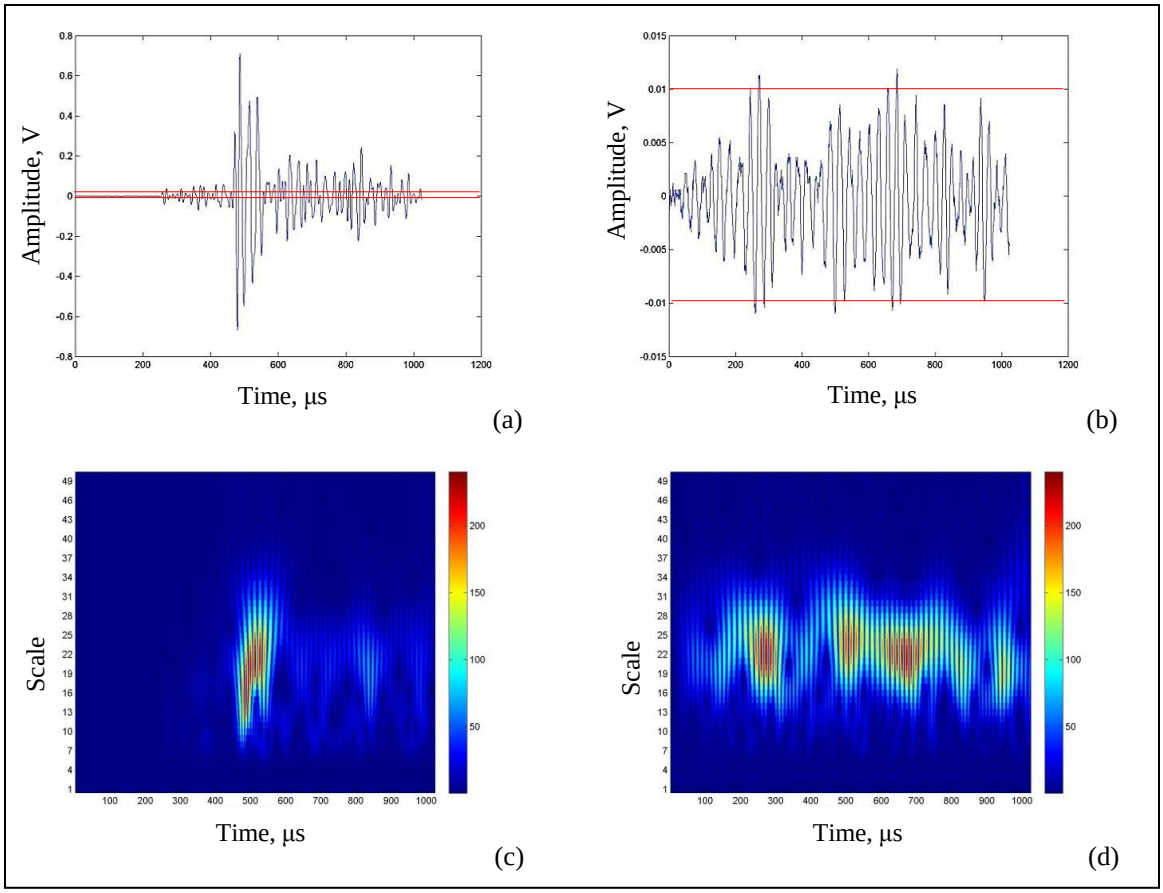

Figure 3.4 AE waveforms and wavelet transform for a target signal ((a) and (c), respectively) and a degraded signal ((b) and (d), respectively).

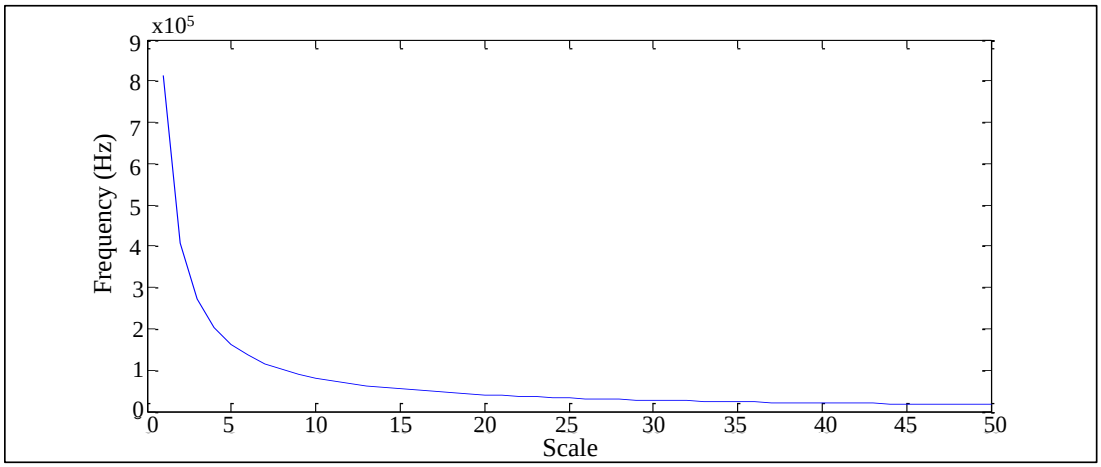

Figure 3.5 Relationship between frequency and scale.

Through visual observation of the wavelet transform results from the training data set, it was observed that high energy tends to be more localized in terms of time and

frequency in the target signal data as compared to data from degraded signals. To enable comparisons, a 3D representation of the wavelet coefficients was obtained as shown in Figure 3.6(a) and Figure 3.6(b) and the coefficient values less than 10% of the maximum value within the same wavelet were set equal to zero as shown in Figure 3.6(c) and Figure 3.6(d). The remaining wavelet coefficients were labeled as 'high energy zones' and the centroid of the high energy zones was obtained and labelled as 'energy density centroid'. Different spatial characteristics of the high energy in the 3D representation were examined as potential filtering criteria including the following:

1. Normalized Area of High Energy (Criterion 1, referred to as 'C1'): The total number of nodes (coefficients) with high energy was calculated and normalized to the summation of the coefficient values at these nodes.
2. Normalized Average Distance (C2): The distance from each high energy node to the energy density centroid was calculated. The average of these distances was normalized to the summation of the coefficient values at these nodes.
3. Normalized Maximum Distance (C3): The maximum distance between high energy nodes and the energy density centroid was calculated and normalized to the summation of the coefficient values at these nodes.
4. Summation of High Energy x Distance (C4): The summation of each high energy coefficient value multiplied by its distance to the energy density centroid was calculated.

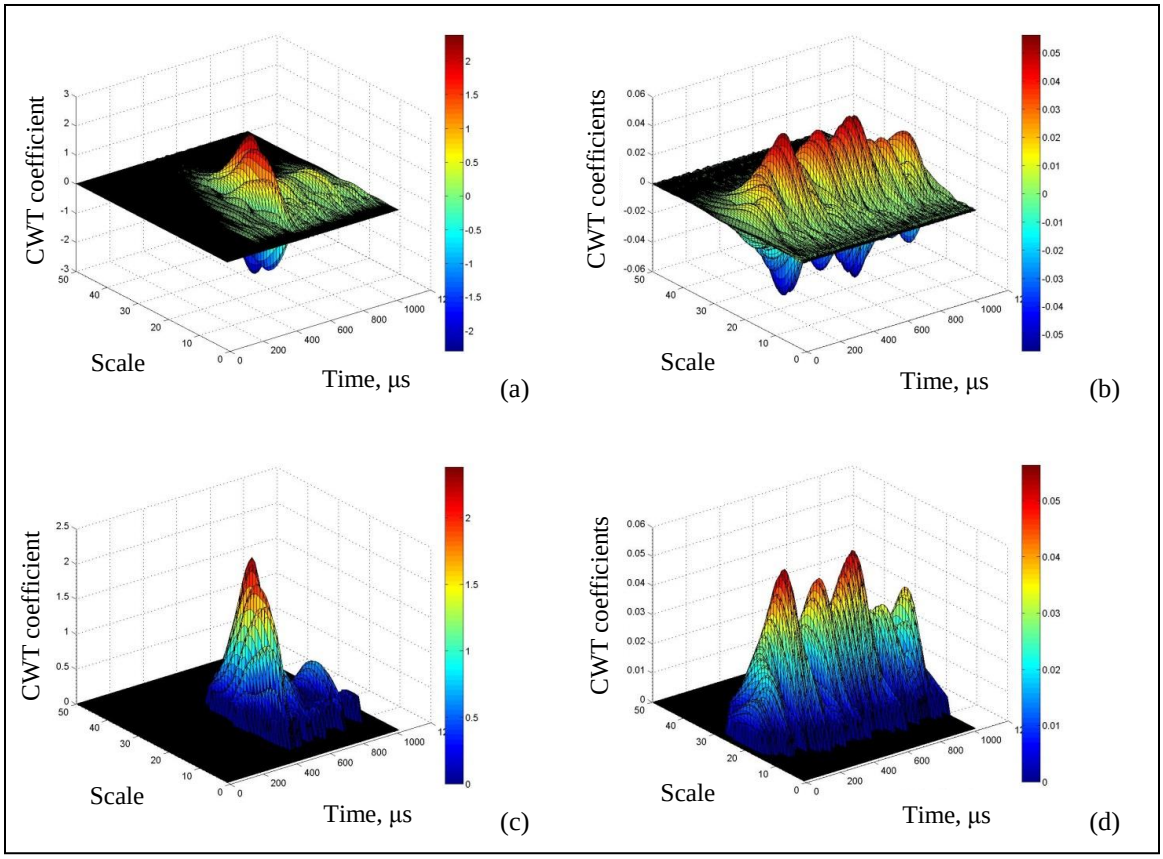

Figure 3.6 3D representation of all wavelet coefficients and the absolute high energy coefficients for a target signal ((a) and (c), respectively) and a degraded signal ((b) and (d), respectively).

3.6 RESULTS AND DISCUSSION

The four candidate criteria described in the previous section were applied to target signal data and degraded signal data generated through PLBs at the centerline of the specimen. Figure 3.7 shows the filtering criteria values for each signal. The data formed two clusters which agree with their known source classification with the exception of a small number of outliers (less than 3%).

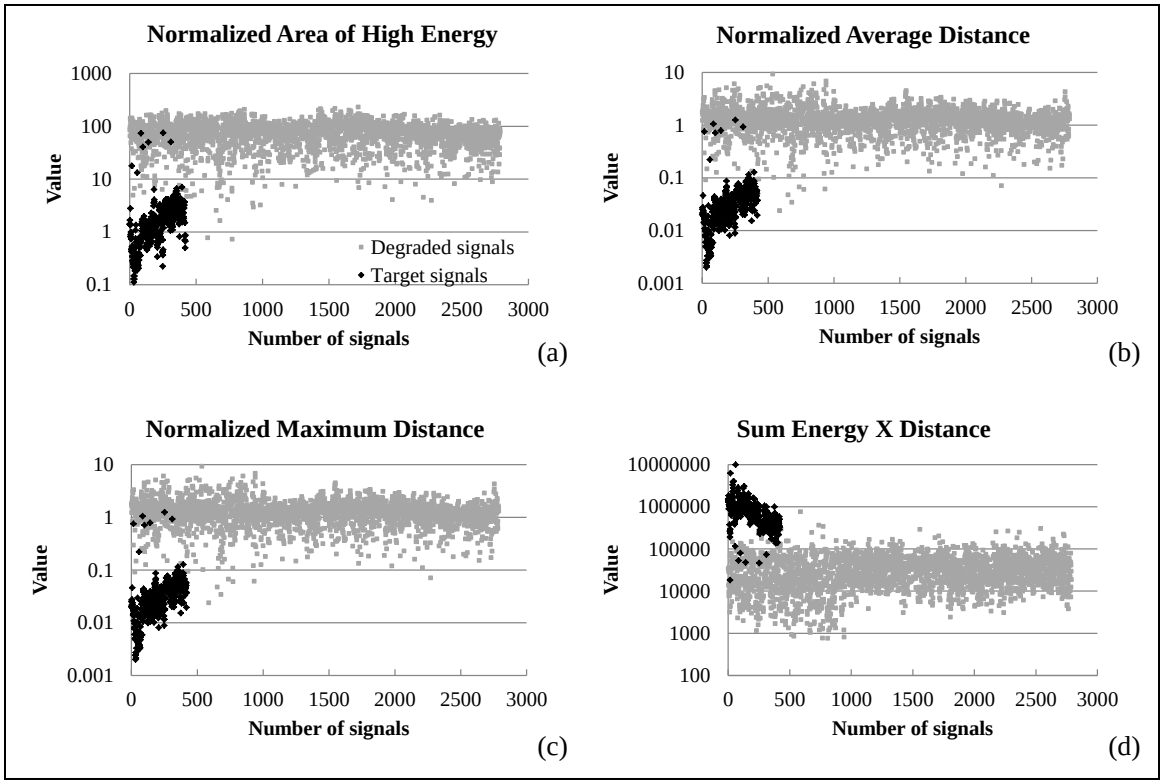

Figure 3.7 Values of criteria for signals obtained from pencil lead breaks at the centerline of the specimen.

The criteria threshold limits were developed using a modified grid search to achieve the highest success rate in data classification. The threshold limit defines the boundary between signals interpreted as target signals and those interpreted as degraded signals. Grid searches normally determine a parameter by applying a uniform adjustment to the parameter and selecting the best value. In this grid search, for a given criterion (C1 - C4), the values calculated for target signals were sorted in ascending order, and each value was evaluated as a potential filtering limit. This approach reduces the search time, as any value between the limits investigated would increase the number of degraded signals attained in the filtered data without gaining additional target signals compared to the previously investigated limit. The success rate for each potential limit was then calculated as "the percentage of target signals correctly classified minus the percentage of degraded signals

incorrectly classified". Figure 3.8 illustrates the values obtained along with the success rate when the criterion "Normalized Area of High Energy (C1)" was investigated. The same procedure was performed for the other three criteria and the limits with the highest success rate were chosen as thresholds for filtering as shown in Table 3.1. All proposed limits yielded relatively accurate classification of data in terms of target signal and degraded signal data. The success rate for each of the four proposed criteria exceeded 97% (Table 3.1).

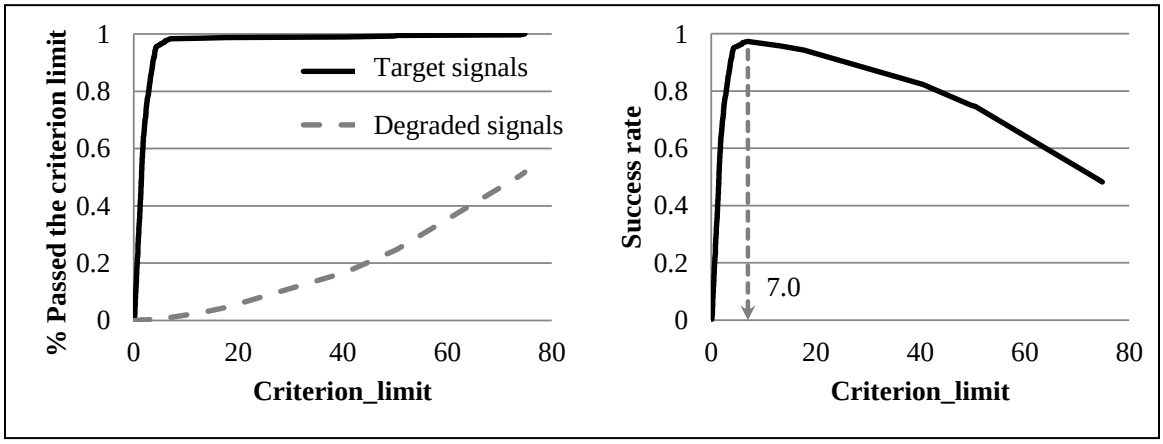

Figure 3.8 Development of filtering limit for criterion C1: (a) percentages of correctly classified target signals and incorrectly classified degraded signals obtained using different limits, (b) success rate for each limit value.

Table 3.1 The proposed limits for each criterion and associated success rates.

Criterion	Proposed limit	Success rate (%)
Normalized Area of High Energy	7.0	97
Normalized Average Distance	0.13	98
Normalized Maximum Distance	0.32	98
Summation of High Energy x Distance	137,120	98

The testing data set (PLBs between sensors 1-4) was used to evaluate the four criteria (C1 - C4). The success rate for each criterion, taking into consideration the

horizontal distance from the PLBs to the sensors, is given in Table 3.2. It can be seen that the filters were able to classify the data properly (higher than 90% success rate) within 775 mm (30.5 in.) from the source. For farther distances from the source [1,867 mm (73.5 in.)], the first three criteria failed to detect some of the target signals, resulting in lower success rates. When examining the cause, it was observed that sensor 10 responded slightly differently from other sensors, especially with farther sources, in the sense that it continued to resonate for a longer time period in comparison to other sensors having the same source-to-sensor distance. This behavior only affected the results of sensor 10. Prior to testing, each sensor was checked for relative sensitivity response through conducting PLBs and examining the peak amplitude response of the sensor, but as is customary this sensitivity test was conducted at 76 mm (3 in.) and 305 mm (12 in.) from each sensor. Appropriate sensor response was demonstrated as the average amplitude response of a sensor was within ± 3 dB of the average amplitude of the sensor group for the PLBs at each distance. This type of test did not reveal the difference related to sensor 10 at larger source-to-sensor distance.

Table 3.2 Success rates for the testing data using proposed limits.

Sensors	Distance from source, mm (in.)	Success rate for each criterion (%)			
		C1	C2	C3	C4
		Limit=7.0	Limit=0.13	Limit=0.32	Limit= 137,120
1,2,3,4	318 (12.5)	92	93	93	90
5,6	775 (30.5)	94	95	95	91
7,8	1,232 (48.5)	86	92	91	97
9,10	1,867 (73.5)	45	51	40	84

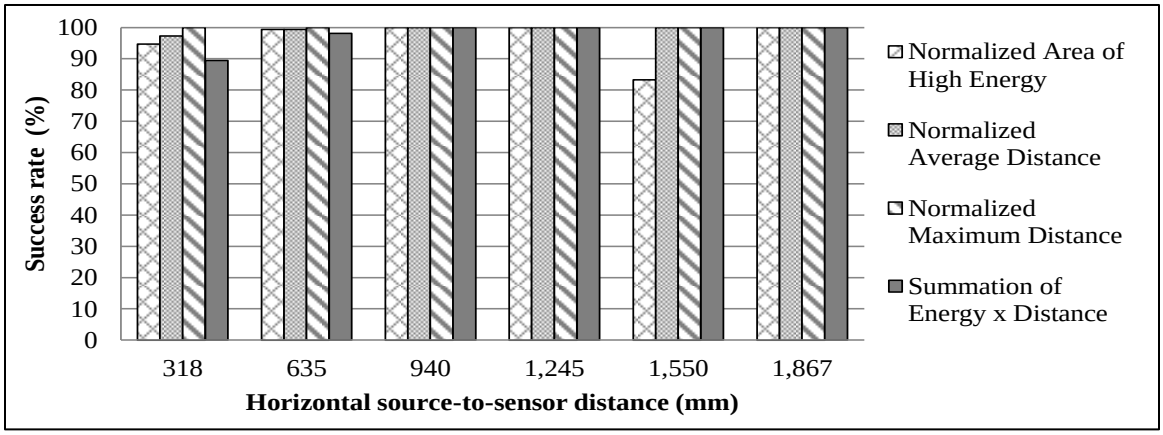

Figure 3.9 Success rates for signals obtained at sensor 2 due to PLBs at different horizontal distances from the sensor.

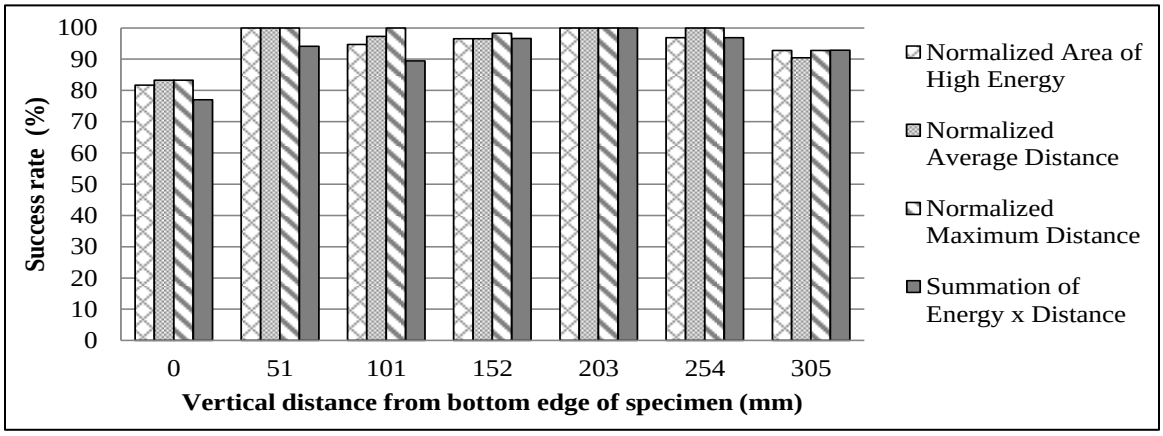

Figure 3.10 Success rates for signals obtained at sensor 2 due to PLBs at different vertical distances at a horizontal distance of 318 mm (12.5 in.) from the sensor.

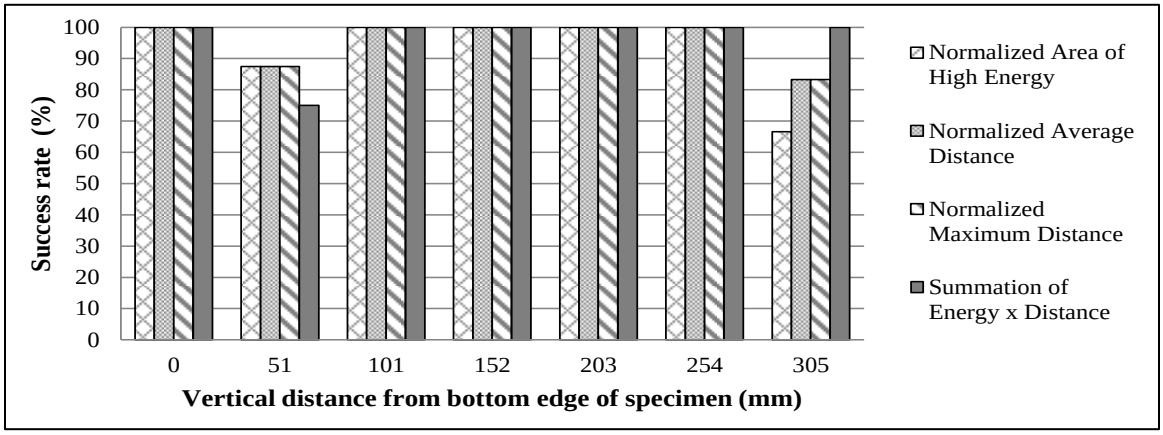

Figure 3.11 Success rates for signals obtained at sensor 2 due to PLBs at different vertical distances at a horizontal distance of 1,867 mm (73.5 in.) from the sensor.

To further investigate the effect of source-to-sensor distance, data collected from sensor 2 due to PLBs at different horizontal distances and the same vertical distance as sensor 2 (100 mm [4 in.] from the bottom of the specimen) was analyzed. As shown in Figure 3.9, all criteria yielded comparable results. These results indicate that the change of horizontal source-to-sensor distance does not affect the quality of the proposed filters within 1.8 m (6 feet) from the source. The same observation was also attained for sources at different vertical distance from sensor 2, placed at 101 mm (4 in.) from the bottom of the specimen. Figure 3.10 shows the success rates achieved for data collected by sensor 2 due to PLBs at different vertical distances at a horizontal distance of 318 mm (12.5 in.) from the sensor. Figure 3.11 shows similar results at a different horizontal distance of 1,867 mm (73.5 in.). This was done to illustrate the effect of a change in vertical distance at a small horizontal distance of 318 mm (12.5 in.) as well as the effect of combined large vertical and horizontal distances. In both cases, acceptable success rates were achieved at different vertical source-to-sensor distances. As expected, lower success rates were achieved when the target signal data was generated at the boundaries (i.e. top and bottom edges of the web).

3.6.1 Comparison between parameter-based filtering approach and the proposed filters

To investigate and quantify the potential improvements offered by the filtering approaches described above, the efficiency of these filters was compared to that of a commonly used parameter based AE filtering method and the results were verified based on known source location. One commonly used filtering method for fiber reinforced pressure vessels is the Swansong II approach discussed by Fowler et al.[23] These filters are

based on the concept that target signals with high duration are associated with high amplitudes and vice versa. Based on this observation, limits based on duration-amplitude (D-A) relationships are set for minimizing non-relevant data. A similar approach is sometimes used for rise time-amplitude (R-A) relationships.

To provide a means of comparison between filtering approaches, D-A/R-A filter limits were developed for the current study related to PLBs. The training and testing data sets described previously were used to develop limits for the D-A/R-A filters. The prior knowledge of the source of each signal (PLB or reflection) in the mentioned data sets was employed to train the filter limits to achieve the highest possible agreement between the filter classification and actual classification of the data. Different sets of limits were investigated as potential D-A/R-A filters and the one that yielded the highest success rate in source classification was chosen to be included in the comparison (Table 3.3). It is noted that the used D-A/R-A filtering limits misclassified most of the degraded signals in the training and testing data sets as target signals (74% and 81%, respectively) and correctly classified most of the target signals (96% and 87% of the training and testing data sets, respectively). However, any refinement to reach higher elimination of unwanted data resulted in higher rejection of target signal data. Thus, the limits mentioned in Table 3.3 were chosen for this study.

Figure 3.12(a) and Figure 3.12(b) show source location results of unfiltered data and data filtered using D-A/R-A filters, respectively. Source location was achieved using AEwin for sensor highway smart monitor software version E4.30, by Mistras Group Inc., based on arrival time (first crossing of data acquisition threshold) of one AE signal at a minimum of four sensors to produce an AE event; i.e. at least four sensors must be triggered

by the same source to produce an event. The AE wave speed in the specimen was measured experimentally using two sensors placed 152 mm (6 in.) apart and is equal to 3,714 m/s (146,200 in/s). The D-A/R-A filters did not provide much improvement to the data. In comparison, when the C2 criterion (normalized average distance) is applied (Figure 3.12(c)), the accuracy of source location improved and the locations where PLBs were applied are more distinct. It is noted that more accurate source location results were achieved when the source was located at the centerline of the rectangular grids of the sensors; for example between sensors 1, 2, 3 and 4. This is attributed to the waves having almost identical propagation distances along the paths to the sensors.

Table 3.4 shows the number of hits remaining after applying each of the approaches (C1 - C4 and D-A/R-A) on AE data generated due to all PLBs as well as their percentage from the raw unfiltered data (which includes 41,254 signals: 6,300 target signals and 34,954 degraded signals). Data reduction achieved with the C1 - C4 criteria is significantly higher than that achieved using the D-A/R-A filters, as shown in Table 3.4. This data reduction may significantly decrease the cost of further analysis of the data.

Table 3.3 Data rejection limits for D-A/R-A filters.

D-A filters		R-A filters	
Amplitude (dB)	Duration (μs)	Amplitude (dB)	Rise time (μs)
40-55	>1,500	40-45	>300
56-60	>5,000	46-50	>400
61-70	>7,500	51-60	>500
71-80	> 11,000	61-100	>700
81-100	>13,000		

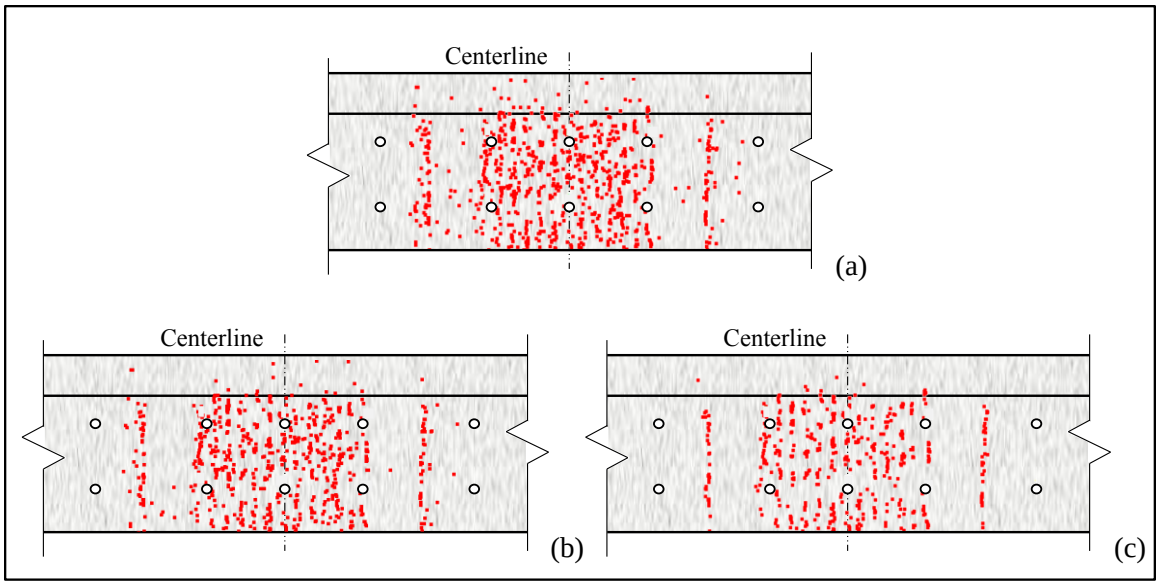

Figure 3.12 Source location results of (a) unfiltered data, (b) filtered data using D-A/R-A filters, and (c) filtered data using normalized average distance (C2) filter.

Table 3.4 Number of hits remaining after applying data filters and its percentage from raw data

	Raw data	D-A/R-A	C1	C2	C3	C4
Number of hits remaining (after filtering)	41,254	31,445	6,793	6,737	6,605	7,445
Filtered/unfiltered hits (percentage)	100%	76.2%	16.4%	16.3%	16.0%	18.0%

For further comparison of the two filtering approaches, a data set of signals due to the 42 PLBs applied at the centerline of the beam specimen (2,490 mm [98 in.] from the left edge of the specimen) was filtered using both methods. This data set included 420 target signals and 2,787 degraded signals. A confusion matrix showing actual data classification and that classified by different filters is shown in Table 3.5 for D-A/R-A filters and in Table 3.6 for the wavelet based filtering approach. Both filtering methods correctly classified most of the target signals as shown in the tables. However, in the case

of D-A/R-A filters 74% of the degraded signals were incorrectly classified as target signals (false positive) which lowered the efficiency of the filters as a data reduction method. The wavelet based filters (criteria C1 – C4) generated better results, where less than 1.5% of the degraded signals were misclassified as target signals as shown in Table 3.6. The data set was reduced to 14% of the unfiltered data as compared to 77% when the D-A/R-A filters were used.

The accuracy of the filtering process using wavelet based filters and D-A/R-A filters was assessed based on a version of the confusion matrix that includes values presented in number of signals instead of percentages. The accuracy term is calculated as the summation of values in the matrix diagonal (true positive and true negative), divided by the summation of all values within the confusion matrix. A perfect result is obtained if the accuracy is equal to 1.0. The confusion matrices in Table 3.5 and Table 3.6 are presented in percentages (not values) to enable interpretation of the data.

Since the number of degraded signals in the AE data set is usually much greater than the number of target signals, the accuracy should not be used as the only measure of performance. For example, in a data set of 1,000 signals having only 20 target signals, if the filters eliminated all degraded signals and kept half of the target signals, the accuracy will be 99% even though the filters rejected 50% of the data of interest. Another measure that is commonly used in cases involving a high proportion of unwanted signals in a data set is *sensitivity* or *true positive rat*e, which is the percentage of positive cases (target signals) that are correctly identified. In our case, this is equal to the true positive cell (top-left cell) in the confusion matrix as the matrix values are presented as percentages. Therefore, both accuracy and true positive rate are used for evaluation as shown in Table

3.7. The wavelet based filters (C1 - C4) offered improved performance in comparison to the D-A/R-A filters.

Table 3.5 Confusion matrix for data collected due to PLBs at the centerline of the specimen classified by D-A/R-A filters.

		Classified by D-A/R-A	
		Target signals	Degraded signals
Actual	Target signals (420 signals)	95.7%	4.3%
	Degraded signals (2,787 signals)	74.1%	25.9%

Table 3.6 Confusion matrix for data collected due to PLBs at the centerline of the specimen classified by proposed filters.

		Classified by C1 (%)		Classified by C2 (%)		Classified by C3 (%)		Classified by C4 (%)	
		TS	DS	TS	DS	TS	DS	TS	DS
Actual	TS* (420 signals)	98.3	1.7	98.3	1.7	98.3	1.7	98.3	1.7
	DS** (2,787 signals)	1.0	99.0	0.8	99.2	0.3	99.7	1.3	98.7

*TS: Target signals; **DS: Degraded Signals

Table 3.7 Accuracy and true positive rate for each filtering method.

	D-A/R-A	C1	C2	C3	C4
Accuracy	0.350	0.990	0.991	0.995	0.987
True positive rate	0.957	0.983	0.983	0.983	0.983

3.7 VERIFICATION OF PROPOSED APPROACH USING LOAD TEST DATA

AE data of actual concrete cracking events collected during cyclic load testing (CLT) of a prestressed concrete beam (Figure 3.13), described in ElBatanouny et al.[11], was used to examine the applicability of the proposed data reduction approach. The beam specimen is similar to that described in the experimental procedure section for the PLBs and was monitored using the same sensor type and layout. Data collected during the last load step in cycle 9, highlighted in red in Figure 3.14, was chosen for further analysis using the wavelet criteria (C1 - C4). This loading portion was selected as it is the last load step before the onset of visible cracking; thus, AE data related to micro-cracking is expected. D-A/R-A filters were developed based on detailed visual inspection of the collected waveforms in the previous study[11], specifically for this specimen shape and loading protocol, to minimize data due to reflections. These D-A/R-A filters limits are considered in this paper for comparison; as they have demonstrated satisfactory source location results as seen in Figure 3.15. It is noted that the limits used for the D-A/R-A filters for the load test differ from those shown in Table 3.3, as those limits were developed for the specific case of PLB sources. The amplitude threshold was set to 40 dB for data acquisition and 60 dB for waveform recording during the load test. ElBatanouny et al. employed an amplitude threshold filter of 60 dB prior to the D-A/R-A filters which will be included in the results described below for filtered data using D-A/R-A filters. The same amplitude filter is used in the wavelet based criteria as waveform data is needed to attain the wavelet transform. Table 3.8 shows the number of hits retained after applying each of the investigated data reduction methods on data collected during the last load step in cycle 9. As seen in the

table, the wavelet based criteria (C1 – C4) resulted in data reduction exceeding 90%, which is comparable to that achieved by D-A/R-A filters.

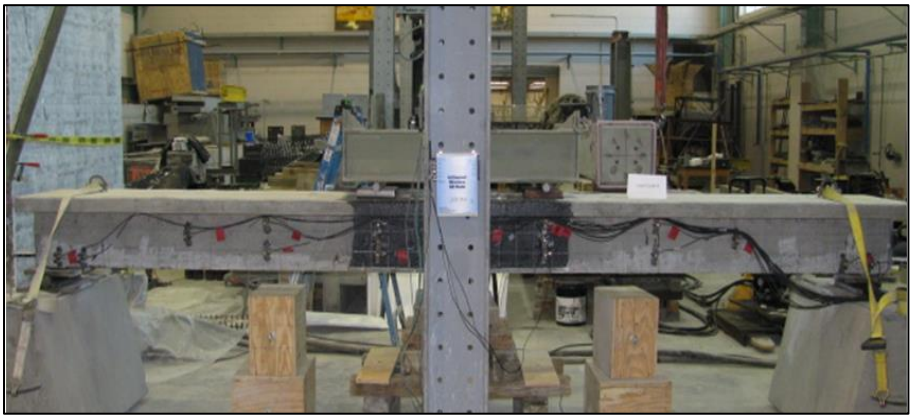

Figure 3.13 Overview of the test setup.

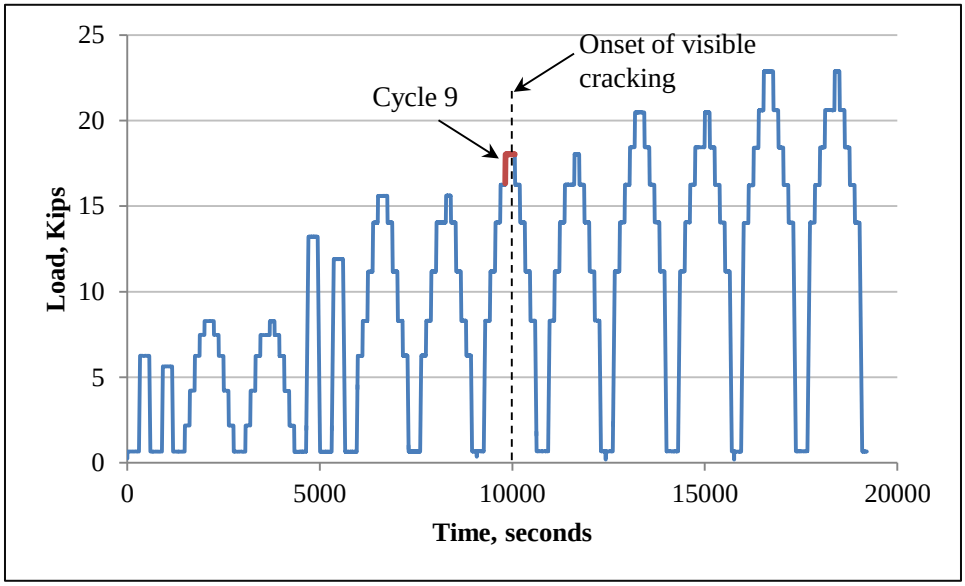

Figure 3.14 Load versus time for cyclic load test on a prestressed concrete beam. Data collected during the highlighted portion in cycle 9 is investigated in this paper.

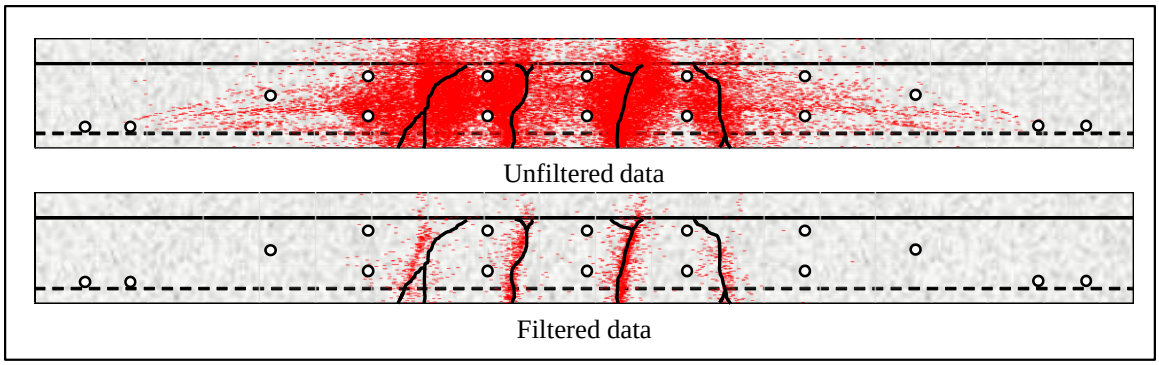

Figure 3.15 Visually detected cracks (plotted in black) superimposed with source location results (plotted as red dots) for acoustic emission data generated by load testing of prestressed concrete beam specimens: unfiltered data (above) and filtered data using D-A/R-A filter (below).[11] Source: reprinted from ElBatanouny et al.[11] with permission from Elsevier.

Table 3.8 Number of hits remaining after applying investigated filters on data collected during the last load step of cycle 9.

	Raw data	Data remaining after filtering				
		D-A/R-A	C1	C2	C3	C4
Number of hits	44,023	3,652	3,065	3,299	2,863	4,292
Percentage remaining	100%	8.3%	7.0%	7.5%	6.5%	9.7%

AE data of interest is related to plastic changes in the monitored material, which in concrete can be stated as the formation of micro-cracks. The relevancy of retained data to micro-cracking can be considered as a measure to assess the applicability of different filtering approaches. Following the hypothesis that micro-cracks are expected to expand and form visible cracks at higher loads, AE events that are in agreement with visible cracking, which forms after the micro-cracking events have been detected, are potentially related to genuine data. In other words, an assumption is made that the number of events located where visible cracks later form is related to the applicability of the filtering

approach. AE events are defined as local change in the material giving rise of AE activity that will cause multiple hits on different sensors, per ASTM E1316.[8]

Figure 3.16 shows source location results of AE events detected during the last load step of cycle 9 as well as the visually detected cracks later observed at the highest load of cycle 11. AE events remaining after filtering with either the D-A/R-A filters or one of the wavelet based filters (C2) plotted close to the cracks that visually appeared afterwards; which suggests the correspondence of these events to micro-cracks. It is noted that more AE events were detected for the C2 filtered data (Figure 3.16c, 65 events) than that for the D-A/R-A filtered data (Figure 3.16b, 26 events) despite the lower number of hits (Table 3.8). This indicates higher agreement between signals in the C2 filtered data set; as an event is only plotted if it is detected by four signals from four different sensors. The lower number of events associated with a higher number of hits, as observed for the D-A/R-A filtered data, can indicate loss of key information.

Wavelet based filter C2 achieved high data reduction and good source location results, as did the D-A/R-A filters. However, the wavelet based filter C2 indicated a higher quality of data retained. In addition, the limits for the D-A/R-A filters were developed subjectively based on the AE expert analyzing the data. On the other hand, the limits for the wavelet based criteria C2 developed from PLB testing achieved good results when used on data collected during load testing of similar specimen and sensor layout. This suggests potential for further development of this approach as an objective filtering tool. Further investigation is recommended to verify the limits of the proposed criteria and to examine its effectiveness on different specimens in both laboratory and field settings.

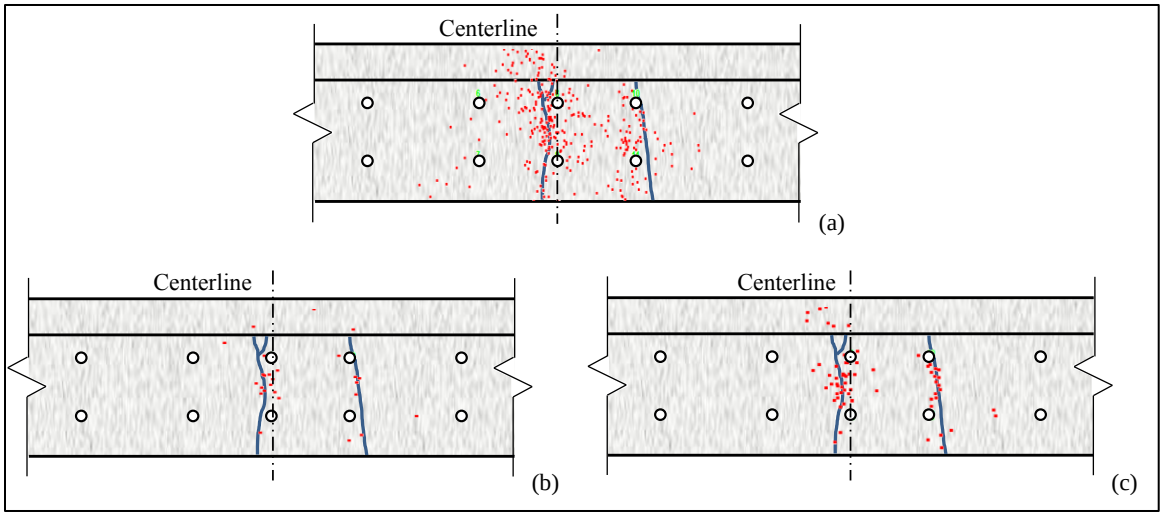

Figure 3.16 Source location results of AE data collected during last load step of cycle 9, superimposed on visually detected cracks. (a) Unfiltered data, (b) filtered data using D-A/R-A filters, and (c) filtered data using normalized average distance (C2) filter.

In field applications, there is less control over possible sources of noise including wind with debris, rain, and hail. The wavelet based filtering approach described in this study appears to hold potential for field applications as it is suited for real-time filtering, thereby enhancing the efficiency of data storage and transfer, and potentially increasing the reliability of AE analysis. This is particularly true for the case of low level acoustic emission (acoustic emission monitoring of slow degradation mechanisms that produce few acoustic emission signals over long period of time) analysis.[52] In this type of analysis, effective data reduction is crucial for detecting damage due to material degradation such as corrosion of steel in concrete or alkali-silica reaction damage at early stages.[10, 53-55]

3.8 CONCLUSIONS

A wavelet based approach for data reduction was developed and assessed for the case of controlled AE data that was generated by an artificial source. A realistically scaled and fabricated prestressed concrete beam served as a test specimen. The objective of the investigation was to assess the relative merits of the wavelet based approach when

compared to more commonly used D-A/R-A filtering approaches for differentiation between induced target signals and degraded signals (noise). Conclusions can be summarized as:

1. Target signals from the artificial source (pencil lead breaks) have different characteristics in terms of high energy distribution in the time-frequency domain as compared to degraded signals (mainly reflections in this study).
2. Data filters based on the wavelet transform were used to distinguish between induced target signals generated by PLBs and degraded signals.
3. When applied to AE data due to PLBs, the developed wavelet based filters provided higher data reduction than the commonly used D-A/R-A filtering approach. The wavelet based approaches eliminated a significantly higher percentage of degraded signals and maintained a higher percentage of the signals in interest.
4. The applicability of one of the proposed filtering criteria was verified for AE data due to concrete cracking during load testing in a laboratory setting. The filters showed significant data reduction without affecting the key information related to material response.
5. The use of the same filtering limits for the case of artificial source data and load testing data shows the potential of this approach to develop objective filters that can be used be less experienced users.

The work described has been intentionally limited to the case of AE sources in a laboratory setting. The proposed filtering approach should be investigated for filtering other sources of noise, including external sources in field environments such as rain and

hail. Further research is needed to verify the applicability of the proposed approach to low level acoustic emission associated with concrete material degradation, such as corrosion and alkali-silica reaction.

3.9 ACKNOWLEDGEMENTS

This material is based upon work supported by the U.S. Department of Energy Office of Science, Office of Basic Energy Sciences and Office of Biological and Environmental Research under Award Number DE-SC-00012530.

3.10 REFERENCES

1. Tabatabai H, Mehrabi AB and Yen W P. Bridge stay cable condition assessment using vibration measurement techniques. *SPIE 3400, Structural Materials Technology III: An NDT Conference*, San Antonio, TX, March 31 1998, pp.194–204.
2. Chang PC and Liu SC. Recent research in nondestructive evaluation of civil infrastructures. *ASCE J Mater Civ Eng* 2003 Jun;15(3):298-304.
3. Ghorbanpoor A, Borchelt R, Edwards M, et al. *Magnetic-Based NDE of prestressed and post-tensioned concrete members—The MFL system*. Final Rep. No. FHWA-RD-00-026, 2000. Federal Highway Administration, Washington, DC.
4. Sansalone M and Street W. Use of the impact-echo method and field instrument for non-destructive testing of concrete structures. *International Symposium ND-Testing in Civil Engineering*, Berlin, 1995 , Vol. 1, pp. 494–502.
5. Komlos K, Popovics S, Nürnbergerová T, et al. Ultrasonic pulse velocity test of concrete properties as specified in various standards. *Cement Concrete Comp* 1996; 18(5): 357-364.

6. Ziehl P. Applications of Acoustic Emission Evaluation for Civil Infrastructure. *SPIE Smart Structures and Materials and Nondestructive Evaluation and Health Monitoring*, San Diego, CA, 9-13 March 2008, pp. 9.
7. Ono K. Application of acoustic emission for structure diagnosis. *Diagnostyka* 2011: 3-18.
8. ASTM E1316: 2016. Standard Terminology for Nondestructive Examinations, American Standard for Testing and Materials, pp. 1-38.
9. Golaski L, Gebski P and Ono K. Diagnostics of reinforced concrete by acoustic emission. *J Acoust Emiss* 2002; 20: 83-98.
10. Mangual J, ElBatanouny M, Ziehl, P, et al. Acoustic-emission-based characterization of corrosion damage in cracked concrete with prestressing strand. *ACI Mater J* 2013; 110(1): 89-98.
11. ElBatanouny M, Ziehl P, Larosche A, et al. Acoustic emission monitoring for assessment of prestressed concrete beams. *Constr Build Mater* 2014; 58: 46–53.
12. Nair A and Cai CS. Acoustic emission monitoring of bridges: Review and case studies. *Eng Struct* 2010; 32 (6): 1704-1714.
13. Ohtsu M, Uchida M, Okamoto T, et al. Damage assessment of reinforced concrete beams qualified by acoustic emission. *ACI Struct J* 2002; 99 (4): 411–417.
14. Larosche A, Ziehl P, Mangual J, et al. Damage evaluation of prestressed piles to cast in place bent cap connections with acoustic emission. *Eng Struct* 2015; 84: 184–194.
15. Lovejoy S. Acoustic Emission Testing of Beams to Simulate SHM of Vintage Reinforced Concrete Deck Girder Highway Bridges. *Structural Health Monitoring* 2008, Vol. 7, 327-346.

16. Colombo S, Main IG and Forde MC. Assessing damage of reinforced concrete beam using "b-value" analysis of acoustic emission signals. *ASCE J Mater Civ Eng* 2003; 15(3): 280-286.
17. ElBatanouny M, Larosche A, Mazzoleni P, et al. Identification of cracking mechanisms in scaled frp reinforced concrete beams using acoustic emission. *Exp Mech* 2014; 54 (1): 69-82.
18. Aggelis, DG, Shiotani T, Momoki S, et al. Acoustic emission and ultrasound for damage characterization of concrete elements. *ACI Mater J* 2009, 106 (6), 509–514.
19. Calabrese L, Campanella G and Proverbio E. Identification of corrosion mechanisms by univariate and multivariate statistical analysis during long term acoustic emission monitoring on a pre-stressed concrete beam. *Corros Sci* 2013; 73: 161-171.
20. Gutkin R, Green CJ, Vangrattanachai S, et al. On acoustic emission for failure investigation in CFRP: Pattern recognition and peak frequency analyses. *Mechanical Systems and Signal Processing* 2011 May 31;25(4):1393-407
21. Ohno K and Ohtsu M. Crack classification in concrete based on acoustic emission. *Constr Build Mater* 2010; 24(12): 2339-2346.
22. Yu J, Ziehl P, Matta F, et al. Acoustic emission detection of fatigue damage in cruciform welded joints. *J Constr Steel Res* 2013; 86: 85-91.
23. Fowler T, Blessing J, Conlisk P, et al. The MONPAC system. *J Acoust Emiss* 1989; (3): 1-8.
24. Tinkey BV, Fowler TJ and Klingner RE. Nondestructive testing of prestressed bridge girders with distributed damage. Research Report 1857-2, 2002: 106.

25. Abdelrahman M, ElBatanouny M and Ziehl P. Acoustic emission based damage assessment method for prestressed concrete structures: modified index of damage. *Eng Struct* 2014; 60: 258–264.
26. Sagasta FA, Torné JL, Sánchez A, et al. Discrimination of acoustic emission signals for damage assessment in a reinforced concrete slab subjected to seismic simulations. *Archives of Acoustics* 2013 Sep 1; 38(3):303-10.
27. Sagasta FA, Benavent-Climent A, Fernández-Quirante T, et al. Modified Gutenberg–Richter Coefficient for Damage Evaluation in Reinforced Concrete Structures Subjected to Seismic Simulations on a Shaking Table. *Journal of Nondestructive Evaluation* 2014 Dec 1;33(4):616-31
28. Anastasopoulos AA, Tsimogiannis AN, Kouroussis DA. Pressure Vessel Evaluation with Pattern Recognition Acoustic Emission Data Analysis. *Proc. EWGAE* 2002, Vol. I, pp. 29.
29. ASTM E976: 2010. Standard Guide for Determining the Reproducibility of Acoustic Emission Sensor Response, American Standard for Testing and Materials, pp. 1-7.
30. Rioul O and Vetterli M. Wavelets and signal processing. *IEEE Signal Proc Mag*, 8 LCAV-article-1991-005, p. 14-38.
31. Grossman A and Morlet J. Decomposiion of hardy functions into square integrable wavelets of constant shape. *SIAM J Math Anal* 1984; 15: 723-736.
32. Meyer Y. Ondelettes et functions splines. *Seminaire Equations aux Derivees Partielles, École Polytechnique*, Paris, 1986.
33. Mallat SG. Multifrequency channel decompositions of images and wavelet models. *Acoustics, Speech and Signal Processing, IEEE Trans* 1989; 37(12): 2091-2110.

34. Mallat SG. Multiresolution approximations and wavelet orthonormal bases of $L^2(R)$. *T Am Math Soc* 1989; 315(1): 69-87.

35. Daubechies, I. Orthonormal bases of compactly supported wavelets. *Commun Pur Appl Math* 1988; 41(7): 909-996.

36. Daubechies, I. Ten lectures on wavelets. *Philadelphia: Society for industrial and applied mathematics* 1992; 61: 198-202.

37. Daubechies I, Landau HJ and Landau Z. Gabor time-frequency lattices and the Wexler-Raz identity. *J Fourier Anal Appl* 1994; 1(4): 437-478.

38. Yoon DJ, Weiss WJ, Shah SP. Assessing damage in corroded reinforced concrete using acoustic emission. *Journal of engineering mechanics* 2000 Mar; 126(3):273-83.

39. Marec A, Thomas JH, El Guerjouma R. Damage characterization of polymer-based composite materials: Multivariable analysis and wavelet transform for clustering acoustic emission data. *Mechanical Systems and Signal Processing* 2008 Aug 31;22(6):1441-64.

40. Hamdi SE, Le Duff A, Simon L, et al. Acoustic emission pattern recognition approach based on Hilbert–Huang transform for structural health monitoring in polymer-composite materials. *Appl Acoust* 2013; 74(5): 746-757.

41. Ni QQ, Iwamoto M. Wavelet transform of acoustic emission signals in failure of model composites. *Eng Fract Mech* 2004; 69, pp. 717–728.

42. Loutas TH, Kostopoulos V, Ramirez-Jimenez C, et al. Damage evolution in center-holed glass/polyester composites under quasi-static loading using time/frequency analysis of acoustic emission monitored waveforms. *Composites science and technology* 2006 Aug 31; 66(10):1366-75.

43. Arumugam V, Kumar CS, Santulli C, et al. Identification of failure modes in composites from clustered acoustic emission data using pattern recognition and wavelet transformation. *Arabian Journal for Science and Engineering* 2013 May 1;38(5):1087-102.
44. Gallego A, Gil JF, Castro E, et al. Identification of coating damage processes in corroded galvanized steel by acoustic emission wavelet analysis. *Surface and Coatings Technology* 2007 Jan 15; 201(8):4743-56.
45. Kharrat M, Ramasso E, Placet V, et al. Acoustic Emission in Composite Materials under Fatigue Tests: Effect of Signal-Denoising Input Parameters on the Hits Detection and Data Clustering. *In31st Conference of the European Working Group on Acoustic Emission (EWGAE)* 2014 Sep 3.
46. Grosse CU, Finck F, Kurz JH, et al. Improvements of AE technique using wavelet algorithms, coherence functions and automatic data analysis. *Constr Build Mater* 2004 Apr 30;18(3):203-13.
47. Zitto ME, Piotrkowski R, Gallego A, et al. Damage assessed by Wavelet scale bands and b-value in dynamical tests of a reinforced concrete slab monitored with acoustic emission. *Mechanical Systems and Signal Processing* 2015 Aug 31;60:75-89.
48. Zitto ME, Piotrkowski R, Gallego A, et al. AE wavelet processing in dynamical tests of a reinforced concrete slab. *J. Acoust. Emiss* 2012 Jan 1; 30:64-75.
49. Ohtsu M. The history and development of acoustic emission in concrete engineering. *Magazine of concrete research* 1996, 48 (177):321-330.
50. Ohno K and Ohtsu M. Crack classification in concrete based on acoustic emission. *Constr Build Mater* 2010; 24(12), 2339-2346.

51. Sause MG. Investigation of pencil-lead breaks as acoustic emission sources. *J Acoust Emiss* 2011 Jan 1; 29:184-96.

52. Ziehl P and ElBatanouny M. Low-Level Acoustic Emission (AE) in the Long Term Monitoring of Concrete. In: Ohtsu M (ed) *Acoustic Emission and Related Non-destructive Evaluation Techniques in the Fracture Mechanics of Concrete: Fundamentals and Applications*, Woodhead Publishing, 2015, pp. 217- 236.

53. Abdelrahman M, ElBatanouny M, Serrato M, et al. Classification of Alkali-Silica Reaction and Corrosion Distress Using Acoustic Emission. *In 42nd Annual Review of Progress in Quantitative Nondestructive Evaluation: Incorporating the 6th European-American Workshop on Reliability of NDE* 2016, Vol. 1706, p. 140001. AIP Publishing.

54. Abdelrahman M, ElBatanouny M, Ziehl, P, et al. Classification of Alkali-Silica Reaction Damage Using Acoustic Emission: A Proof-of-Concept Study. *Constr Build Mater* 2015, V. 95, pp. 406-413.

55. ElBatanouny M, Mangual J, Ziehl P, et al. Early Corrosion Detection in Prestressed Concrete Girders Using Acoustic Emission. *ASCE J Mater Civ Eng* 2014; 26(3), pp. 504–511.

CHAPTER 4

CLASSIFICATION OF ALKALI-SILICA REACTION DAMAGE USING ACOUSTIC EMISSION: A PROOF-OF-CONCEPT STUDY[2]

[2]Abdelrahman, M., M. ElBatanouny, P. Ziehl, J. Fasl, C. Larosche, and J. Fraczek. 2015. *Construction and Building Materials.* V. 95: 406-413.
Reprinted here with permission of publisher (Appendix C).

4.1 ABSTRACT

Alkali-silica reaction (ASR) is a concrete degradation mechanism that generates internal cracks in concrete material as a result of volumetric expansion. This mechanism is currently affecting many structures throughout the United States, especially in Texas and the Pacific Northwest. In this study, an accelerated ASR test was implemented at the University of South Carolina Structures and Materials Laboratory on twelve specimens with dimensions of 3 x 3 x 11.25 in. (76 x 76 x 286 mm). The specimens were cast using reactive aggregate and mortar with a high alkali content and placed in a controlled environment with high humidity and temperature to accelerate the reaction, while being continuously monitored with acoustic emission. Length change measurements and petrographic examination were conducted periodically to serve as benchmarks for ASR damage detection. Micro-cracking associated with ASR damage was detected by AE and the rate of AE activity was correlated to the rate of ASR damage. An AE based Intensity Analysis chart that enables ASR damage classification in correlation with petrographic analysis was developed.

4.2 INTRODUCTION

Concrete degradation is one of the crucial issues that face infrastructure owners and the civil engineering community. The heterogeneous nature and low tensile strength of concrete make it susceptible to cracking induced by service loads in addition to material degradation through various mechanisms including corrosion of reinforcement, sulfate attack, alkali-aggregate reaction (AAR), freeze-thaw cycling, leaching, radiation, elevated temperatures, salt crystallization, and microbiological attack [1]. Degradation of concrete often affects the safety and serviceability of structures which leads to economic losses and,

in some cases, catastrophic failures and fatalities. This has raised the need for advanced monitoring techniques to determine the current structural state of the concrete members and to assist in the evaluation of repairs.

This study focuses on alkali-silica reaction (ASR) degradation, which is currently affecting many structures across the United States [2]. This degradation mechanism has gained more attention since the presence of ASR induced cracks in the Seabrook Nuclear Power Plant [3]. Figure 4.1 shows a map of states with ASR degradation and a photograph of ASR cracks in a highway bridge. ASR degradation is affected by material selection of the concrete matrix and initiates when certain types of reactive siliceous aggregates are combined with cement paste having high alkali content. The ASR mechanism requires as little as 80-percent relative humidity to occur and only permits a few mitigation techniques once the structure is in-service [4]. The reaction product is a gelatinous material that swells when moisture is absorbed and can cause expansion and cracking [5]. Figure 4.2 shows a schematic of the mechanism of ASR damage in concrete.

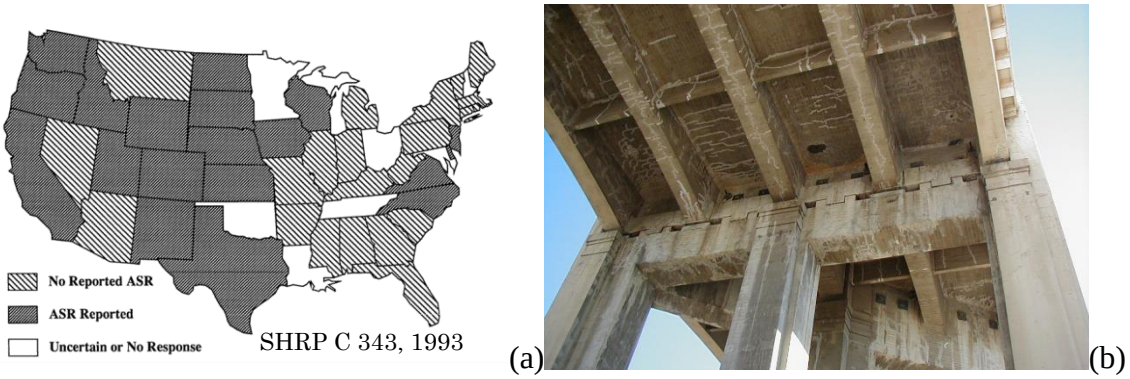

Figure 4.1 (a) Map of states with ASR degradation [2], and (b) example of ASR induced cracks.

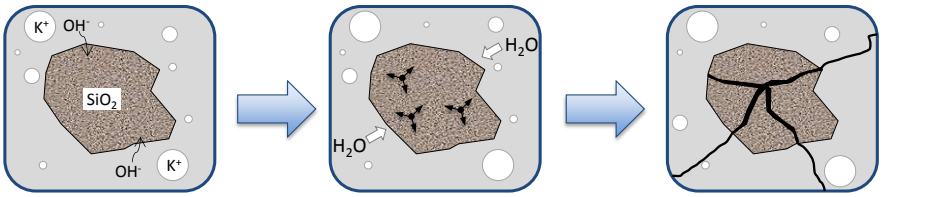

Figure 4.2 Mechanism of ASR damage in concrete [www.journal.hep.com.cn].

Currently ASR damage in field structures is evaluated through length change measurements, visual inspection of cracks, and/or concrete coring with subsequent petrographic examination [6]. Length change measurements can be inconsistent given the high precision required (in the micro-range) and their susceptibility to temperature changes. On the other hand, visual inspection is subjective and only detects damage after visual signs are apparent while the petrographic examination is a local, qualitative, and destructive method which may not be allowed in some structures, such as nuclear power plants. In addition, all the above methods, with exception to length change, are used for periodic inspection and are not suitable for continuous monitoring. Therefore, there is a need for a nondestructive evaluation/structural health monitoring (NDE/SHM) method to enable detection and monitoring of ASR degradation.

Acoustic emission (AE) is a promising method for health monitoring of concrete structures which gained more attention in the last decade. AE is defined as transient stress waves produced by a sudden release of energy, such as crack formation or growth [7, 8]. The high sensitivity of the sensors, in the kHz range, enables it to detect cracks long before they are visible [9, 10]. This research effort is motivated by recent studies that show the ability of the method to detect other concrete degradation mechanisms, particular corrosion and cracking in reinforced and prestressed concrete specimens [11-17]. It is noted that a

previous study investigated the use of AE to detect ASR damage in cylindrical specimens [18]. The results of this study showed that AE can detect early cracking associated with ASR; however, the rate of AE activity plateaued at the end of the test.

The study described herein examines the ability of AE to detect and classify ASR degradation. To achieve meaningful data within a reasonable period of time (one year), the laboratory test was intentionally accelerated in general conformance with ASTM C1293 [19]. The test environment was carefully controlled to minimize variability and to maintain conformance with ASTM C1293. The specimens were continuously monitored using AE and two benchmark measurements for ASR degradation were used: discrete length change measurements to measure longitudinal expansion and petrographic examination (resulting in a damage rating index). The results of this study demonstrate the ability of AE to detect and assess the rate of ASR induced degradation in concrete structures.

4.3 RESEARCH SIGNIFICANCE

ASR degradation is currently affecting many structures in the United States including highway bridges and nuclear power plants (Figure 4.1). The excessive cracking associated with this degradation mechanism results in serviceability concerns which require repair or complete replacement of the affected structure. This study demonstrates the ability of AE, as a non-invasive SHM method, to detect and assess the extent of ASR damage. An algorithm for ASR damage classification was also developed, which can help infrastructure owners evaluate the current condition of the structure and assess the effectiveness of repairs.

4.4 EXPERIMENTAL PROGRAM

4.4.1 Tests specimens

An accelerated ASR test was designed to degrade the specimens in a reasonable time. The test program included twelve conditioned specimens and three control specimens (cast using nonreactive aggregate during an earlier study), all having dimensions 3 x 3 x 11.25 inches (76 x 76 x 286 mm) similar to ASTM C1293 [19]. An alkalinity concentration of 5% $Na_2O_{(Eq)}$ was used in the concrete mix of the ASR specimens, as opposed to the specified concentration of 1.25% in ASTM C1293. A highly reactive aggregate (Knife River) from Cheyenne, Wyoming was used in the ASR specimens. Table 4.1 and Table 4.2 show the ASTM C1293 specifications and the concrete mix design used to cast the ASR specimens with a water/cement ratio of 0.48. The conditioned specimens were cast using two identical batches (six specimens per batch). The control specimens were cast with ordinary Portland cement and innocuous aggregates.

All specimens were placed in a controlled environment with 100 ± 2˚F temperature and 100% relative humidity. An insulated chamber was constructed to control the temperature while sealed polypropylene containers, conforming to the specifications identified in section 5.2.2 of ASTM C1293, were used to achieve 100% relative humidity. Four containers were used with three specimens in each container (Figure 4.3).

The duration of the test was one year. At ages of 14, 28, and 56 days, three specimens were removed for petrographic examination. The specimens are named in 'XY-Z' format. 'X' specifies the type of specimen; S for ASR specimens and C for control specimen. 'Y' denotes the number of the specimen; specimens from batch one are numbered 1 through 6, while specimens from batch two are numbered 7 through 12. 'Z'

denotes the duration of conditioning in days. For example, S2-28 is an ASR specimen from batch one with 28 days of conditioning.

Table 4.1 ASTM C1293 Specifications

w/c ratio*=	0.45
Cement content=	26.22 lb/ft3
Volume of coarse aggregate per unit volume of concrete=	0.70
Alkali content**=	5.0% Na2Oeq

***Based upon aggregate saturated surface dry conditions**
**** Modified from ASTM C1293 (1.25% Na_2O_{eq})**

Table 4.2 Mix design

Constituent	Weight (lbs/cy)
Cement	700
Water	340
Coarse Aggregate	1830
Fine Aggregate	1100
NaOH Admixture	40
Total	4010

Figure 4.3 Test setup. Controlled temperature chamber (left) and specimens placed in 100% relative humidity buckets (right).

4.4.2 Length Change measurements

Length change measurements were taken at discrete intervals to quantify the degree of expansion. During the first two months of the test, the measurements were taken at 5, 10, 14, 28, and 56 days of exposure. Additional readings were taken for the three specimens that continued the test for a period of one year. Length change measurements were compared to an initial reading at an age of 3 days (after conditioning). This was done to minimize the change in length due to thermal effects. Measurements were taken using a length comparator apparatus as specified in ASTM C157 [20]. However, the use of AE monitoring prohibited taking the measurements in strict conformance with Section 10.2.2 of ASTM C1293 [19]. In particular, the specimens were not placed in a moist cabinet for 16 hours in order to minimize the time of length change measurements, as AE data cannot be collected during this process. Rather, length change measurements were taken immediately after removing the specimens from the controlled environment and the specimens were kept moist with wet burlap after the reading was taken. Figure 4.4(a) shows a photograph of a specimen in the length comparator apparatus.


(a)


(b)

Figure 4.4 (a) Comparator length change measurements, and (b) photograph of specimens with AE sensors installed.

4.4.3 Petrographic examination

Petrographic examination is a destructive testing method that can assess damage in concrete by visual inspection of concrete slices, usually extracted from concrete cores, under a microscope [21]. Petrographic examination was conducted at the Wiss, Janney, Elstner Associates, Inc., Austin office (WJE-Austin) using the Damage Rating Index (DRI) procedure. This method is used in Europe and Canada to semi-quantitatively define distress in concrete due to ASR. The Federal Highway Administration (FHWA) references this procedure in their published manual on concrete petrography [6]. DRI is estimated by measuring certain features and multiplying each of them by a correspondent weighting factor. There are many versions of the DRI method, differing mainly in the assignment of weighting factors. WJE has modified the method to include deterioration in the fine aggregate in the rating index. The modified distress features and the corresponding weighting factors, adopted from FHWA, are shown in Table 4.3.

Table 4.3 ASR Damage Rating Index (DRI) Features and Weighting Factors

Distress Feature	Weighting Factor
Cracks in either coarse or fine aggregate (CAgg)	0.25
Cracks and gel in coarse or fine aggregate (C+GAgg)	2.0
Aggregate debonded (DAgg)	3.0
Reaction rims around aggregate (RR)	0.5
Cracks in cement paste (CCP)	2.0
Cracks and gel in cement paste (C+GCP)	4.0
Air voids with gel (GAV)	0.5

The samples were prepared as for a typical petrographic examination, including curing and lapping. After the samples are lapped, the following two steps were taken:

- A 0.156 in^2 (1-cm square) transparency grid was overlaid on the lapped concrete surface. The transparency was trimmed to the size of the sample and securely taped to the concrete so that it will not move during examination.
- The stereomicroscope was set to a magnification of 16X and a ring light was used to achieve uniform lighting. The magnification was adjusted as necessary to better assess the distress; however, all DRI measurements were done at 16X for consistency.

The DRI was then calculated by moving across the sample and tallying each occurrence of each feature in each 0.156 in^2 (1-cm square) and multiplying the tally for each feature with its weighting factor. A final DRI value is then obtained by averaging the results of all the 0.156 in^2 (1-cm square) examined and multiplying by 100.

4.4.4 Acoustic emission

AE is defined as transient stress waves emitted from sudden release of energy, such as crack initiation or growth [8]. Each AE signal is called a 'hit' and is associated with a waveform that can be used to calculate different parameters such as amplitude, duration, rise time, absolute energy, and signal strength, along with different frequency parameters. Two types of sensors were used to monitor AE activity in the specimens. One 55 kHz resonant AE sensor having 40 dB integral pre-amplification (R6I) was used on each specimen and placed at the mid-length of the specimen. Four of the specimens were also instrumented with a broadband AE sensor (WDI). This study only focuses on the data

collected from the resonant sensors. Data collection threshold was set for amplitude of 40 dB.

A two part epoxy was used to attach the sensors to the surface of each specimen as shown in Figure 4.4(b). Due to the high temperature and humidity, the coupling between the sensors and some of the specimens was weakened. Therefore, after two weeks of exposure, a two part epoxy manufactured specifically for these conditions was used to re-attach the sensors. AE data was recorded continuously during the test except for the short pauses when length change measurements were taken.

4.5 RESULTS

4.5.1 AE Data Filters

Development of robust data filters is an essential step for AE data analysis to ensure minimizing of non-relevant data. A pre-test was conducted to check for 'noise' by placing AE sensors on control specimens in the environmental chamber. This test showed a minimal presence of mechanical and electrical noise. This test was also used to determine front end filters of hit definition time (HDT: enables determination of the end of the hit and closes out the measurement processes), and hit lockout time (HLT: inhibits the measurement of signals after the hit is stored to avoid measuring reflections) of 200 and 800 microseconds, respectively. However, elimination of false data using only front end filters is not possible; therefore, post-processing filters are also needed.

For the ASR test, the main source of noise in the AE data is from wave reflections, which is the primary concern in small scale specimens where the AE waves reflect from the specimen's boundaries and do not attenuate within their small travel distance.

Therefore, an extensive filtering plan was adopted using different parameter based data filters.

The first filter used is a duration-amplitude filter (D-A), also known as a Swansong II filter [9, 15, 22-25]. This filter is based on the fact that genuine AE hits with long durations are associated with high amplitudes and vice versa. The limits of the filter were determined through visual inspection of AE waveforms. The second filter is a rise time-amplitude (R-A) filter and it follows the same logic as the D-A filter. The data limits for D-A and R-A filters are shown in Table 4.4.

The third filter rejects data with a signal strength that exceeds 10,000,000 pVs (pico-volts second). Filter four is based on the relation between counts and amplitude, and it rejects data with low counts (less than 2) and amplitude exceeding 50 dB. The last two filters are frequency based and depend upon the operational frequency range of the sensor and the characteristics of acoustic emission in concrete. The first frequency based filter rejects data with average frequency not between 10 and 200 kHz while the second frequency filter rejects data with peak frequency less than 20 kHz. The limits of all described filters were based on in-depth inspection of AE waveforms.

Figure 4.5 shows the filtered data for a control specimen (C1-365) and ASR specimen (S10-365), both were placed in the controlled environment for one year. As seen in the figure, minimal activity was measured in the control specimen as compared to the ASR specimen. The total number of hits detected in the control specimen is 117 hits while 14,295 hits were detected in the ASR specimen. This indicates that the developed filters are effective and can eliminate the majority of noise collected during the test. In addition, the majority of the hits collected from the control specimen took place at the beginning of

their exposure (14 days after exposing the ASR specimens) and, therefore, can be attributed to the high relative humidity and temperature in the controlled environment which may lead to minor cracking in the concrete. A photograph of both specimens is shown in Figure 4.6.

Table 4.4 Data rejection limits for D-A and R-A filters

D-A filter				R-A filter	
Rejection limits		Rejection limits		Rejection limits	
Amp (dB)	Duration (µs)	Amp (dB)	Duration (µs)	Amp (dB)	Rise time (µs)
40-44	400	66-70	1,500	40-50	100
45-48	500	71-75	2,500	51-60	200
49-52	600	76-80	3,500	61-70	300
53-56	700	81-95	5,000	71-100	400
57-60	800	96-100	10,000	-----	-----
61-65	1,000	-----	-----	-----	-----

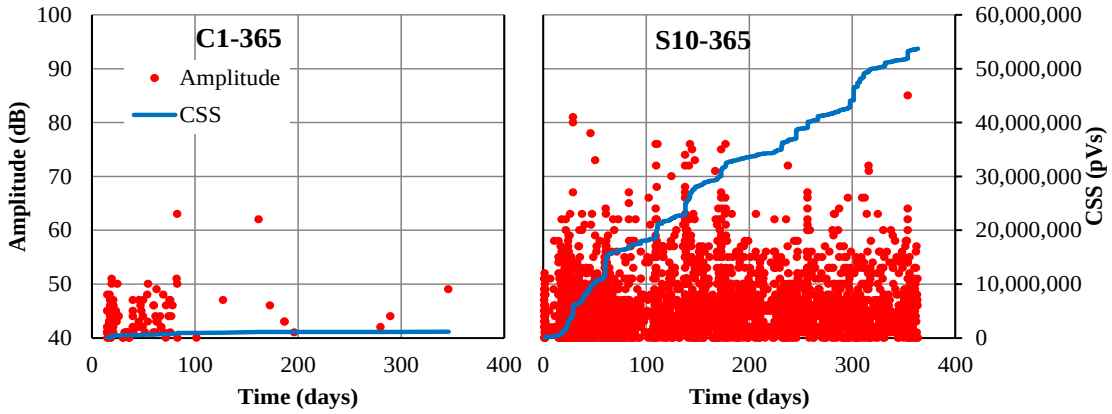

Figure 4.5 AE activity from control (C1-365) and ASR specimen (S10-365), CSS refers to cumulative signal strength of AE hits.

Figure 4.6 Photograph of control specimen (C1-365, left) and ASR specimen (S10-365, right) after 365 days of exposure.

4.5.2 AE versus Length Change measurements

The results of AE cumulative signal strength (CSS) and length change measurements for all the conditioned specimens are shown in Figure 4.7. As seen in the figure, AE activity increases with the increase of the duration of exposure which shows the ability of the method to assess the rate of ASR damage. In addition, CSS continued to increase for the specimens that were conditioned for one year which proves that the sensors can detect generation of micro-cracks with progression of ASR damage, regardless of the attenuation caused by such cracks.

Figure 4.7 also shows that length change measurements increase with the increase of duration of exposure, which agrees with the results of AE activity. The maximum length change was measured in specimen S10-365 with a value 0.044%. The ASTM C1293 prescribes a 0.04% expansion after one year of testing as the threshold for identifying an aggregate as potentially susceptible to deleterious ASR expansion. Therefore, this measurement indicates that the aggregates used in the study are reactive which agrees with: a) the known reactivity of the type of aggregates used, and b) the petrographic analysis results which showed ASR damage as presented in the next section.

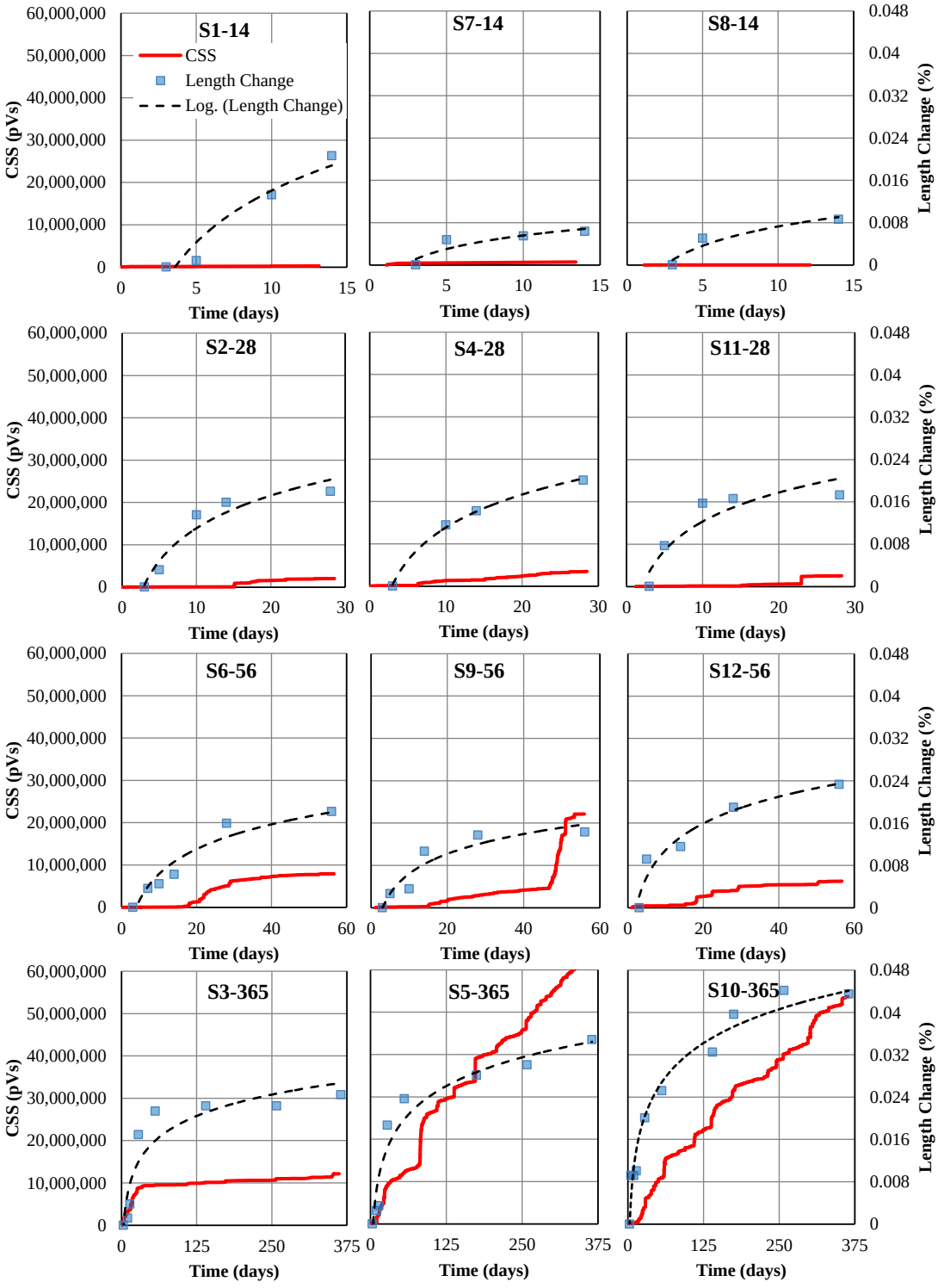

Figure 4.7 AE and length change measurement versus time for all the specimens (S5-365 CSS=6.48e7 pVs).

The correlation coefficient of the results shown in Figure 4.7, length change measurements and CSS, was calculated as 0.81; which indicates a linear correlation between the two variables. This result shows that AE activity can be used to determine the rate of expansion associated with ASR damage and, therefore, may offer a useful tool for the detection and eventual quantification of this degradation mechanism.

4.5.3 Petrographic examination

The results of petrographic examination of six specimens (conducted after 14, 28, and 56 days; two specimens at each) are shown in Figure 4.8. The least DRI value was obtained from a specimen conditioned for 14 days while the highest value was obtained from a specimen condition for 56 days. It can also be seen that the average DRI value, for each exposure duration, increases with the increase in duration. For the tested specimens, the main ASR damage features were cracking of the cement paste, cracks with gel in the cement paste, formation of gel in air voids, and cracking of the aggregates.

Table 4.5 shows length change results and DRI results for six specimens. It can be seen that some variability exists between the results of both methods for different specimens. This can be attributed to the qualitative nature of the DRI measurements and the high precision needed to measure the length change (differences in the comparator tool measurements are in terms of micrometers).

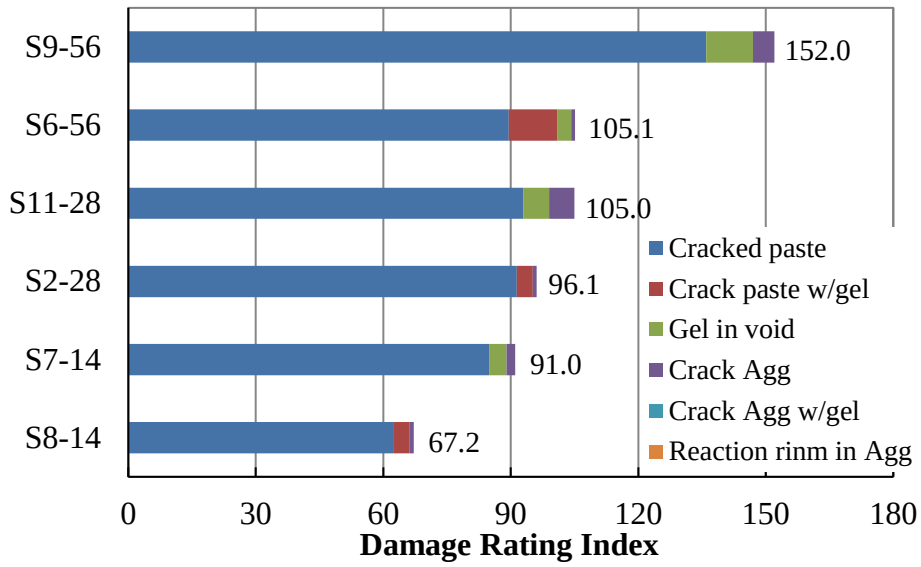

Figure 4.8 DRI measurements for six specimens.

Table 4.5 Length change, DRI and AE results

Specimen	Duration (days)	Length change* (%)	DRI	Historic index	Severity (pVs)
S7-14	14	0.006	91.0	1.5142	1.38E+04
S8-14		0.009	67.2	1	1.40E+03**
S2-28	28	0.018	96.1	1.7075	2.68E+04
S11-28		0.017	105.0	2.9828	4.89E+04
S6-56	56	0.018	105.1	2.1676	9.13E+04
S9-56		0.014	152.0	3.2464	2.15E+05

***Measured at the end of the exposure duration.**
****Average of signal strength from available hits as number of hits was less than 50.**

4.5.4 ASR damage quantification using AE

AE Intensity Analysis (IA) was used to classify ASR damage. This approach was developed by Fowler et al. 1989 [23] to assess damage in fiber reinforced polymer vessels. The technique is listed in an ASTM standard for detection of damage in Fiberglass Reinforced Plastic Resin (FRP) Tanks/Vessels [26]. IA has been used to detect damage in

prestressed concrete structures during load tests [9, 27] and recently to classify corrosion damage in prestressing strands [14]. The method uses the signal strength to calculate two parameters: historic index and severity. Historic index, *H(t)*, is a form of trend analysis that estimates the change of slope of CSS with respect to time while severity, S_r, is the average signal strength of the largest 50 hits. Historic index and severity can be calculated using Equation 4.1 and Equation 4.2 where: N is number of hits up to time (t), S_{oi} is the signal strength of the i-th event, and K is an empirically derived factor that varies with the number of hits. In this study, the value of K was selected to be: a) N/A if $N \leq 50$, b) $K=N-30$ if $51 \leq N \leq 200$, c) $K=0.85N$ if $201 \leq N \leq 500$, and d) $K=N-75$ if $N \geq 501$ [28].

$$H(t) = \frac{N}{N-K} \frac{\sum_{i=K+1}^{N} S_{oi}}{\sum_{i=1}^{N} S_{oi}} \tag{4.1}$$

$$S_r = \frac{1}{50} \sum_{i=1}^{i=50} S_{oi} \tag{4.2}$$

IA chart is obtained by plotting the maximum severity and historic index acquired for each specimen during the test where the points plotted towards the top-right corner of the figure indicates more damage. Figure 4.9 shows the IA and DRI results for six specimens (only six specimens had DRI measurements). The specimen with the least DRI damage plotted in the bottom-left corner of the figure. As DRI measurements increase, IA data points trend towards the top-right corner of the figure indicating that more damage is occurring. Based on DRI results, the chart can be divided in three regions: A-No damage; B-Minor damage; and C-Moderate damage. No heavy damage was observed from available DRI results. It is noted that the specimens conditioned for 365 days are still in testing and have the highest IA results, except for S3-365. This indicates that more damage has occurred in these specimens, which is reasonable given their longer duration of exposure.

From Table 4.5, the correlation coefficient between the DRI measurements and historic index was calculated as 0.88 while the correlation coefficient between the DRI measurements and severity was found to be 0.95. These results show that DRI measurements have a stronger linear correlation with AE activity as compared to the length change measurements. It also validates the established relation between AE activity and DRI measurements as shown in Figure 4.9.

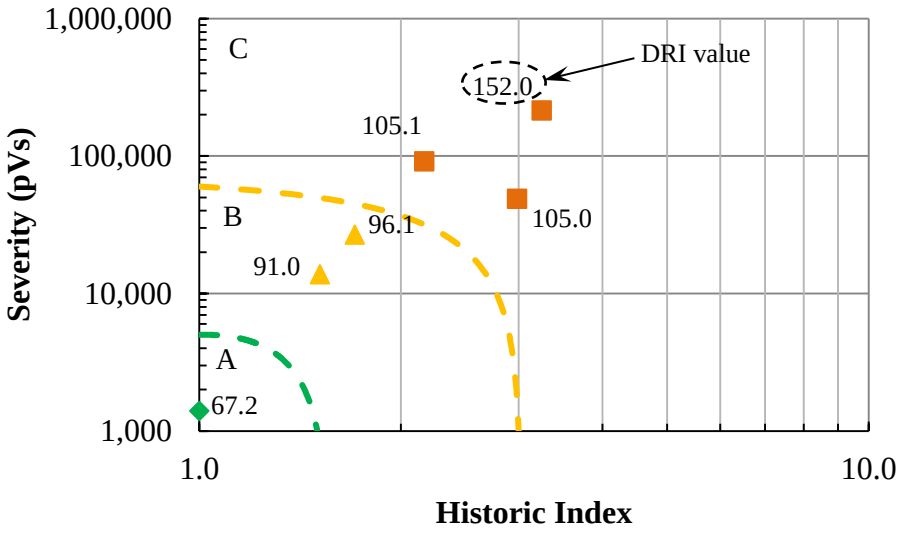

Figure 4.9 ASR classification chart, Intensity Analysis and DRI results.

4.6 SUMMARY AND CONCLUSIONS

This study reports the results of acoustic emission monitoring for detection of ASR degradation in laboratory concrete specimens. AE activity as a result of ASR damage is compared to two standard ASR diagnostic measurements: length change and petrographic examination. Unlike the used ASR benchmarks, AE is a truly non-invasive technique which eliminates or limits the need for taking core samples for petrographic examination, which may be prohibited in some structures such as nuclear power plants. In addition, the method is virtually immune to changes in environmental conditions such as relative

humidity and temperature while measurements of length change should be corrected for such variations to avoid errors. The availability of self-powered and wireless AE equipment gives this technique additional advantage especially for purposes of long-term assessment and monitoring of ASR damage. The findings of this study can be summarized as follows:

- Acoustic emission can detect ASR damage. Continual AE activity was recorded from the specimens conditioned for one year, which shows that formation of micro-cracks and ASR by-products do not inhibit collection of AE data.
- The rate of AE activity can be related to the rate of ASR degradation as shown by the linear correlation between AE measurements and the used ASR benchmarks. This can help evaluate the efficiency of ASR mitigation strategies by comparing the rate of AE activity before and after the repair for a prescribed duration.
- An acoustic emission Intensity Analysis chart for ASR damage classification was proposed by correlating AE results with petrographic examination (DRI measurements). This chart can be used for health monitoring to enable proper identification of the extent of ASR damage. More data is needed to validate the proposed limits and extend the chart to include heavy ASR damage.

It is noted that immediate applications of the proposed method include verification of reactivity of aggregate/concrete mixture in conjunction with ASTM C1293 and assessment of repair techniques by comparing AE activity of active ASR specimens before and after repair. Future studies should investigate implementation of this method in field conditions where dimensions of the structures are different than the laboratory specimens. Environmental conditions in the field (such as rain or windborne debris) may result in noise

in the AE data set; therefore, the limits of the proposed filters should also be tested. Previous experience of the authors indicates that proper filters could be developed for these conditions; however, this is beyond the scope of the current work.

Acoustic emission is a structural monitoring and assessment method, and therefore it is necessary to collect data over an extended period of time such as 20 days or more for ASR damage, depending on the application, to enable proper analysis of the data. This has recently become more feasible due to the commercial availability of self-powered and wireless acoustic emission monitoring systems.

4.7 ACKNOWLEDGMENTS

Special thanks are extended to the personnel of the University of South Carolina Structures and Materials Laboratory, in particular to Mr. Matthew Jones, and to Mr. Eddie Deaver of Holcim Cement for his valuable input.

4.8 REFERENCES

[1] Clifton, J. R. (1991). "Predicting the Remaining Service Life of Concrete," NISTIR 4712, U.S. Department of Commerce, National Institute of Standards and Technology, Gaithersburg, Maryland.

[2] Stark, D., Morgan, B., and Okamoto, P. (1993). "Eliminating or Minimizing Alkali-Silica Reactivity," Report No. SHRP-C-343.

[3] NRC IN 2011-20. (2011). "Concrete Degradation by Alkali-Silica Reaction," Nuclear Regulatory Commission (NRC), Washington, DC, November 18.

[4] Eskridge, A.E., Klahorst, J.T., Klingner, R.E., and Kreger, M.E. (2005) "Mitigation Techniques for In-Service Structures with Premature Concrete Deterioration: Synthesis Report", FHWA/TX-05/0-4069-3.

[5] Saouma, V.E., Perotti, L., and Shimpo, T. (2007). "Stress Analysis of Concrete Structures Subjected to Alkali-Aggregate Reactions," ACI Structural Journal, V. 104, No. 5, pp. 532-541.

[6] Fournier, B., Berube, M. A., Folliard, K. J., and Thomas, M. (2010). Report on the Diagnosis, Prognosis, and Mitigation of Alkali-Silica Reaction (ASR) in Transportation Structures (No. FHWA-HIF-09-001).

[7] Pollock, A.A. (1986). "Classical Wave Theory in Practical AE Testing," Progress in AE III, Proceedings of the 8th International AE Symposium, Japanese Society for Nondestructive Testing, pp. 708-721.

[8] ASTM E1316-13c. (2013). "Standard Terminology for Nondestructive Examinations," American Standard for Testing and Materials, pp.1-38.

[9] ElBatanouny, M.K., Ziehl, P., Larosche, A., Mangual, J., Matta, F., and Nanni, A. (2014). "Acoustic Emission Monitoring for Assessment of Prestressed Concrete Beams," Construction and Building Materials, V. 58, pp. 46–53.

[10] Ziehl, P., and Pollock, A. (2012). "Acoustic Emission," Chapter 1: Acoustic Emission for Civil Infrastructure, Intech (ISBN 979-953-307-372-8).

[11] Mangual, J., ElBatanouny, M.K., Ziehl, P., and Matta, F. (2013). "Acoustic-Emission-Based Characterization of Corrosion Damage in Cracked Concrete with Prestressing Strand," ACI Materials Journal, V. 110, No. 1, pp.89-98.

[12] Mangual, J., ElBatanouny, M.K., Ziehl, P., and Matta, F. (2013). "Corrosion Damage Quantification of Prestressing Strands Using Acoustic Emission," Journal of Materials in Civil Engineering, V. 25, No. 9, pp. 1326–1334.

[13] Di Benedetti, M., Loreto, G., Matta, F., and Nanni, A. (2013). ”Acoustic Emission Monitoring of Reinforced Concrete under Accelerated Corrosion.” J. Mater. Civ. Eng., 25(8), 1022–1029.

[14] ElBatanouny, M.K., Mangual, J., Ziehl, P., and Matta, F. (2014). “Early Corrosion Detection in Prestressed Concrete Girders Using Acoustic Emission”, Journal of Materials in Civil Engineering, V. 26, No. 3, pp. 504–511.

[15] ElBatanouny, M.K., Larosche, A., Mazzoleni, P., Ziehl, P. H., Matta, F., & Zappa, E. (2014). “Identification of Cracking Mechanisms in Scaled FRP Reinforced Concrete Beams using Acoustic Emission,” Experimental Mechanics, V. 54, No. 1, pp. 69-82.

[16] Iliopoulos, S., Aggelis, D. G., Pyl, L., Vantomme, J., Van Marcke, P., Coppens, E., and Areias, L. (2015). “Detection and Evaluation of Cracks in the Concrete Buffer of the Belgian Nuclear Waste Container Using Combined NDT Techniques”, Construction and Building Materials, V. 78, pp. 369-378.

[17] Kawasaki, Y., Wakuda, T., Kobarai, T., and Ohtsu, M. (2013). “Corrosion Mechanisms in Reinforced Concrete by Acoustic Emission”, Construction and Building Materials, V. 48, pp. 1240-1247.

[18] Pour-Ghaz, M., Spragg, R., Castro, J., and Weiss, J. (2012). “Can Acoustic Emission be used to Detect Alkali Silica Reaction Earlier than Length Change Tests?,” 14th International Conference On Alkali Aggregate Reaction in Concrete, May 20-25, Austin, TX.

[19] ASTM C1293-08b. (2008). “Standard Test Method for Determination of Length Change of Concrete Due to Alkali-Silica Reaction,” American Standard for Testing and Materials, pp. 1-7.

[20] ASTM C157/C157M-08e1. (2008). “Standard Test Method for Length Change of Hardened Hydraulic-Cement Mortar and Concrete”, American Standard for Testing and Materials, pp. 1-7.

[21] Shrimer, F.H. (2000). “Application and Use of Damage Rating Index in Assessment of AAR-Affected Concrete - Selected Case Studies,” Proceedings of the 11thInternational Conference on Alkali-Aggregate Reaction in Concrete, Quebec City, Canada, Editors: M.A. Bérubé, B. Fournier and B. Durand, pp. 899-908.

[22] Tinkey, B.V., Fowler, T.J., Klingner, R.E. (2002). “Nondestructive Testing of Prestressed Bridge Girders with Distributed Damage,” Research Report 1857-2, pp. 106.

[23] Fowler, T., Blessing, J., Conlisk, P., Swanson, T.L. (1989). “The MONPAC System,” Journal of Acoustic Emission, V. 8, No. 3, pp. 1-8.

[24] Ziehl, P., Engelhardt, M., Fowler, T., Ulloa, F., Medlock, R., and Schell, E. (2009). “Design and Live Load Evaluation of a Hybrid FRP/RC Bridge Superstructure System,” ASCE Journal of Bridge Engineering, V. 14, No. 5, pp. 309-318.

[25] Anay, R., Cortez, T., Jáuregui, D., ElBatanouny, M., Ziehl, P. (2015). “On-Site Acoustic Emission Monitoring for Assessment of a Prestressed Concrete Double-Tee Beam Bridge without Plans”, ASCE Journal of Performance of Constructed Facilities (in press).

[26] ASTM E1067/E1067M-11. (2011). “Standard Practice for Acoustic Emission Examination of Fiberglass Reinforced Plastic Resin (FRP) Tanks/Vessels,” American Standard for Testing and Materials, pp.1-15.

[27] Golaski, L., Gebski, P., and Ono, K. (2002). “Diagnostics of Reinforced Concrete by Acoustic Emission,” Journal of Acoustic Emission, Vol. 20, p. 83-98.

[28] ElBatanouny, M.K., Jones, M., and Ziehl, P. (2014). “Assessment of Alkali-Silica-Reaction using Acoustic Emission,” 2014 International Congress on Advances in Nuclear Power Plants (ICAPP), Charlotte, North Carolina, April 6-9, pp.5.

CHAPTER 5

REMOTE MONITORING AND EVALUATION OF DAMAGE AT A DECOMMISSIONED NUCLEAR FACILITY USING ACOUSTIC EMISSION[3]

[3]Abdelrahman, M., M. ElBatanouny, K. Dixon, M. Serrato and P. Ziehl. To be submitted to *Journal of Performance of Constructed Facilities*.

5.1 ABSTRACT

Reinforced concrete systems used in the construction of nuclear reactor buildings, spent fuel pools, and related nuclear facilities are subject to degradation over the long term. Corrosion of steel reinforcement and thermal cracking are potential degradation mechanisms that adversely affect durability. Remote monitoring of such degradation can be used to enable informed decision making for facility maintenance operations and projecting remaining service life. Acoustic emission (AE) monitoring has been successfully employed for the detection and evaluation of damage related to cracking and material degradation in laboratory settings. This paper describes the use of AE sensing systems for remote monitoring of active corrosion regions in a decommissioned reactor facility for a period of approximately one year. In parallel, a representative block was cut from a wall at a similar nuclear facility and monitored during an accelerated corrosion test in the laboratory. Electrochemical measurements were recorded periodically during the test to correlate AE activity to quantifiable corrosion measurements and to allow for service life prediction. The results of both investigations demonstrate the feasibility of using AE for corrosion damage detection and classification as well as its potential as a remote monitoring technique for structural condition assessment and prognosis of aging structures.

5.2 INTRODUCTION

The vast presence of aging infrastructure throughout the nation, including transportation and energy-related infrastructure, has raised concerns regarding the level of service, reliability and vulnerability to natural disasters. The American Society of Civil Engineers (ASCE) latest Report Card stated a grade of "D^{+}" for US infrastructure and an estimated investment of $3.6 trillion needed by 2020 for upkeep. One of the major

challenges facing decision makers is resource allocation which is dependent on available information related to the current state of each structure. Reliable monitoring techniques that can effectively assess the structural condition are needed to evaluate the robustness of such structures and the urgency of any repair, replacement or maintenance activities.

Monitoring nuclear facilities, in particular, is of special interest due to safety considerations and the relatively long half-life of nuclear waste products. Reinforced concrete elements are used to construct several portions of nuclear facilities. Potential degradation mechanisms of reinforced concrete (Clifton 1991) include corrosion of reinforcement (Mangual et al., 2013a and b; ElBatanouny et al., 2014a; and Abdelrahman et al., 2016), alkali-silica reaction (Fournier et al., 2010; Abdelrahman et al., 2015; Abdelrahman et al., 2016), freeze-thaw cycling, sulfate attack, deformation mechanisms including creep and shrinkage, stresses due to structural constraint combined with seasonal effects such as thermal cycling and precipitation, and extreme events (Braverman et al., 2007; Kojima, 2009; Abdelrahman et al., 2014).

Advances in computing and data transfer over the last several decades have allowed for the development of wireless systems and remote monitoring. Acoustic emission (AE) is one emerging monitoring method that has proven potential for early damage detection through laboratory and field applications (Ono, 2010; Golaski, 2002). As a passive piezoelectric sensing technique, acoustic emission is able to detect stress waves (in the kHz range) emitted from sudden releases of energy such as cracking of the concrete matrix (ASTM E1316, 2016; Pollock, 1986). The method is suitable for real-time monitoring over the long term, and its high sensitivity enables it to detect active cracks long before they become visible (micro-cracking).

Corrosion of reinforcing steel is a degradation mechanism that affects the durability of concrete structures. The cracking of the concrete matrix associated with corrosion damage makes acoustic emission a well-suited method for monitoring its progression. Early investigations related to acoustic emission monitoring of corrosion damage in reinforced concrete date back to the 1980s (Weng et al., 1982; Dunn et al., 1983; Zdunek et al., 1995). Several investigations demonstrated the potential of utilizing AE for this degradation mechanism (Li et al., 1998; Assouli and Idrissi, 2005; Ohtsu and Tomoda, 2008; James, 2003). However, the quantification of damage was not fully resolved. Quantification of corrosion damage in reinforced concrete structures has been more recently addressed in a series of publications using accelerated corrosion results in laboratory settings (Di Benedetti et al., 2013; Mangual et al., 2013a; Mangual et al., 2013b) as well as natural corrosion tests (ElBatanouny et al., 2014a; Velez et al., 2015; Appalla et al., 2015).

This study investigates the applicability of deploying acoustic emission for the remote monitoring of selected areas at the Savannah River Site (SRS) 105-C Reactor Facility, Aiken, South Carolina (Figure 5.1). This is an inactive nuclear facility under surveillance and maintenance operations as well as deactivation and decommissioning operations. AE monitoring was conducted at areas known to have active corrosion damage and/or visible cracking. This allows for examining the applicability of previously developed AE methods for corrosion damage detection and classification.

To aid in the development of damage algorithms and to provide a more controlled study, an aged reinforced concrete block specimen cut from a similar reactor facility was maintained and monitored in the University of South Carolina Structures and Materials

Laboratory for the majority of the project duration. This specimen was subjected to wet/dry cycling to accelerate the corrosion process. Electrochemical measurements were periodically recorded, whereas acoustic emission was monitored continuously.

The activities undertaken and reported in this study represent a step toward the development of an acoustic emission based approach for assessment of reinforced concrete structural systems through remote monitoring.

Figure 5.1 Reactor building 105-C at the Savannah River Site.

The study is divided into two main activities: 1) Remote acoustic emission monitoring and analysis of data collected at the 105-C Reactor Facility, and 2) Accelerated corrosion testing to assess corrosion damage within an aged reinforced concrete block supplied by SRNS at the University of South Carolina Structures and Materials laboratory.

5.3 EXPERIMENTAL PROGRAM: AE MONITORING AT THE 105-C REACTOR FACILITY

5.3.1 Acoustic Emission Sensing Systems

Two separate AE systems were utilized for remote monitoring at the 105-C Reactor Facility. These systems are referred to as a ‘wired’ AE system, and a ‘wireless’ AE system. All acoustic emission system components and software were manufactured by Mistras Group, Inc. of Princeton Junction, New Jersey. The wired system utilized both R6I (peak

resonance near 55 kHz) and WDI (relatively broadband) sensor types (calibration sheets for both sensor types are available in the manufacturer's website). Both sensor types utilize integral pre-amplifiers within the stainless steel sensor housing. The resonant sensors are more sensitive to damage in reinforced concrete structures than the broadband sensors. However, the broadband sensors provide higher fidelity frequency data which can be useful for data reduction and interpretation. The sensors were connected to a 16-channel DiSP acoustic emission data acquisition system which utilizes four high speed data acquisition boards specifically designed and manufactured for the acquisition and processing of acoustic emission data as well as specialized software (AEWin).

The wireless acoustic emission system (type 1284), includes 4-channels and utilizes low power PK6I acoustic emission sensors. These sensors are resonant in the vicinity of 55 kHz and utilize integrated preamplifiers within the stainless steel housing. The sensors were connected to the 1284 system, where preliminary processing of the data is performed. The data is transmitted through an antenna and received through a base station module that is connected to a conventional laptop computer. Specialized wireless acoustic emission software (AEWin for Wireless) is used for controlling the data acquisition. This system was powered through solar panels connected to 12V DC batteries.

5.3.2 Installation of Acoustic Emission Systems

Prior to installation at the Savannah River Site (SRS), the consistency of the sensor readings was checked using pencil lead breaks on an acrylic rod (ASTM E 2075, 2015; ASTM E 2374, 2015). Six pencil lead breaks were performed for each sensor. Appropriate sensor response was demonstrated as the average amplitude response of a sensor type was within ± 6 dB of the average amplitude of the sensor group. A threshold of 40 dB was used

for data collection. An analog filter was used to collect signals with frequency between 1 kHz and 1 MHz. The waveform sampling rate was 1 million samples per second (MSPS) with 256 micro-seconds pre-trigger and 1 kilobyte length. Peak definition time (PDT), hit definition time (HDT) and hit lock-out time (HLT) were set to 200, 400, and 200 micro-seconds, respectively. Each AE system was connected to a cellular modem to allow for remote monitoring, and each system was remotely controlled though appropriate software. This allowed for altering system settings and saving of data at the University of South Carolina.

Crane Maintenance Area: The wired AE system was installed to monitor the activity in this area of building 105-C with ten sensors; five resonant sensors (type R6I) and five broadband sensors (type WDI). The sensors were installed at three different locations. The first location was near a column to roof interface (referred to as the 'vertical column to roof interface location'). This area had been visually assessed by Savannah River Nuclear Solutions/Savannah River National Laboratory (SRNS/SRNL) personnel and is known to have deteriorated in comparison to the majority of the structural system comprising the 105-C reactor building. Spalling has occurred in this area in the recent past and ongoing corrosion activity is suspected. The area has undergone at least one repair activity in the past. A total of six sensors (three resonant and three broadband) were installed at this location as shown in Figure 5.2. The locations of the sensors were chosen to be near exposed reinforcing bars showing visual signs of corrosion damage. The locations of the sensors with respect to the red dot shown in Figure 5.2 are provided in Table 5.1.

The second location was chosen on a horizontal beam that forms the connection with the previously described column (referred to as the 'horizontal beam location'). Two sensors (one resonant and one broadband) were installed at a distance of twelve inches below the beam to roof interface where signs of deterioration were visually observed (Figure 5.3a). The spacing between the sensors was six inches. The third location was chosen at an area where no signs of damage were observed (referred to as the 'control location'). Two sensors (one resonant and one broadband) were installed at this location as shown in Figure 5.3b. The horizontal distance between the two sensors is six inches. The data collected from the control location was used to evaluate the effectiveness of data reduction approaches.

Table 5.1 Location of sensors shown in Figure 5.2.

Sensor type - channel	Horizontal dimension (in.)	Vertical dimension (in.)
WDI-9	0	-10.5*
R6I-10	8.5	16
R6I-11	5.5	9
WDI-12	11	5.5
R6I-13	14.5	16
WDI-14	15.5	8.5

**Positive dimension indicates below the red dot shown in Figure 5.2. Negative dimension indicates above the red dot shown in Figure 5.2.*

Figure 5.2 Photographs of the crane maintenance area: (a) main sensor grid, (b) close-up of sensor on side of column, and (c) view of main grid from floor level (red dot is at corner).

Figure 5.3 Photograph of: (a) horizontal beam location, and (b) control location.

+48 Level: The wireless AE system was installed at the +48 level to monitor a vertical crack that may penetrate an exterior wall, as shown in Figure 5.4, using four resonant sensors (type PK6I). Sensor layout and spacing is also shown in the figure.

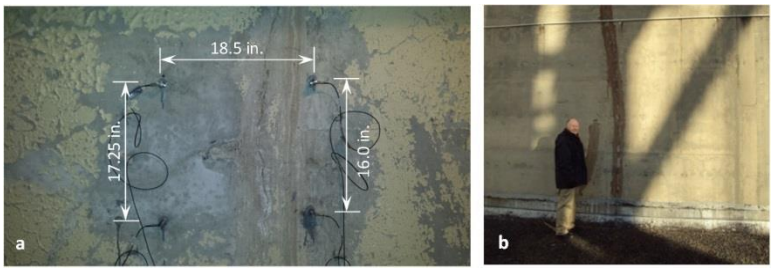

Figure 5.4 Photographs at +48 level: (a) sensor grid from interior, and (b) vertical crack from exterior.

5.4 RESULTS AND DISCUSSION: AE MONITORING AT THE 105-C REACTOR FACILITY

5.4.1 Remote Monitoring at Crane Maintenance Area

Remote monitoring at the Crane Maintenance Location was performed from September 10, 2014 (commencement of test) through August 25, 2015. A cellular connection was utilized to remotely operate the wired system. Data loss due to power outage at the system occurred between December 18, 2014 and January 20, 2015. The raw data was analyzed and appropriate filters were used to reject data arising from signals not related to initiation or growth of cracks, such as wave reflections. The filters are primarily parameter based filters that were developed based on visual inspection of AE waveforms, similar to those described in ElBatanouny et al. (2014a). The first is a Duration-Amplitude filter (D-A), also referred to as a Swansong II type filter, while the second is a Rise time-Amplitude filter (R-A) as described in Table 5.2. Additional filters, Duration and RMS filters, were developed during this study to minimize electrical noise. The additional filters were developed based on data collected from the concrete block discussed in the following sections.

Table 5.2 Data rejection limits.

D-A filter		R-A filter		Duration	RMS filter (V)
Amp (dB)	Duration (μs)	Amp (dB)	Rise time (μs)		
45-50	> 500	45-50	> 40	≤ 100 μs	0.0019-0.0041
51-55	> 1000	51-65	> 100	-----	-----
56-65	> 2000	66-100	> 150	-----	-----
66-75	> 3000	-----	-----	-----	-----
76-100	> 4000	-----	-----	-----	-----

Figures 5.5 and 5.6 show the AE activity detected at the three monitored locations in the crane maintenance area for the resonant and broadband sensors, respectively. As shown in the figures, AE activity at the locations associated with visually observable damage (‘vertical column to roof interface location’ and ‘horizontal beam location’) was significantly higher than the AE activity at the control location. This indicates that the filters used were suitable for this application and also that intrinsic noise such as that potentially caused by electro-magnetic interference is not an obstacle for this application. The relatively high levels of AE activity indicate that damage (corrosion and related cracking) associated with aging of reinforced concrete is progressing at the vertical column to roof interface and horizontal beam locations.

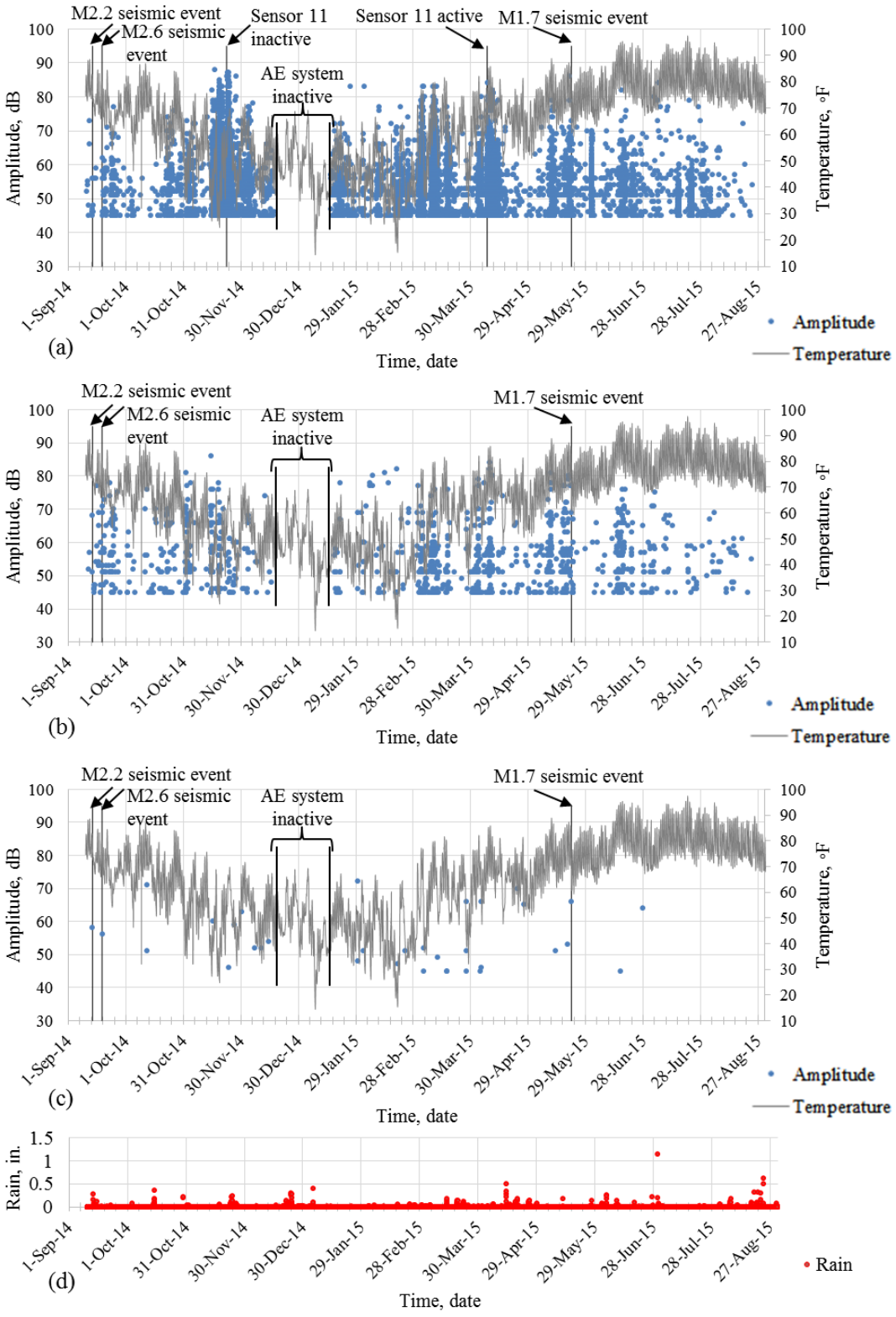

Figure 5.5 Amplitude and temperature versus time for resonant sensors: (a) vertical column to roof interface location, (b) horizontal beam location, and (c) control location, and (d) rain versus time.

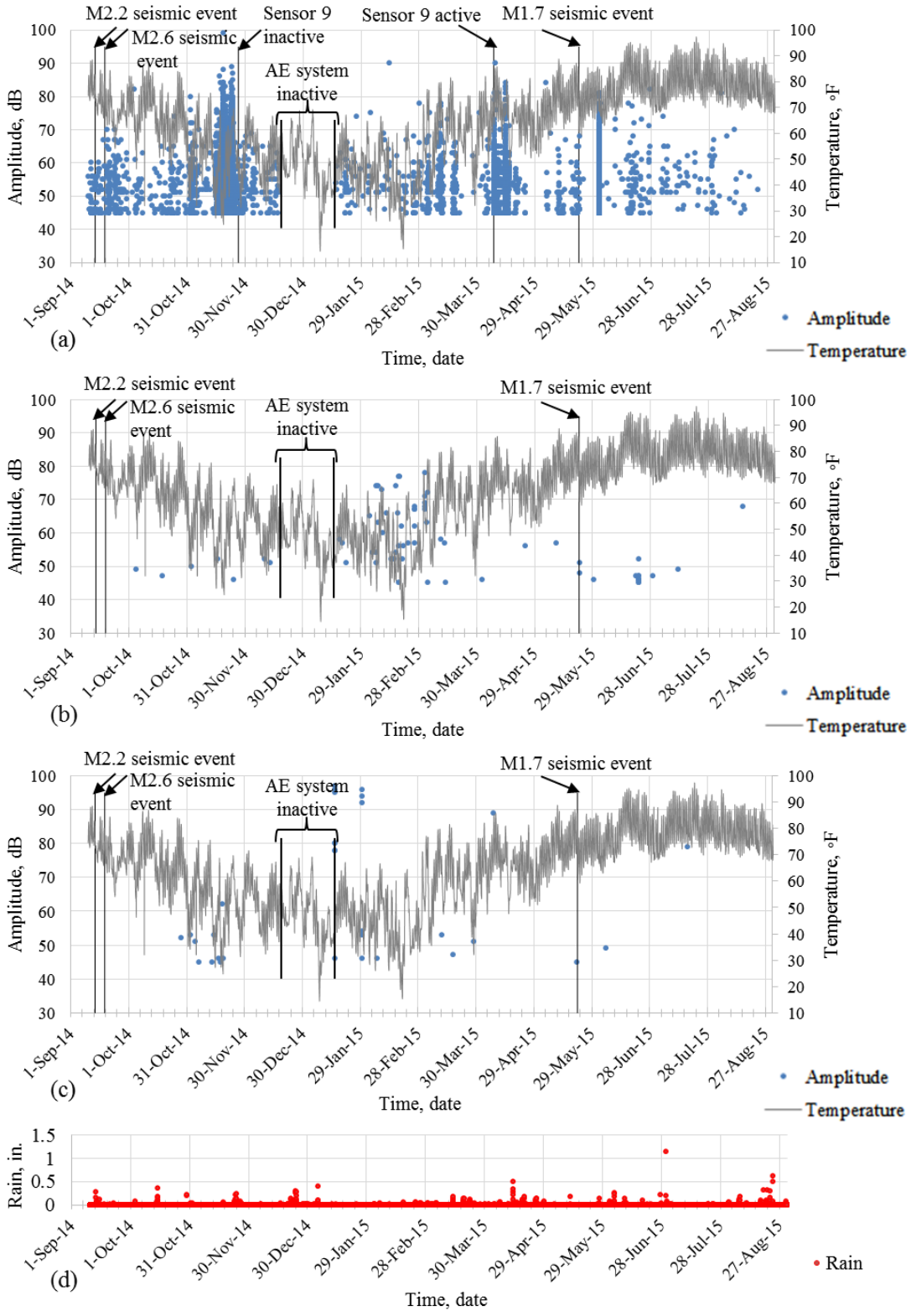

Figure 5.6 Amplitude and temperature versus time for broadband sensors: (a) vertical column to roof interface location, (b) horizontal beam location, and (c) control location, and (d) rain versus time.

Rain and temperature data were provided by SRNL to investigate the effect of environmental conditions on AE activity. Seasonal temperature fluctuations affected the data more significantly than daily temperature fluctuations. This may be attributed to the low coefficient of thermal expansion of concrete, causing volumetric changes to be associated with prolonged exposure to temperature differentials. As a general statement, increased AE activity was recorded when temperatures decreased during the winter months. Rain events were not as closely correlated to AE activity as were temperature fluctuations. However, associated moisture and repeated wet/dry cycling from rain events may lead to acceleration of the degradation process. During one of the site visits, remnants of a crack sealing material were found on the floor of the 105-C building, indicating one potential source of moisture intrusion in this area.

The wired AE system was inactive between December 18, 2014 and January 20, 2015 due to moisture related event that adversely affected the laptop. Sensors corresponding to channels 9 and 11 (both at the vertical column to roof interface location) detached from concrete surface on November 27, 2014 and November 23, 2014, respectively. Localized spalling that occurred at these locations during this time period is presumed to be the cause of the detachment. Both sensors were reattached on April 8, 2015.

Three seismic events occurred during the monitoring period: September 14, 2014 (M2.2); September 19, 2014 (M2.6); and May 22, 2015 (M1.96). Close inspection of data collected during this period did not reveal a correlation between these events and the AE data. Referring to the definition of acoustic emission (transient stress waves caused by a rapid release of energy within a material, ASTM E 1316c, 2013), AE sensors would potentially be capable of detecting crack growth events caused by a seismic event provided

the crack growth event or events occurred within the range of sensitivity of the sensors. In the application at 105-C, the range of sensitivity for minor crack growth events (similar in energy to that caused by a pencil lead break) is in the range of three to ten feet from each sensor. Due to the frequency range of AE sensors (30 kHz to 300 kHz), the sensors are not sensitive to global structural vibrations such as those potentially related to seismic activity.

5.4.2 Evaluation of Data at Crane Maintenance Area

Figure 5.7a and Figure 5.7b show the cumulative signal strength (abbreviated as CSS) at each monitored location for resonant and broadband sensors, respectively. Signal strength of an AE hit is a measure of the area under the recorded signal envelope (sometimes referred to as MARSE, Measured Area under the Rectified Signal Envelope) (ASTM E 1316c, 2013). Higher levels of signal strength are associated with higher levels of energy release due to crack growth events.

While the signal strength of an AE hit is related to the intensity of damage growth at a particular instant in time, cumulative signal strength is related to increases in damage growth rates over a particular testing period. Rapid increases in the cumulative signal strength curve are related to rapid increases in damage growth. The relationship between rapid changes in the cumulative signal strength curve and damage growth has been utilized to assess damage in different structural systems (Fowler et al., 1989) including reinforced concrete bridges (Golaski et al., 2002) and corrosion damage in reinforced concrete laboratory specimens (Mangual et al., 2013a and 2013b).

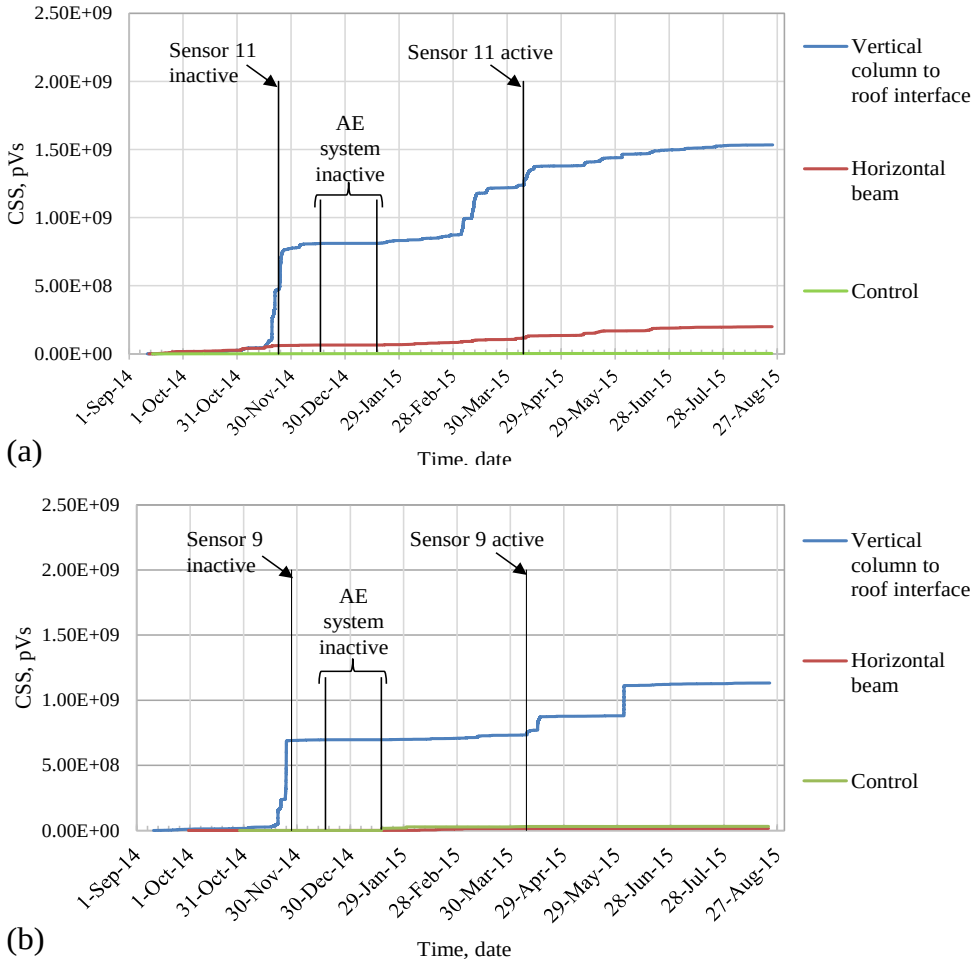

Figure 5.7 Cumulative signal strength (CSS) of: (a) resonant sensor, and (b) broadband sensors.

In both Figure 5.7a and Figure 5.7b, it is apparent that sharp changes in the slope of cumulative signal strength, indicating sharp increases in damage progression, related to the vertical column to roof interface location occurred in several different instances. For example, a sharp increase in damage growth is noticed at the end of November; between March 4, 2015 and March 13, 2015; and between April 8, 2015 and April 15, 2015. These sharp increases were noticed for both the resonant and broadband sensor types. As expected, the broadband sensors exhibit slightly lower values of cumulative signal strength owing to the relatively low sensitivity of this sensor type.

The highest change of slope for resonant and broadband sensors at the vertical column to roof interface occurred at the end of November, 2014. This sudden increase in cumulative signal strength was accompanied by localized spalling of concrete, which may have caused the detachment of two sensors as previously mentioned. This spalling supports the findings that significant damage occurred during this time period.

To allow for comparison of AE activity from each sensor, the response of broadband sensors was normalized to that of resonant sensors. The normalization was determined based on the application of a simulated source (ASTM E 2374-15) applied at both resonant and broadband sensor locations on the reactor concrete block (described later). Pencil lead breaks (PLBs) were applied at different angles around a resonant sensor (0, 45, 90, 135 and 180 degrees) at distances of 3 in. and 6 in. in each direction; three PLBs were applied at each distance. The CSS recorded from PLBs applied at each distance was calculated separately. The same procedure was repeated for a broadband sensor. The ratio of CSS detected from the resonant sensor to the CSS from the broadband senor was calculated for the cases of 3 in. and 6 in. from the sensor. The average of the ratios achieved at the two distances was found to be approximately equal to 10. Thus, cumulative signal strength detected from WDI sensors was normalized using a factor of 10.

Figure 5.8a is a visual representation of the intensity of damage at each sensor location using a contour plot. The plot is based on cumulative signal strength results (units of pico-Volt seconds), where high cumulative signal strength is plotted in red, indicating high damage, while low cumulative signal strength is plotted in blue, indicating lower damage. The contour plots show relative intensity of AE activity.

As seen in the plot, the highest normalized cumulative signal strength values were detected at the top left of the elevation face sensors and at sensor 9 at the side of the vertical column. The 2D source location results (for the data detected from the five sensors at the same plane) show that most AE events were also detected at the top left of the sensor grid, suggesting that damage is progressing at this location (Figure 5.8b). Figure 5.8c likewise indicates very high damage progression in the vicinity of sensor 9; with the highest value of normalized CSS detected at sensor 9.

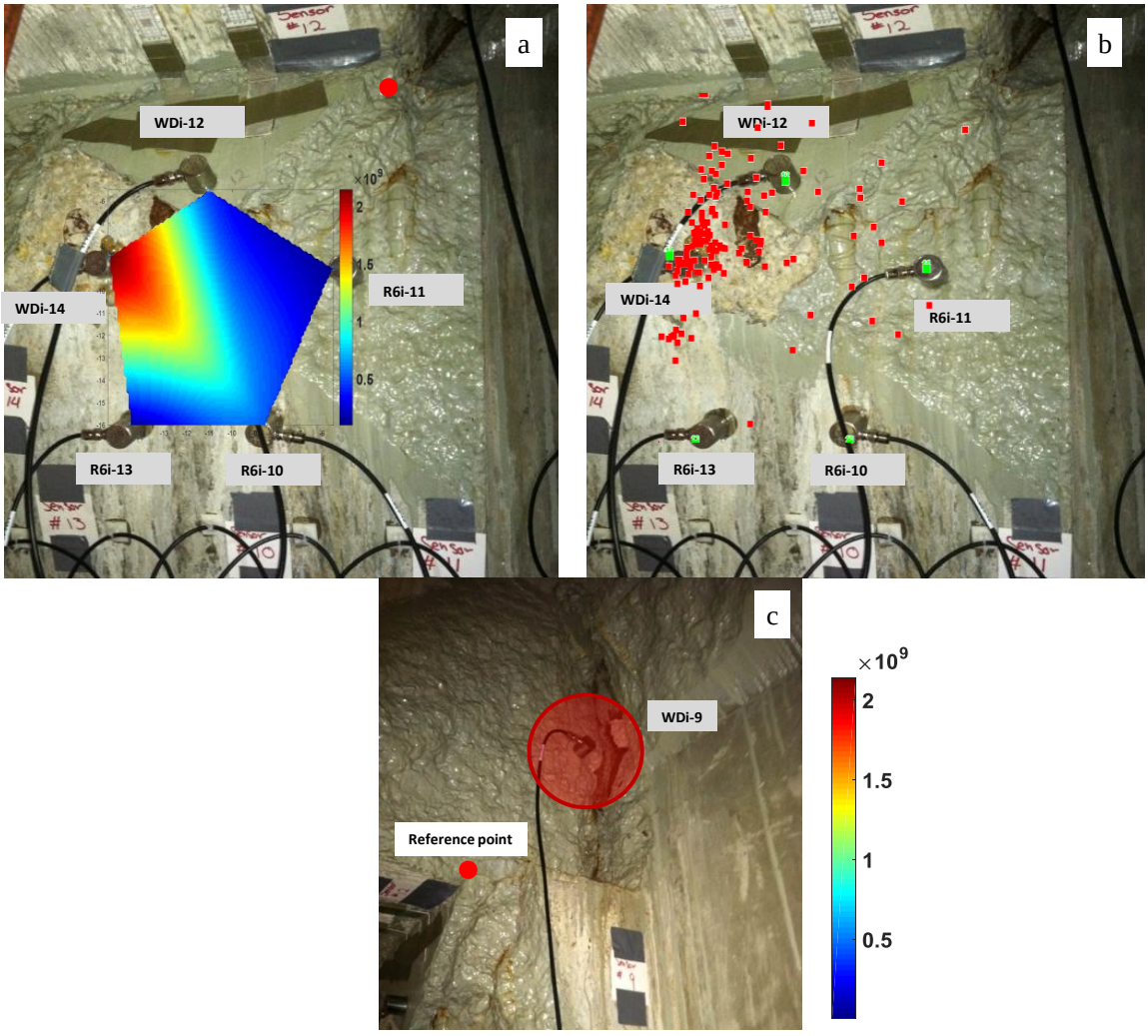

Figure 5.8 Vertical column to roof interface: (a) signal strength contour plot at elevation face sensors, (b) source location at elevation face sensors, and (c) signal strength contour plot at side face sensor.

Figure 5.9 shows similar contour plots at the horizontal beam and control locations. Similar to the vertical column to roof interface location, normalized data was used to generate the plot. The same contour scale as in Figure 5.8 was used to generate the plots. As seen in Figure 5.9, lower damage occurred at the horizontal beam location (Figure 5.9a) and the control location (Figure 5.9b) when compared to vertical column to roof interface location.

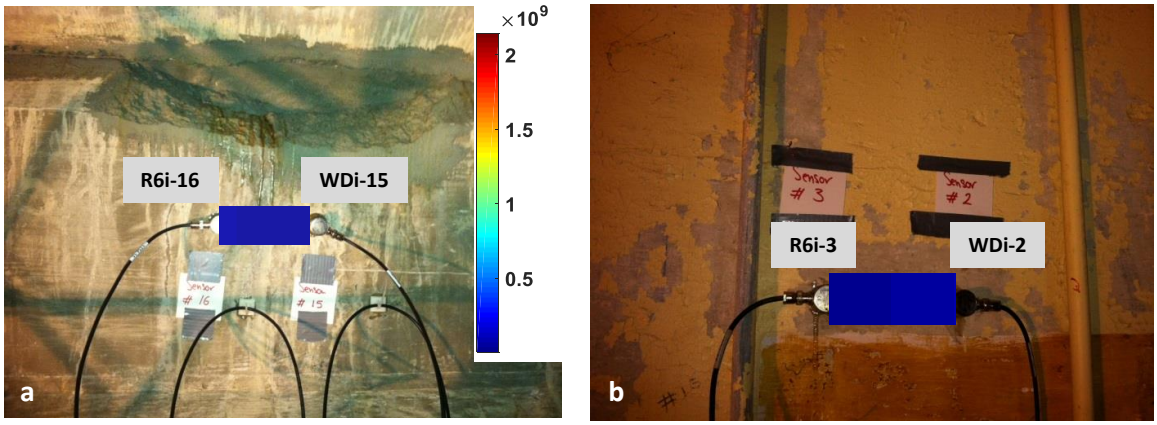

Figure 5.9 Signal strength contour plot: (a) horizontal beam location, and (b) control location.

5.4.3 Damage Classification using Acoustic Emission

To provide a means for interpretation of the data, Intensity Analysis graphs were developed at each AE monitoring location. The method was first introduced by Fowler and others (Fowler et al., 1989) for the evaluation of fiber reinforced polymer vessels and is based entirely on signal strength. Intensity Analysis is a graphical method which differs from many other forms of acoustic emission assessment in the sense that it is focused on trends in the AE data as opposed to individual events. Intensity Analysis uses two parameters, both based on signal strength: a) historic index (plotted on the horizontal axis), and b) severity (plotted on the vertical axis).

Historic index and severity can be calculated using Equation 5.1 and Equation 5.2 where N is the number of hits up to time (t), S_{oi} is the signal strength of the i-th event, and K is an empirically derived factor that varies with the number of hits. The value of K has been previously selected in one case as: a) N/A if $N \leq 50$, b) $K = N - 30$ if $51 \leq N \leq 200$, c) $K = 0.85N$ if $201 \leq N \leq 500$, and d) $K = N - 75$ if $N \geq 501$ (ElBatanouny et al., 2014a).

$$H(t) = \frac{N}{N-K} \frac{\sum_{i=K+1}^{N} S_{oi}}{\sum_{i=1}^{N} S_{oi}} \quad (5.1)$$

$$S_r = \frac{1}{50} \sum_{i=1}^{i=50} S_{oi} \quad (5.2)$$

Historic index, H(t), is a form of trend analysis that incorporates historical data in the current measurement. It is sensitive to changes of slope in cumulative signal strength versus time and compares the signal strength of the most recent hits to a value of cumulative hits. Severity, S_r, is defined as the average signal strength for the 50 hits having the highest numerical value of signal strength. The intensity analysis method has been widely used for assessment of structural systems during load testing, including reinforced concrete systems (Golaski et al., 2002; Nair and Cai, 2010; ElBatanouny et al., 2014), and has been extended to the case of corrosion damage in prestressed concrete specimens (Mangual et al., 2013a and 2013b; ElBatanouny et al., 2014a; Velez et al. 2015).

By plotting the maximum historic index and severity values obtained over the duration of the test, an Intensity Analysis plot is generated. Due to the relationship between AE signal strength and damage growth, points that plot upward and to the right are associated with higher levels of damage.

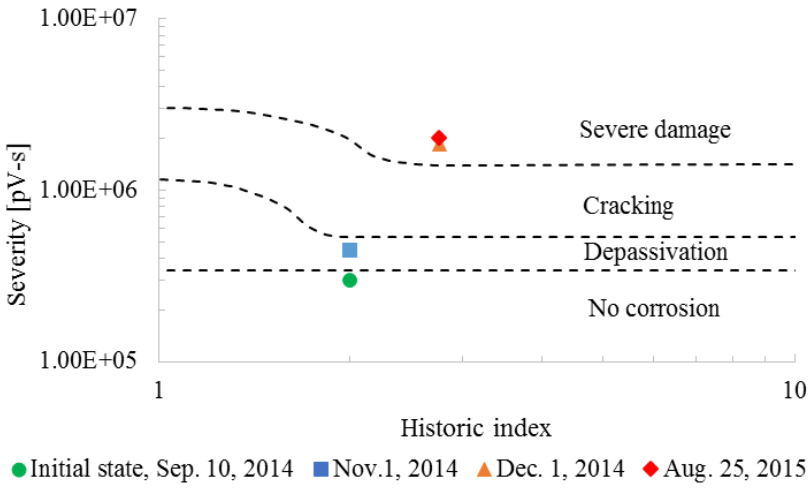

(a)

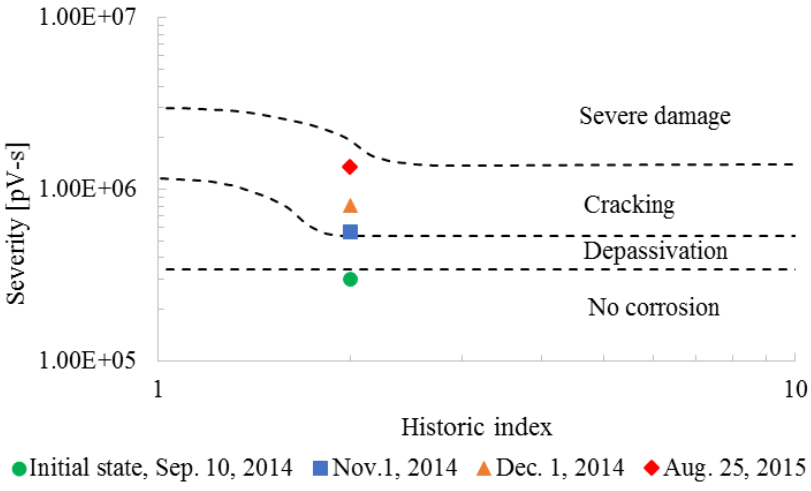

(b)

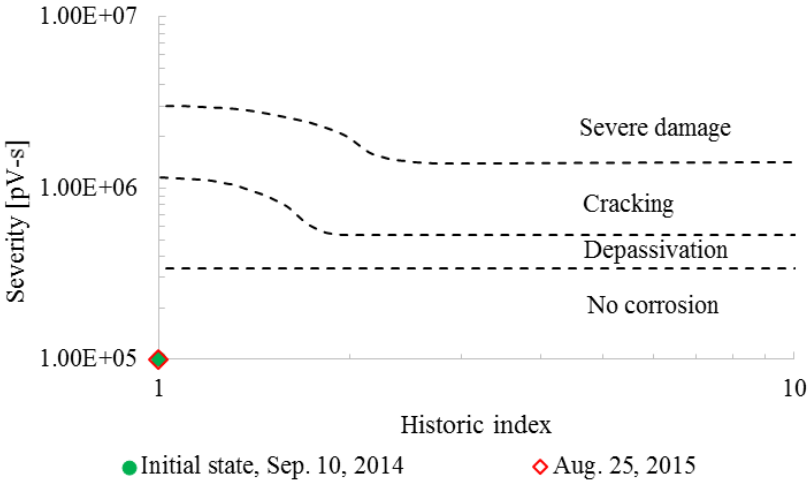

(c)

Figure 5.10 Intensity Analysis results for resonant sensors: (a) roof to column interface, (b) horizontal beam location, and (c) control location.

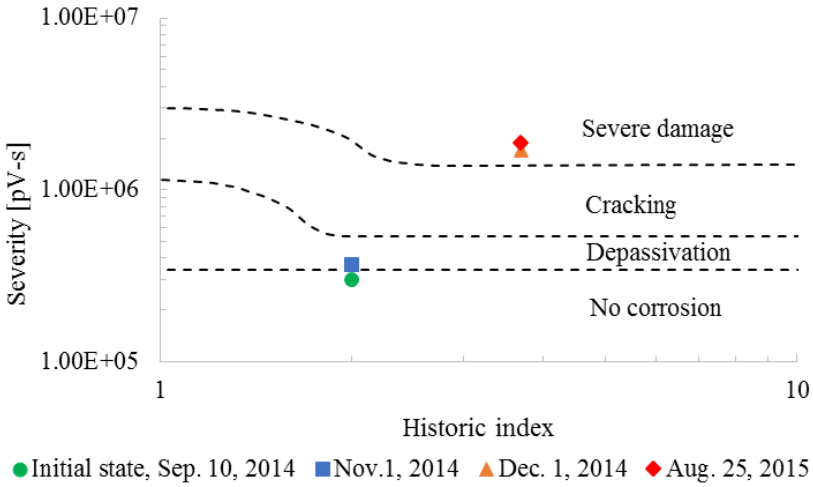

(a)

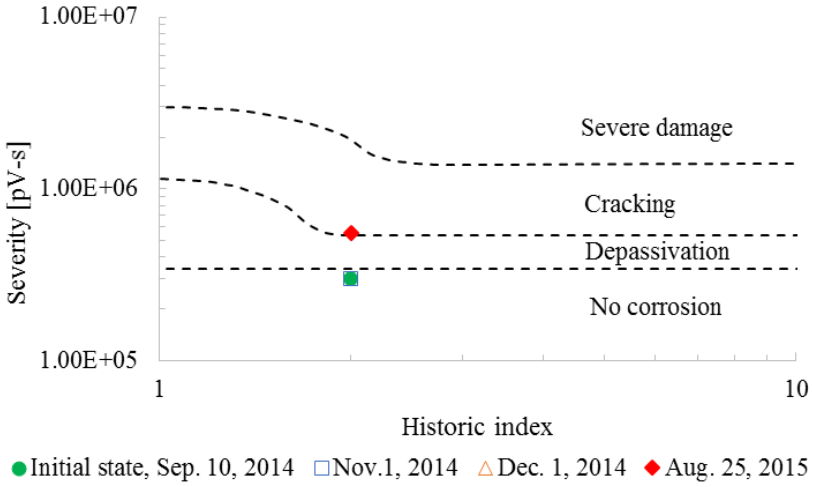

(b)

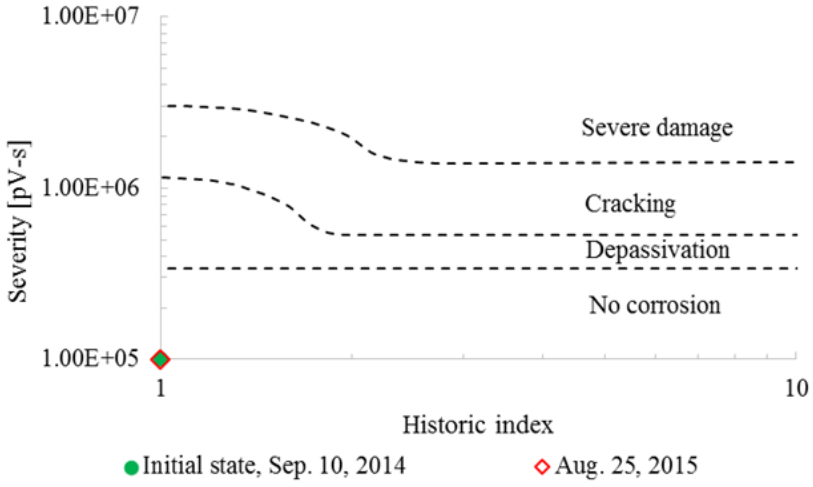

(c)

Figure 5.11 Intensity Analysis results for broadband sensors: (a) roof to column interface, (b) horizontal beam location, and (c) control location.

Because IA uses historical information, an initial point on the Intensity Analysis plot must be chosen. This may be approached through visual inspection, numerical modeling, electrochemical measurements (in the case of corrosion damage), coring and petrographic examination, and other methods including suitable nondestructive evaluation techniques. Only visual inspection was practicable for the monitored locations within 105-C. Therefore the initial point was chosen based on visual inspection.

The values of historic index and severity for the initial point were considered to account for pre-existing damage such that the historic index value at any time cannot be less than that for the initial point. For the severity, the distribution of the highest fifty signal strength values collected during the monitoring period, in terms of their scattering from the mean value, was used to develop the other fifty signal strength values with the same distribution but with a mean value equal to the severity of the initial point. Then the highest fifty numerical values from the collective set of one hundred signal strengths; fifty from the monitoring period and fifty developed from the initial point, are used to calculate an updated severity value that takes into account the pre-existing condition.

Figure 5.10 and Figure 5.11 are plots of Intensity Analysis results from the period beginning September 10, 2014 and ending August 25, 2015 for data recorded from resonant and broadband sensors, respectively. For the majority of field applications, only resonant sensors would be utilized due to the increased sensitivity of this sensor type in comparison to broadband sensors. The use of resonant sensors therefore reduces the number of sensors needed for a given application. However, resonant sensors do not provide high fidelity representations of the frequency content in comparison to broadband sensors. One purpose of using the two different sensor types is to investigate the associated differences in the

results. The limits of the Intensity Analysis chart were developed based on data from resonant sensors (Mangual et al., 2013a), thus it is expected that data collected from broadband sensors may yield underestimated damage classification if the same limits are used.

The preliminary estimation of damage was based on visual inspection during the initial visit to 105-C and was located near the border between the 'no damage' and the 'depassivation' regions of the chart (severity = 300,000 and historic index = 2.0) for both the vertical column to roof interface location and the horizontal beam location. It is noted that this assumed level of damage underestimated the actual condition of the structures, since these areas are known to have ongoing corrosion damage. Ideally, this initial point would be established through a combination of methods including visual inspection and electrochemical methods. Electrochemical methods, however, were not collected during this part of the study. For the control location no damage was assumed and, therefore, the initial point was located at the left corner in the 'no corrosion' region of the chart.

Acoustic emission activity during the monitoring period (approximately one year) at the vertical column to roof interface location indicated a progression from the initial state to the severe damage state for both sensor types. It is noted that the results of IA after approximately 2 months of monitoring (November 1, 2014) showed that corrosion is ongoing at this location. On December 1, 2014, Intensity Analysis results indicated that severe damage occurred. For monitoring over this relatively short duration, such a progression from the initial state to the 'severe' damage state is indicative of a relatively high level of ongoing damage growth in the monitored areas. For this plot, the term 'cracking' refers to micro-cracking that is generally non-visible, whereas 'severe damage'

refers to visible cracking that may be accompanied by spalling. This result is supported by the spalling that occurred at this location during the monitoring period.

Acoustic emission data from the resonant sensor and the broadband sensor at the horizontal beam location progressed from the initial state to the cracking state over the duration of the monitoring period. This result is also an indication of ongoing damage growth at this location when the relatively short monitoring period is considered. The broadband sensors results (Figure 5.11b) indicated less damage than the resonant sensor results (Figure 5.10b), especially during the first 3 months of monitoring. This can be attributed to the lower sensitivity of the broadband sensors.

In contrast to the roof interface location and the horizontal beam location, the intensity analysis results for the control location indicate no damage progression during the monitoring period, and therefore the initial state and final state coincide (plot on top of one another) for the control location.

5.4.4 Remote Monitoring at +48 Level

A cellular connection was used to remotely operate the wireless acoustic emission data acquisition system. Data from the wireless system was collected between September 9, 2014 (commencement of test) and November 13, 2014. Due to loss of power from the solar power/battery system, ten days of data were lost starting from September 11, 2014. The power was reconnected and the system continued to monitor until October 15, 2014 when a thunderstorm caused a power outage and data was lost for another thirteen days. The system continued to collect data afterwards until the data acquisition laptop was damaged on November 13, 2014; most likely by moisture, and was not repairable.

As described for the wired system data, the raw data was analyzed and appropriate data filters were used to separate meaningful data from spurious emissions. The limits of the data filters are shown in Table 5.2. Figure 5.12 shows acoustic emission activity in terms of amplitude versus time (showing both rain and temperature data) collected between September 9, 2014 and November 13, 2014 from the wireless acoustic emission system. This data set contains a significant number of hits having amplitude exceeding 80 dB. These hits are of relatively high amplitude and may be correlated to ongoing damage.

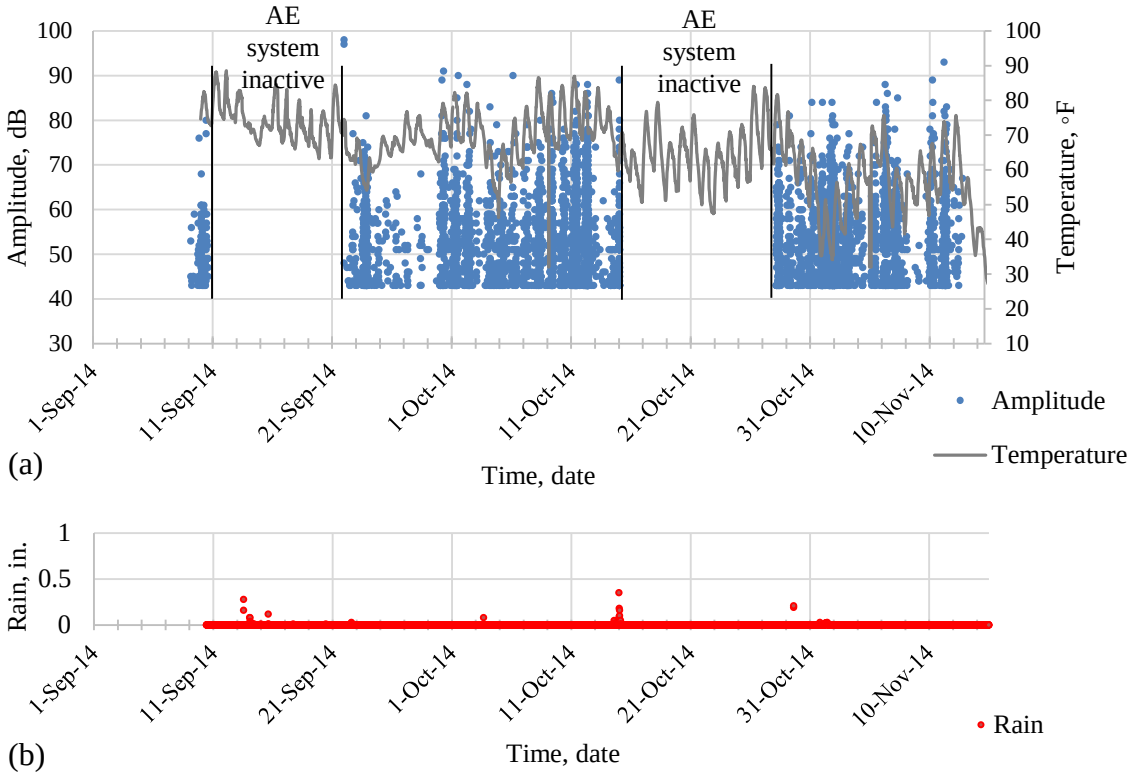

Figure 5.12 (a) Amplitude and temperature versus time for four wireless sensors at +48 level, and (b) rain versus time.

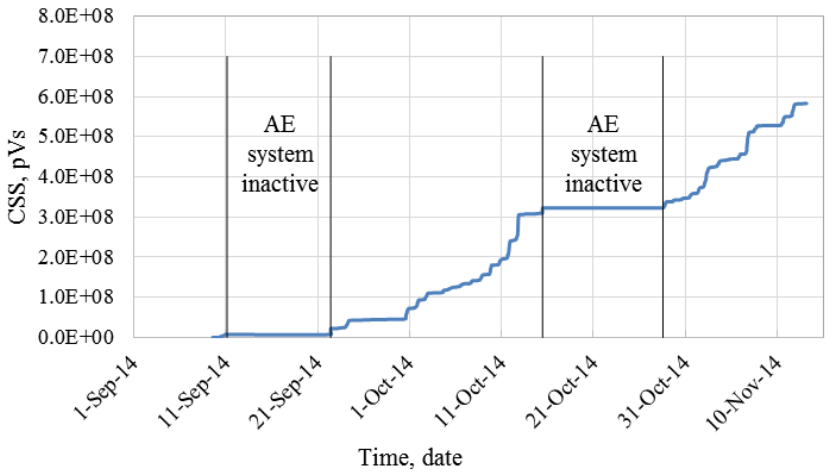

Figure 5.13 Cumulative signal strength (pVs) versus time (days) for four wireless sensors at +48 level.

One objective of monitoring this location was to assess whether the large vertical crack in the wall is still active. This vertical crack has a width between 0.125 and 0.25 in. with several small hairline cracks extending from it in the horizontal direction. Figure 5.13 plots the cumulative signal strength (units of pico-Volt seconds) versus time (days) for the collected signals over the monitoring period. An increasing trend in the acoustic emission activity is observed in the figures, indicating that damage may be progressing at this location.

To further investigate the trends in this data set, triangulation algorithms were used to investigate if AE events were generated from crack growth. Figure 5.14 shows the source location results from filtered acoustic emission data. In this figure, each red dot indicates a located acoustic emission event, meaning that all four sensors received data with a specified time increment. The time increment was determined based on the characteristic wave speed of the structure, which was experimentally determined during the installation site visit, and the geometry of the sensor grid. Source location from raw data was inconclusive as it showed acoustic emission activity throughout the monitored area. Six acoustic emission events from the filtered data set were located in the vicinity of the vertical

crack. These results imply that crack growth or friction between crack surfaces was ongoing in this area during the monitoring period.

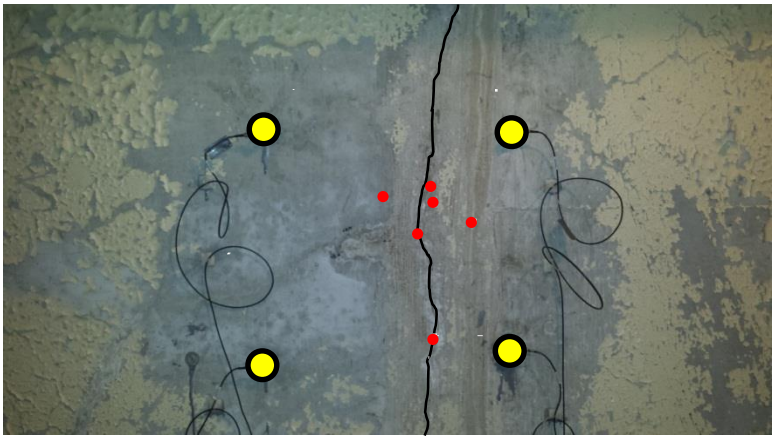

Figure 5.14 Source location results at +48 level; red dots indicate located AE events.

5.5 EXPERIMENTAL PROGRAM: ACCELERATED CORROSION TESTING OF THE REACTOR CONCRETE BLOCK

A reinforced concrete block was cut from the reactor facility with a length, width, and depth of 7 ft. 4 in., 3 ft. and 3 ft. 4 in., respectively. Accelerated corrosion test was conducted to corrode three different areas over the course of this study. Three concrete cores were drilled (3 in. in diameter and 9 in. in length) at three locations to create different concrete cover thickness for three vertical steel reinforcing bars adjacent to the cores (Figure 5.15). During the coring process, a transverse reinforcing bar was unavoidably cut at a depth of approximately six inches from the surface of the concrete test block specimen.

The test was initiated by placing 3% NaCl solution in the drilled holes to a depth of 3 in. on December 2, 2014. The solution was maintained in the drilled holes for two months to ensure that chloride concentration reached needed level for corrosion initiation (Nilsson et al., 2011; Vélez et al., 2012). Wet/dry cycles were then initiated (three days wet and four days dry) on February 19, 2015 to accelerate the corrosion process. A galvanic

cell was created during the wet days by inserting a copper plate in the cored locations. Figure 5.15d shows the 'as measured' concrete cover after the cores were drilled.

The first location has a concrete cover of 0.25 in. and was monitored using three broadband sensors (WDI) and one resonant sensor (R15I) while the second location has a cover of 1.0 in. and was monitored using four resonant sensors (R6I). The third location has a cover of 0.125 in. and was monitored using eight resonant sensors (R6I). On May 22, 2015 one of the sensors at the 1.0 inch cover location was removed from the test block and on May 27, 2015 it was placed on a small concrete specimen (control specimen) having dimensions of 3.0 in. x 3.0 in. x 11.25 in. The control specimen is not reinforced and therefore is known not to have corrosion activity. Data collected from the control specimen was used to verify the efficiency of the data filters developed during the course of the project. Acoustic emission activity was recorded continuously throughout the test period.

Half-cell potential (HCP) and linear polarization resistance (LPR) measurements were recorded once a week with the objective of providing insight related to the corrosion process of targeted reinforcement locations. HCP method is described in ASTM C876 (ASTM C876, 2009) and is traditionally employed to determine the likelihood of corrosion activity as described in Table 5.3. Linear polarization resistance (LPR) is a method used to measure polarization resistance (*Rp*) which can be used to calculate corrosion current (*Icorr*), and corrosion current density (*icorr*). These parameters can be used to estimate the corrosion rate (*CR*). Figure 5.16 shows a schematic of the test setup and acoustic emission sensor layout to monitor the corrosion process of the reinforcing bars. A schematic of the aged concrete block control specimen is also shown in this figure.

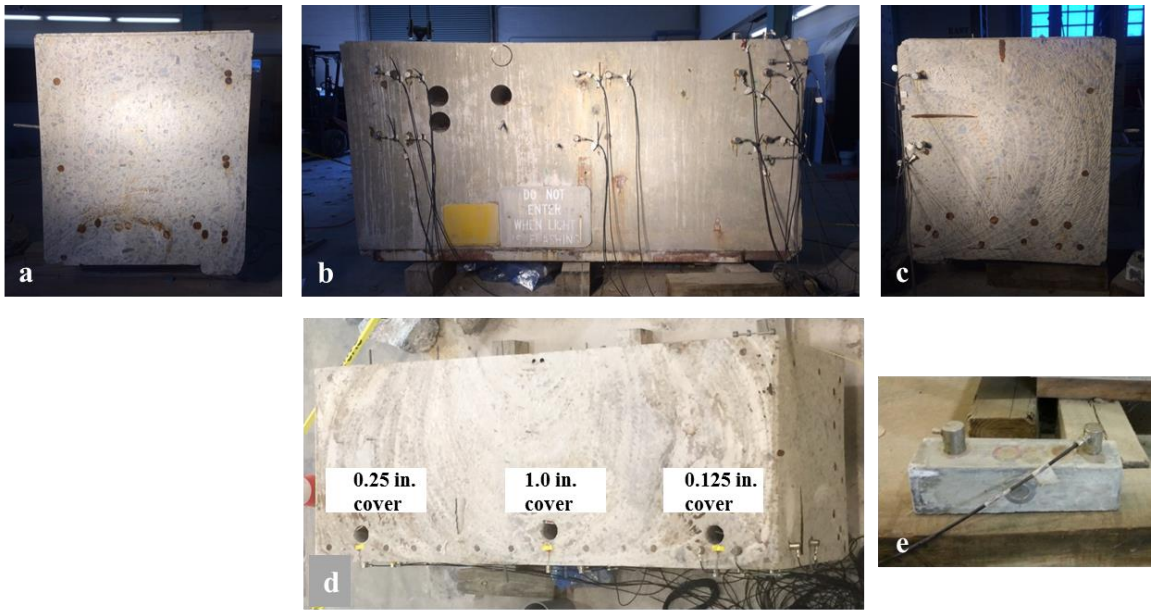

Figure 5.15 Aged concrete block specimen: (a) left side view, (b) front view, (c) right side view, (d) top view, and (e) control location.

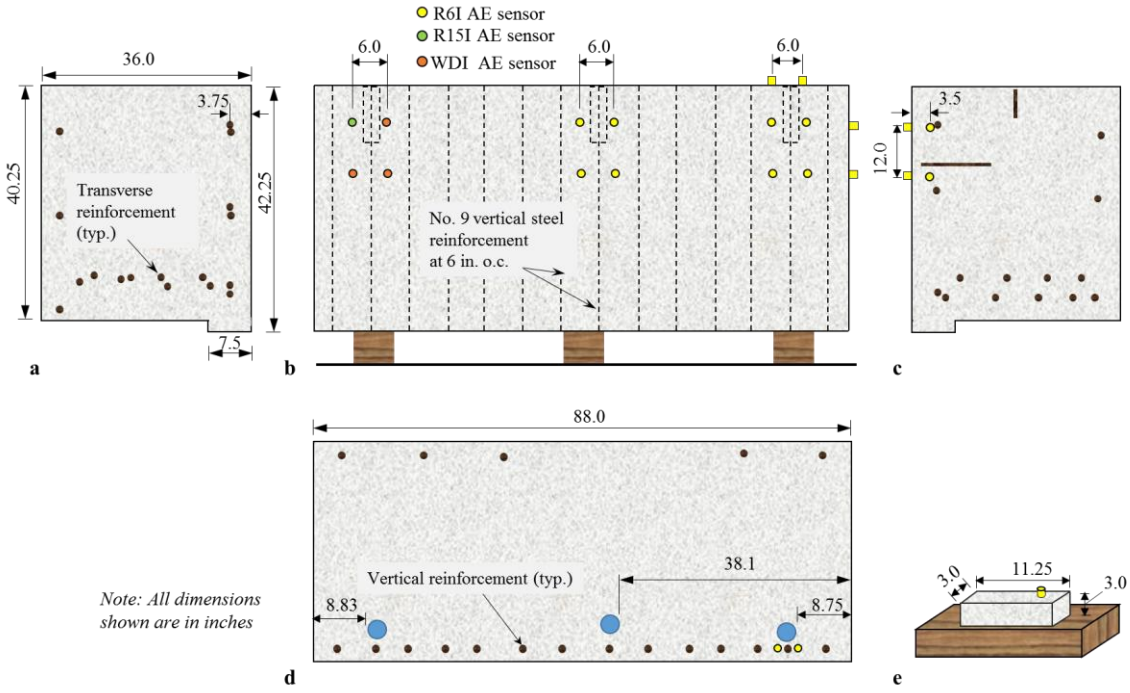

Figure 5.16 Schematic of aged reactor concrete test block: (a) left side view, (b) front view, (c) right side view, (d) top view, and (e) control location.

Table 5.3 ASTM corrosion for Cu-CuSO4 reference electrode (ASTM C876, 2009).

Potential Against Cu-CuSO4 Electrode	Corrosion Condition
> – 200 mV	Low Risk (10% probability of corrosion)
– 200 to – 350 mV	Intermediate corrosion risk
< – 350 mV	High corrosion risk (90% probability)
< – 500 mV	Severe corrosion damage

5.6 RESULTS AND DISCUSSION: ACCELERATED CORROSION TESTING OF THE REACTOR CONCRETE BLOCK

5.6.1 Electrochemical measurements

Initial electrochemical measurements, half-cell potential, were taken prior to initiation of the conditioning period. These measurements indicated a passive state of the steel reinforcement. The NaCl solution was then placed in the cored areas on December 2, 2015 and electrochemical readings were recorded weekly thereafter. As shown in Figure 5.17, three weeks after conditioning, half-cell potential values were observed to be more negative than -350 mV (referred to as the corrosion threshold) at all three locations. At the conclusion of the wet/dry cycles, half-cell potential readings indicated high corrosion risk in one of the three locations (0.25 in. cover location) and severe corrosion damage (more negative than -500 mV) in the other two locations (0.125 in. and 1.0 in. cover locations). The 1.0 in. cover location is known to have leakage associated with it as the NaCl solution drained continuously from this location from the commencement of the testing. While chloride diffusion is often assumed to be the primary initiator of corrosion damage, the presence of cracking in the concrete matrix may have a more profound effect on corrosion in some instances. The 0.125 in. cover and the 0.25 in. cover locations did not experience

similar issues with leakage. The bottom of the hole at the 1.0 in. cover location was sealed with epoxy in the first week of April, 2015.

Figure 5.18 shows linear polarization resistance results at the three locations with a logarithmic fit of the data points. The x-axis in Figure 5.18 represents the number of days after the solution was placed in the cored areas (initiated on December 2, 2014). The results indicate that all locations had relatively high corrosion rates as the polarization resistance was less than 100 ohms (ElBatanouny et al., 2014a). As seen in the figure, data was not collected between December 24, 2014 and February 19, 2015 (between 22 and 79 days) due to a malfunction with the potentiostat/galvanostat cable over that time period. This was addressed and the testing was resumed after February 29, 2015. Because these readings are taken weekly over a time span of 300 days, and due to the instantaneous nature of the readings, trends in the data set are more important than readings taken on a particular day. Therefore, trend lines with both upper and lower estimates are shown in the figures. A statistical method was used to eliminate outliers with low values to obtain the upper estimate and eliminate outliers with high values to obtain the lower estimate.

5.6.2 Detection of Damage using Acoustic Emission

Figure 5.19 shows the acoustic emission activity, in terms of amplitude versus time, recorded at locations monitored with resonant sensors (the 1.0 in. concrete cover location, the 0.125 in. concrete cover location, and the control location which initiated on May 27, 2015). Figure 5.20 shows the acoustic emission activity recorded using broadband sensors at the 0.25 in. concrete cover location. The data shown in Figure 5.19 and Figure 5.20 was filtered using the data filters discussed in Table 5.2. An unusual amount of data that had characteristics related to electromagnetic interference was continually collected at the

control location, potentially due to damage in the sensor or cable during the removal and re-installation process. RMS and Duration data rejection limits were developed and were able to delete the majority of the false data without affecting data collected from other locations.

As seen in Figure 5.19 and Figure 5.20, acoustic emission activity at the 1.0 in. concrete cover location and the 0.125 in. concrete cover location was higher than the acoustic emission activity at the 0.25 in. concrete cover location. This is attributed to the inherently higher sensitivity of the resonant sensors. It is noted that the rate of activity recorded at 1.0 in. concrete cover location decreased during wet days after sealing the bottom of the hole.

To reduce the possibility of contaminating the acoustic emission data set with unrelated data generated from ongoing work in the University of South Carolina Structures and Materials Laboratory, the acoustic emission data acquisition system was intentionally paused on several occasions. Significant pauses in data acquisition are shown in the figures. A video camera monitoring system was utilized to cross-verify and to aid in the development of data filters that are specific to ongoing work in the laboratory environment.

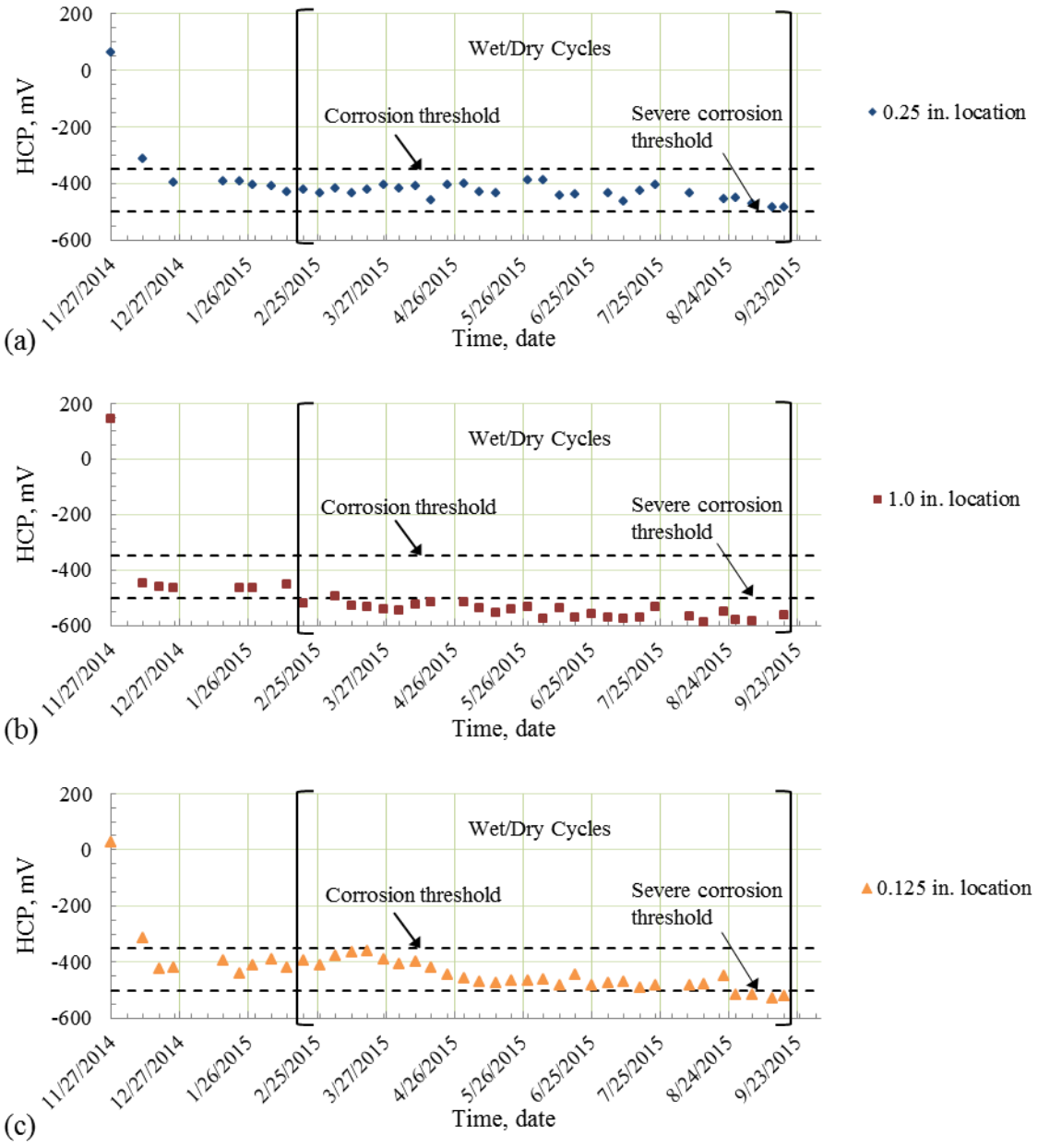

Figure 5.17 Half-cell potential measurements at: (a) 0.25 inch concrete cover location, (b) 1.0 inch concrete cover location, and (c) 0.125 inch concrete cover locations.

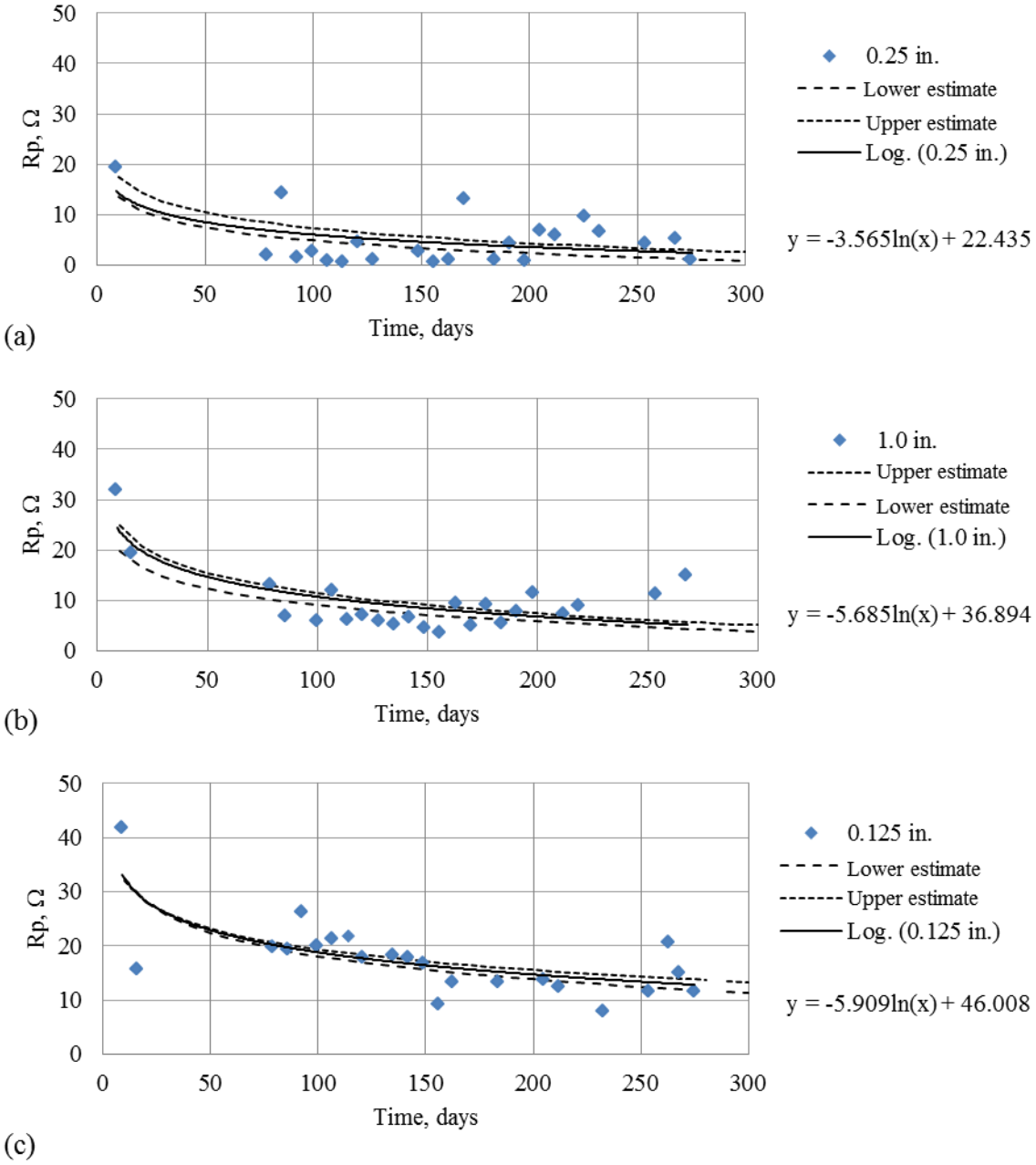

Figure 5.18 Linear polarization resistance (LPR) measurements at: (a) 0.25 inch concrete cover location, (b) 1.0 inch concrete cover location, and (c) 0.125 inch concrete cover location.

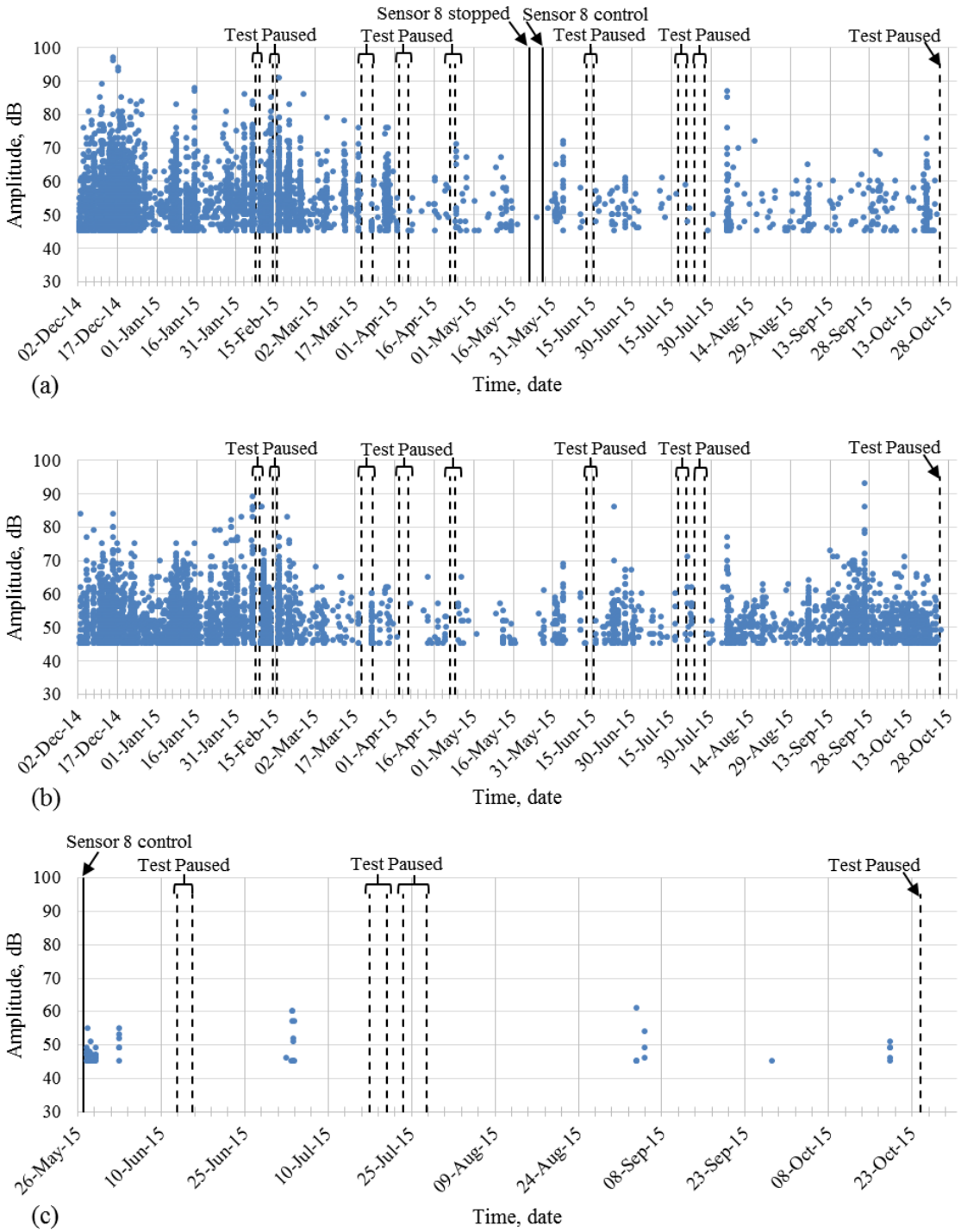

Figure 5.19 AE data recorded from resonant sensors on the reactor concrete block specimen: (a) 1.0 inch concrete cover location, (b) 0.125 inch concrete cover location, and (c) control location.

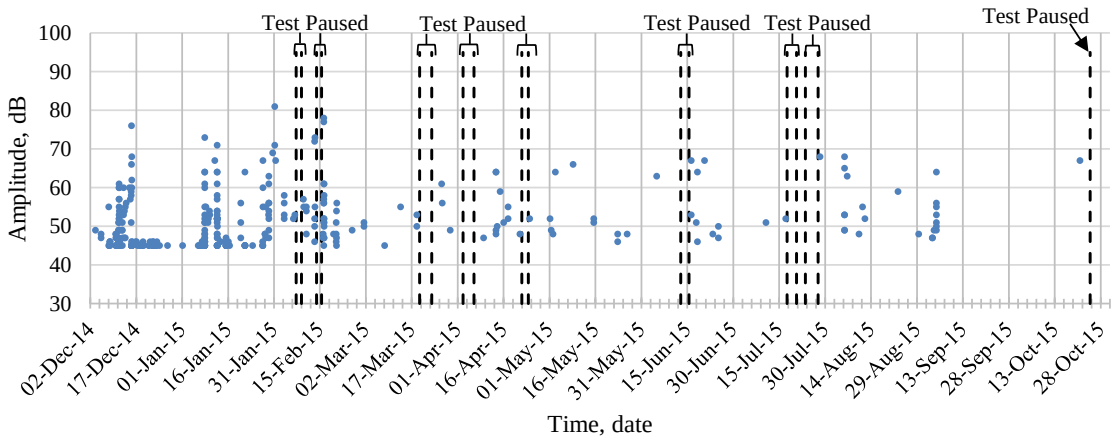

Figure 5.20 AE data recorded from broadband sensors on the reactor concrete block specimen at the 0.25 inch concrete cover location.

Figure 5.21 shows cumulative signal strength versus time at locations monitored using resonant sensors. It can be seen from this figure that cumulative signal strength increases rapidly at the beginning of the test, corresponding to a period of rapid damage growth associated with corrosion initiation, enters a dormant period, and then increases slightly near the end of the testing period for the 1.0 inch and 0.125 inch locations. This trend in the data mirrors a trend noticed in the linear polarization resistance plots. The magnitude of the cumulative signal strength is greater for the 1.0 inch location when compared to the 0.125 inch location, which indicates increased acoustic emission activity and therefore increased damage growth at the 1.0 inch location. This is consistent with the electrochemical readings at this location and may be attributable to the presence of cracking in this location. The control location has minimal cumulative signal strength magnitude as would be expected. The relatively low cumulative signal strength magnitude at the control location demonstrates that unwanted acoustic emission data caused by ongoing laboratory activities in the vicinity of the test block specimen were minimized in the data sets.

The broadband sensor data shows a similar trend of rapidly increasing damage early in the testing period, followed by a relatively dormant period at the 0.25 in. location, as shown in Figure 5.22. The magnitude of cumulative signal strength from the broadband sensors is lower in comparison to the resonant sensors, as is expected due to the lower sensitivity of the broadband sensors.

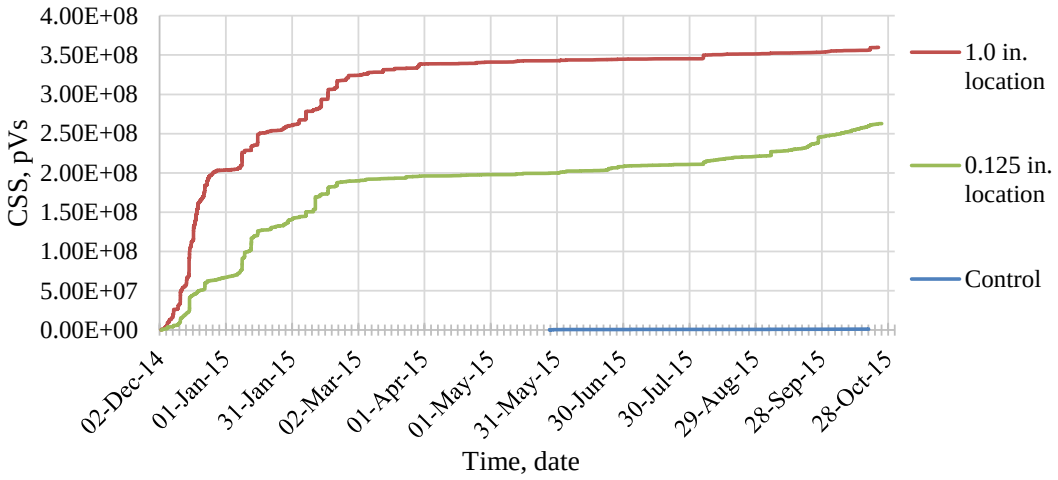

Figure 5.21 Cumulative signal strength from resonant sensors on the aged concrete block specimen.

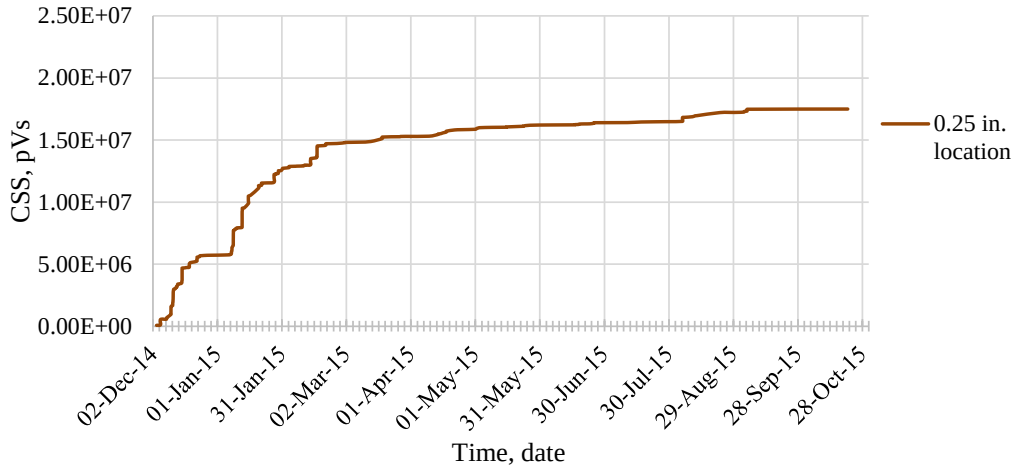

Figure 5.22 Cumulative signal strength versus time from broadband sensors on the aged concrete block specimen.

Figure 5.23 and Figure 5.24 show the Intensity Analysis results calculated at each location. The estimation of initial damage for the aged concrete block specimen, based on visual inspection and electrochemical results, was located near the border between the 'no damage' region and the 'depassivation' region of the chart. For the control location, a lower initial damage state was used since no corrosion damage is expected in this specimen. AE activity from the resonant sensors at the 1.0 in. concrete cover location progressed from the initial state to the severe damage zone over the duration of the monitoring period. AE activity from the resonant sensors at the 0.125 in. concrete cover location progressed from the initial state to the border of the cracking and severe damage zones. For the broadband sensors at the 0.25 in. concrete cover location, acoustic emission activity progressed from the initial state to the border of the cracking and severe damage zones.

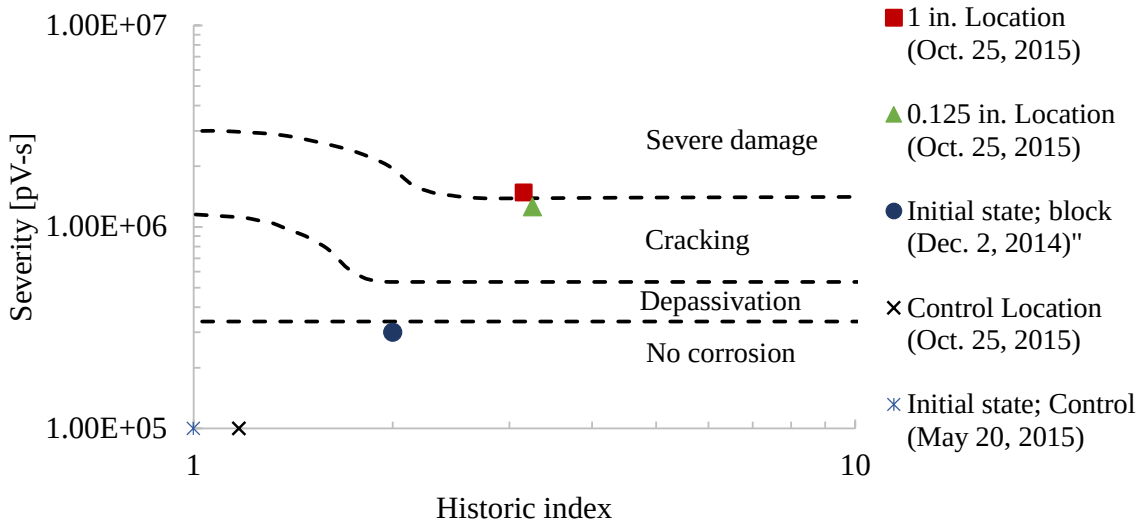

Figure 5.23 Intensity Analysis for resonant sensors on reactor concrete block specimen.

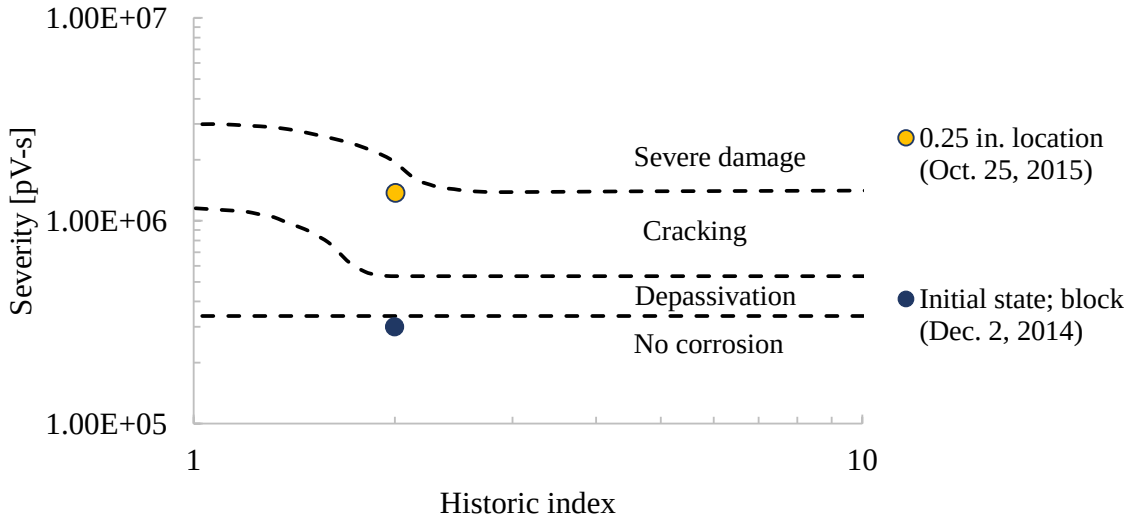

Figure 5.24 Intensity Analysis for broadband sensors on reactor concrete block specimen.

The above results are indicative of cracking in the concrete matrix due to corrosion activity at all three locations. As with the electrochemical measurements, the acoustic emission activity indicated that the most severe damage occurred at the 1.0 inch concrete cover location. As mentioned above, this location is affected by cracking as noticed through leakage of the NaCl solution at this location. While many degradation models for reinforced concrete are based on diffusion and therefore do not directly address the presence of cracking in the matrix, the effect of cracking in the matrix may nonetheless be significant. Similarly, many models assume a homogeneous concrete matrix. The lack of homogeneity in the concrete matrix for actual structures, such as the concrete test block, may also play a significant role in the results.

5.6.3 Potential Approach for Service life Predication

Many approaches are available in the literature for the prediction of remaining service life based on corrosion damage. In some cases, the end of functional service life is defined as first surface cracking due to corrosion activity (Maaddawy and Soudki, 2007).

Prediction of first surface cracking is considered to be overly conservative for an application such as 105-C, where the structure is no longer in use and has been decommissioned.

The approach taken for this investigation is based on calculations of the reduction in steel reinforcement cross-sectional area due to corrosion damage. Once the reduction in cross-sectional area is estimated, its effect on the load capacity of the member can be calculated. Service life prediction can then be performed based on this information combined with an agreed upon value of reduction in cross-section corresponding to the end of service life.

To perform this process a particular corrosion deterioration model must be adopted. A commonly referenced model is that presented by Tuutti (1982) which consists of two main phases; a) initiation period where chlorides permeate the concrete cover until chloride concentration around the steel reaches the corrosion initiation threshold, and b) a corrosion propagation period as shown in Figure 5.25.

Commercial software packages focusing on prediction of service life using time to corrosion initiation are available, for example Life-365 and STADIUM (Software for Transport and Degradation in Unsaturated Materials). Both software packages can be used to predict the initiation period based on concrete properties and exposure conditions; making use of diffusion models to predict initiation of chloride induced corrosion. These software packages were not utilized in this investigation as corrosion was accelerated and, based on HCP measurement, corrosion initiated within the first three weeks of exposure.

Prediction of remaining service life once corrosion initiates (the propagation phase) is not covered in either software package. For bridges, as a reference, Tuutti's

recommendations for time of corrosion propagation up to failure are 5 to 10 years for chloride initiated corrosion and 10 to 20 years for carbonation initiated corrosion.

For corrosion propagation, Andrade et al. (1990) employed Tuutti's conceptual model to estimate the loss in reinforcing bar cross section during the propagation period as shown in Equation 5.3.

$$\theta(t) = \theta_i - 0.023 * i_{corr} * t \qquad (5.3)$$

where;

$\theta(t)$: the rebar diameter at time t (mm)

θ_i: the initial diameter of the rebar (mm)

i_{corr}: the corrosion current density or corrosion rate ($\mu A/cm^2$)

t: the time after the beginning of the propagation period (years)

0.023: The conversion factor of $\mu A/cm^2$ into mm/year

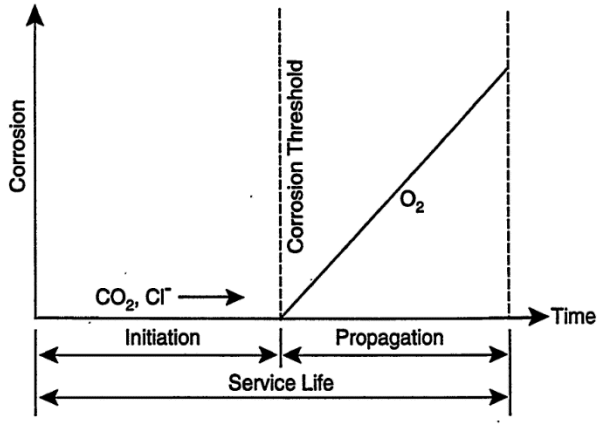

Figure 5.25 Schematic representation of conceptual model of corrosion of steel reinforcement in concrete (Tuutti, 1982).

To demonstrate one approach that may be used for prediction of service life based on corrosion damage, Equation 5.3 was used to estimate the reduction in cross-sectional area of the steel reinforcement in the aged concrete block specimen. The initial diameter

of the vertical reinforcing bar in the concrete block is equal to 1.128 inches (No. 9 bar) with initial cross sectional area of 1.0 in^2. The corrosion current, I_{corr}, was calculated from the linear polarization measurements using Equation 5.4, where B is a constant equal to 26 for the active corrosion condition. The corrosion current density, i_{corr}, was calculated by assuming a corroding surface area of the steel reinforcement.

$$R_p = \frac{\Delta E}{\Delta i} = \frac{b_a \times b_c}{2.303 \times I_{corr}(b_a + b_c)} = \frac{B}{I_{corr}} \qquad (5.4)$$

This approach for calculating the reduction in cross-sectional area of steel reinforcement involves a number of assumptions:

1. Uniform corrosion around the steel rebar surface; meaning no pitting or localized corrosion
2. Constant corrosion rate once corrosion has initiated
3. Linear relationship between the loss in rebar diameter and corrosion rate
4. No loss in rebar diameter during the initiation process
5. The corroding surface area of the steel rebar must be assumed to obtain i_{corr}. For this study, the corroding surface area is assumed to be equal to the perimeter of the reinforcing bar multiplied by a length of 3 inches (this is equal to the depth of the NaCl solution during the wet days in the wet/dry cycles).
6. The initiation period in this study was assumed to be 16 days which corresponds to half-cell potential measurements indicating 90% probability of corrosion activity at all three cored locations.

To obtain representative corrosion rate values the weekly linear polarization measurements were used to develop an equation to model the trends at each location; as shown in Figure 5.18. Given the inherent variability in linear polarization measurements a

statistical approach was used to exclude outliers in the data and obtain upper and lower estimates for the LPR results. The equations of the trend lines were used to obtain upper and lower estimates for the corrosion rate and sectional area loss at each of the three cored locations.

The vertical reinforcing bars diameters at September 17, 2015 (the last day of wet/dry cycles) for the three cored locations were estimated using the trend lines equations calculated at each location. The corresponding estimated cross-sectional areas of the vertical steel reinforcing bars are shown in Table 5.4. The 0.25 inch concrete cover location had the highest estimated loss in reinforcing bar cross-sectional area (11% loss, based on all LPR data points) and the 0.125 inch cover location had the lowest estimated loss (3% loss, also based on all LPR data points).

The estimated number of years needed for the reinforcing bar cross-sectional area to reach 50% of its initial value was calculated for the three cored locations, with the results shown in Table 5.5. The calculation procedure is based on the assumptions listed above, including a constant corrosion rate after September 17, 2015.

The values shown in Table 5.4 and Table 5.5 provide insight into procedures that may be utilized to estimate cross-sectional area loss due to corrosion activity based on electrochemical measurements. The test period available to accelerate the corrosion process was significant but was not in the range that would be ideal to establish reliable trends in the electrochemical measurements. Therefore, a longer test period is recommended. The time associated with the longer testing period is dependent on the rate of the corrosion process. A reasonable estimate based on the data available is between one to two additional years of wet/dry cycles.

Table 5.4 Estimated reinforcement cross sectional area as percentage of the initial value (after 289 days of conditioning)

	Estimated remaining cross sectional area (%)		
	0.25 inch location	1.0 inch location	0.125 inch location
Lower estimate	83	93	97
Upper estimate	91	95	97
All data	89	94	97

Table 5.5 Estimated number of years to reach 50% loss of cross-sectional area.

	Estimated number of years to reach 50% sectional area loss		
	0.25 inch location	1.0 inch location	0.125 inch location
Lower estimate	0.6	3.3	10.0
Upper estimate	2.1	4.5	11.3
All data	1.7	3.9	11.3

5.7 SUMMARY AND CONCLUSIONS

This investigation explores the implementation of acoustic emission monitoring as a remote structural assessment method. Acoustic emission systems were used to monitor corrosion damage and cracking in a decommissioned nuclear reactor facility as well as to monitor corrosion damage in a concrete block cut from the nuclear facility in laboratory conditions. The monitoring period in this study extended to approximately one year.

The study showed that long-term remote monitoring of ongoing damage in large scale existing structures is feasible using acoustic emission systems. For the wired system, AC power and cellular network connection are required for successful operation of the system. No major issues were encountered in terms of electromagnetic interference with

the sensors, external noise and remote monitoring and data transfer. The wireless system used has the potential to be used with solar power paired with cellular connection for the remote monitoring which makes this approach well suited for long-term monitoring efforts. However, adequate protection to the electrical components is required especially in humid environments, as illustrated by the failure of the data acquisition laptop due to moisture damage.

For the Reactor Building 105-C Crane Maintenance Area, the acoustic emission activity recorded at the 'vertical column to roof interface location' and 'horizontal beam location' varied throughout the monitoring period and tended to be associated with seasonal temperature fluctuations. The acoustic emission activity recorded at the 'control location' was significantly less when compared to the activity from the other two locations. Intensity Analysis was used to quantify the damage progression over the course of the monitoring period for both the broadband and resonant sensor types. The results of this method were in agreement with visually observed distress in the monitored locations. The assessed condition of the actively corroding areas progressed from the assumed condition of 'no corrosion/approaching depassivation' to 'severe damage' over the monitoring period while no change was observed in the state of the control location. It is noted that the assessed condition based on Intensity Analysis progressed to 'cracking/severe damage' within the first two months of monitoring. This shows the feasibility of this technique to successfully qualify active corrosion damage in structures in relatively small monitoring periods.

For the Reactor Building 105-C +48 level, the acoustic emission activity at the +48 location also varied with seasonal temperature fluctuations. This area contained a vertical

crack in the exterior wall and it is possible that crack growth or friction between surfaces of this crack was the cause of much of the acoustic emission activity. Source location was carried out at this location and events were located in the vicinity of the vertical crack which shows the feasibility of acoustic emission to detect and locate ongoing damage from cracking given that appropriate data filters are used.

For the Aged Concrete Test Block, both electrochemical results and acoustic emission cumulative signal strength versus time indicated that the corrosion activity occurred primarily during the first three to four months of conditioning and then continued at a reduced rate. Intensity Analysis based on the acquired data indicated that damage progressed from the assumed initial condition of 'no corrosion/approaching depassivation', determined based on electrochemical results upon arrival at the laboratory, to 'cracking/severe damage' over the monitoring period for all three locations and for both sensor types. This Intensity Analysis result is similar to that reported for the 'vertical column to roof interface location'.

One of the main areas that hinder wide implementation of structural health monitoring systems is the large amounts of data that is collected and the subsequent effort needed to interpret and analyze this data in order to produce meaningful assessment of the condition of the structures. An important contribution of this study is that it proved the ability of well-developed data reduction and damage assessment algorithms to provide accurate evaluation of the condition of the structures. The results of the study showed that the developed filtering techniques along with the Intensity Analysis chart used for corrosion damage classification were able to successfully qualify the damage in the monitored areas. These methods can be easily programed and used to provide meaningful

information to facility managers without the need of further assessment of large data sets. This can subsequently help in maintenance planning and prioritization especially in large scale and complex infrastructure systems.

5.8 REFERENCES

Abdelrahman, M., ElBatanouny, M., and Ziehl, P. (2014). Acoustic Emission Based Damage Assessment Method for Prestressed Concrete Structures. Engineering Structures, Vol. 60, pp. 258 – 264.

Abdelrahman, M., ElBatanouny, M., Ziehl, P., Fasl, J., Larosche, C., and Fraczek, J. (2015). Classification of Alkali–Silica Reaction Damage using Acoustic Emission: A Proof-of-Concept Study. Construction and Building Materials, Vol. 95, pp. 406-413.

Abdelrahman, M., ElBatanouny, M., Serrato, M., Dixon, K., Larosche, C., and Ziehl, P. (2016). Classification of Alkali-Silica Reaction and Corrosion Distress Using Acoustic Emission. In 42nd Annual Review of Progress in Quantitative Nondestructive Evaluation: Incorporating the 6th European-American Workshop on Reliability of NDE (Vol. 1706, p. 140001). AIP Publishing.

Andrade, C., Alonso, M.C., Gonzalez, J.A. (1990). An Initial Effort to Use Corrosion Rate Measurements for Estimating Rebar Durability Corrosion Rates of Steel in Concrete. ASTM STP 1065, N.S. Berke et al. editors. ASTM, Philadelphia 1990, 29-37.

Appalla, A., ElBatanouny, M., Velez, W., and Ziehl, P. (2015). Assessing Corrosion Damage in Post-Tensioned Concrete Structures using Acoustic Emission. Journal of Materials in Civil Engineering, 04015128, pp. 10.

Assouli, B., Simescu, F., Debicki, G., and Idrissi, H. (2005). Detection and Identification of Concrete Cracking during Corrosion of Reinforced Concrete by Acoustic

Emission Coupled to the Electrochemical Techniques. NDT & E International, 38(8), pp. 682-689.

ASTM C876-09. (2009). Standard Test Method for Half-Cell Potentials of Uncoated Reinforcing Steel in Concrete. ASTM International, West Conshohocken, PA, pp. 1-8.

ASTM E1316-16a. (2016). Standard Terminology for Nondestructive Examinations. ASTM International, West Conshohocken, PA, pp.1-38.

ASTM E2374-15. (2015). Standard Guide for Acoustic Emission System Performance Verification. ASTM International, West Conshohocken, PA, pp. 1-5.

ASTM E2075/E2075M-15. (2015). Standard Practice for Verifying the Consistency of AE-Sensor Response Using an Acrylic Rod. ASTM International, West Conshohocken, PA, pp. 1-5.

Braverman, J.I., Xu, J., Ellingwood, B.R., Costantino, C.J., Morante, R.J., and Hofmayer, C.H. (2007). Evaluation of the Seismic Design Criteria in ASCE/SEI Standard 43-05 for Application to Nuclear Power Plants. U.S. Nuclear Regulatory Commission, Job Code N6112, pp. 1-73.

Clifton, J. F. (1991). Predicting the remaining service life of concrete. No. NISTIR--4712. National Inst. of Standards and Technology, Gaithersburg, Maryland (United States), Center for Atomic, Molecular and Optical Physics.

Di Benedetti, M., Loreto, G., Matta, F., and Nanni, A. (2013). Acoustic Emission Monitoring of Reinforced Concrete under Accelerated Corrosion. Journal of Materials in Civil Engineering, 10.1061/(ASCE)MT.1943¬5533.0000647,pp. 1022-1029.

Dunn, S. E., Young, J. D., Hartt, W. H., and Brown, R. P. (1984). Acoustic Emission Characterization of Corrosion Induced Damage in Reinforced Concrete. Corrosion, 40(7), 339-343.

ElBatanouny, M., Mangual, J., Ziehl, P., and Matta, F. (2014a). Early Corrosion Detection in Prestressed Concrete Girders Using Acoustic Emission. Journal of Materials in Civil Engineering, 26(3), pp. 504– 511.

ElBatanouny, M., Ziehl, P., Larosche, A., Mangual, J., Matta, F., and Nanni, A. (2014b). Acoustic Emission Monitoring for Assessment of Prestressed Concrete Beams. Construction and Building Materials, Vol. 58, pp. 46-53.

Fournier, B., Berube, M. A., Folliard, K. J., and Thomas, M. (2010). Report on the Diagnosis, Prognosis, and Mitigation of Alkali-Silica Reaction (ASR) in Transportation Structures (No. FHWA-HIF-09-001).

Fowler, T., Blessing, J., Conlisk, P., Swanson, T.L. (1989). The MONPAC system. Journal of Acoustic Emission, V.8, No. 3, pp.1–8.

Golaski, L, Gebski, P., and Ono, K. (2002). Diagnostics of Concrete Bridges by Acoustic Emission. Journal of Acoustic Emission, Vol. 20, 83-98.

Kojima, F. (2009). Structural Health Monitoring of Nuclear Power Plants using Inverse Analysis in Measurements. MFPT.

Li, Z., Zudnek, A., Landis, E., and Shah, S., (1998). Application of Acoustic Emission Technique to Detection of Reinforcing Steel Corrosion in Concrete. ACI Materials Journal, 95(1), pp. 68-76.

Maaddawy, T., and Soudki, K. (2007). A Model for Prediction of Time from Corrosion Initiation to Corrosion Cracking. Cement and Concrete Composites, 29(3):168-175.

Mangual, J., ElBatanouny, M., Ziehl, P., and Matta, F. (2013a). Acoustic-Emission-Based Characterization of Corrosion Damage in Cracked Concrete with Prestressing Strand. ACI Materials Journal, V. 110, No. 1, pp. 89-98.

Mangual, J., ElBatanouny, M., Ziehl, P., and Matta, F. (2013b). Corrosion Damage Quantification of Prestressing Strands Using Acoustic Emission. Journal of Materials in Civil Engineering, 25(9), pp. 1326–1334.

Nair, A., and Cai, C.S., (2010). Acoustic Emission Monitoring of Bridges: Review and Case Studies. Engineering Structures, 32(6), 1704-1714.

Nilsson, L.O., Sandberg, P., Poulsen, E., Tang, L., Andersen, A., Frederiksen, J.M. (2011). HETEK, a System for Estimation of Chloride Ingress into Concrete, Theoretical Background. Danish Technological Institute.

Ohtsu, M., and Tomoda, Y. (2008). Phenomenological Model of Corrosion on Process in Reinforced Concrete Identified by Acoustic Emission. ACI Materials Journal, 105, 194-199.

Ono, K. (2010). Application of Acoustic Emission for Structure Diagnosis. Konferencja Naukowa, pp. 317-341.

Pollock, A.A. (1986). Classical Wave Theory in Practical AE Testing. Progress in AE III, Proceedings of the 8th International AE Symposium, Japanese Society for Nondestructive Testing, pp. 708-721.

Tuutti, K. (1982). Corrosion of Steel in Concrete. Swedish Cement and Concrete Institute, Stockholm.

Vélez, W., ElBatanouny, M., Matta, F., and Ziehl, P. H. (2012). Assessment of Corrosion In Prestressed Concrete Piles In Marine Environment With Acoustic Emission. NACE International.

Vélez, W., Matta, F. and Ziehl, P. (2015). Acoustic Emission Monitoring of Early Corrosion in Prestressed Concrete Piles. Structural Control and Health Monitoring, 22: 873–887. doi: 10.1002/stc.1723.

Weng, M. S., Dunn, S. E., Hartt, W. H., and Brown, R. P. (1982). Application of Acoustic Emission to Detection of Reinforcing Steel Corrosion in Concrete. Corrosion, 38(1), 9-14.

Zdunek, A.D., Prine, D.W., Li, Z., Landis, E., and Shah, S. (1995). Early Detection of Steel Rebar Corrosion by Acoustic Emission Monitoring. No.16, Northwestern University Infrastructure Technology Institute.

CHAPTER 6

SUMMARY AND CONCLUSIONS

6.1 SUMMARY

AE monitoring is a promising technique that can be used to assess and evaluate damage in aging infrastructure. The current state of practice does not allow for full implementation due to uncertainties related to reliability of data interpretation. In this research, three studies were conducted to further the development of AE as a monitoring and damage assessment tool for infrastructure. The studies focused on addressing current gaps associated with AE monitoring by a) developing an innovative AE data filtering technique to differentiate between data from actual cracking events and data from wave reflections or spurious noise sources, and b) developing and applying damage assessment algorithms for evaluation of concrete degradation mechanisms in laboratory and field structures.

The first study was conducted to develop data reduction techniques to differentiate between AE signals related to damage (target AE signals) and other signals from noise or wave reflections (degraded signals). Artificial AE sources (pencil lead breaks) were used to generate the target AE signal dataset while wave reflections were used to form the degraded signal dataset. All tests were conducted on a medium-scale prestressed concrete specimen instrumented with ten AE sensors. Wavelet analysis was used to analyze the collected data in the time-frequency domain. The results showed that the characteristics of the target signals are different than those of the degraded signals in

terms of energy distribution. These results were used to develop four different criteria for data filtering. Following the development of the data reduction criteria, AE data collected from concrete cracking during load testing was used to validate the method. The use of the same filtering limits for the case of artificial source data and load testing data shows the potential of this approach to develop objective filters that can be automated, therefore increasing the potential reliability of assessment based on AE data.

The second study aimed to prove the feasibility of AE to detect ASR damage in concrete structures. ASR damage results in micro-cracks in the concrete matrix which can later extend into aggregates to develop visible damage. The test program included twelve ASR specimens and three control specimens. The ASR specimens were cast using reactive aggregate and elevated alkali content. All specimens were placed in a controlled environment with 100% relative humidity and a 100 ± 2 ^{0}F environment to accelerate damage while AE was continuously monitored. The specimens were conditioned for different periods up to one year and standard ASR measurements (length change and petrographic analysis) were recorded periodically. The results of this study showed that damage due to ASR was apparent in the AE data at early stages, and also after considerable degradation occurred. An acoustic emission Intensity Analysis chart for ASR damage classification was proposed by correlating AE results with petrographic examination. This chart can be used for health monitoring to enable proper identification of the extent of ASR damage.

The third study summarizes the results of AE monitoring of corrosion damage and thermal cracking in a decommissioned nuclear facility. Two AE systems were installed at different locations to monitor corrosion damage and thermal cracking in the structure for a

period of approximately one year. Previously developed data reduction and corrosion damage assessment algorithms were adapted for this application. A statistical technique was developed to extend the use of the damage assessment algorithm to the case of existing damage. This was performed through integration of the observed current state using other techniques as a prior in the algorithm. The results of the study showed the feasibility of AE to accurately assess existing and ongoing corrosion damage in the monitored locations. AE damage classification chart results indicated a condition of cracking/severe damage in the structure which was also indicated by concrete spalling that occurred during the monitoring period. This high level of damage was detected in the first two months of monitoring. Accelerated corrosion testing was also conducted on a concrete block cut from a similar nuclear facility. The results of this test reinforced the findings of the field study. In addition, an approach for estimating the sectional mass loss and predicting remaining service life was presented.

6.2 CONCLUSIONS

Several conclusions can be drawn from each of the studies:

- The characteristics or signature of AE signals associated with cracking and signals due to noise differ from one another. Wavelet based criteria were developed and proposed, based on tests using simulated cracking events and wave reflections, to enable reliable filtering of AE data.
- Results from the filtering study showed that higher data reduction was achieved using the developed wavelet based filters as compared to the commonly used Swansong II filtering approach. The wavelet based approaches eliminated a

significantly higher percentage of degraded signals and maintained a higher percentage of the signals of interest.

- Data collected from formation of cracks during a load test was used to verify the applicability of the developed filtering criteria. Significant data reduction was observed without losing the key information related to material response. The use of the same filtering limits for the case of artificial source data and load testing data shows the potential of this approach to develop more objective filters, thereby increasing reliability of the interpretation.
- The wavelet based filtering approach described in this study appears to hold potential for field applications as it is suited for real-time filtering, thereby enhancing the efficiency of data storage and transfer while also increasing the reliability of interpretation.
- Acoustic emission can be used to detect and classify ASR damage in concrete structures. This was shown by the filtering approach and damage classification chart developed to evaluate ASR damage in laboratory specimens and verified through more traditional means.
- A linear correlation was observed between AE measurements and ASR benchmarks, indicating the feasibility of the method to detect the rate of ASR distress. This can help evaluate the efficiency of ASR mitigation strategies by comparing the rate of AE activity before and after the mitigation for a prescribed duration.

- The results of the ASR study show that formation of micro-cracks in the concrete matrix due to concrete material degradation does not preclude the ability of AE to detect ongoing damage.
- AE is suitable for long-term, remote monitoring of concrete degradation in field structures. The data reduction and damage assessment algorithms simplified the analysis of the large datasets collected and can provide meaningful results after short periods of monitoring. This was shown through the results of a first-of-a-kind monitoring study where ongoing corrosion damage in a decommissioned nuclear reactor building was qualified using AE data collected for a period of one year.
- Daily temperature changes did not significantly affect the collected AE data while seasonal temperature changes caused slight variations in the collected AE data as indicated by the results of the field monitoring study. However, the effect of this variation does not appear to have impact on the damage classification algorithms as it is based on analysis of trends in the AE data over extended periods of time.
- A technique for inclusion of existing corrosion damage in AE based corrosion damage assessment algorithms was developed. This has significant importance for evaluation of damage in aging structures with known or estimated degrees of deterioration.
- Source location of damage was carried out at a location in the nuclear reactor where a vertical crack existed. AE events were located in the vicinity of the

vertical crack, indicating the potential of using AE data to detect and locate ongoing cracking provided that appropriate data filters are used.

- An approach for service life prediction during accelerated corrosion of a concrete block taken from similar nuclear reactor building was presented. This approach utilized linear polarization resistance and corrosion rate measurements to estimate the sectional mass loss in the reinforcing steel and incorporates this information for damage prognosis.

6.3 RECOMMENDATIONS AND FUTURE WORK

This research aimed to build-on and augment previous research conducted in the area of condition assessment and structural health monitoring using AE. Future research to enhance the findings of this study includes:

- The wavelet filtering criteria was developed and validated using data collected from artificial sources and cracking during load testing. The suitability of this approach for filtering data associated with low-level AE activity such as corrosion damage and alkali-silica reaction is unknown. This is especially true as the energy level and signal amplitude collected from low-level AE activity may be similar to that collected from wave reflections during load tests. Therefore, it is recommended to validate the proposed limits or propose new limits that are tied to the amount of energy detected in the AE signals.
- The ASR damage classification chart is based on limited data collected from controlled testing that included fifteen specimens. More data is needed to validate the proposed limits and extend the chart to include heavy ASR damage. Future studies should also investigate the implementation of the proposed

method in field conditions. The appropriateness of the developed data filters to omit noise in the AE dataset from environmental conditions in the field (such as rain or windborne debris) should also be investigated.

- AE was used to perform long-term, remote monitoring of corrosion damage in a decommissioned nuclear facility. A technique for inclusion of existing damage was developed and applied to the collected data. The results of this study showed the feasibility of AE to provide meaningful information regarding the state of damage in existing structures. Future studies are needed to verify and extend the proposed techniques to help with standardization of the method.

REFERENCES

Abdelrahman, M. (2013). Assessment of Damage in Concrete Structures Using Acoustic Emission. M.Sc. Thesis, University of South Carolina.

Abdelrahman, M., ElBatanouny, M., and Ziehl, P. (2014). Acoustic Emission Based Damage Assessment Method for Prestressed Concrete Structures. Engineering Structures, Vol. 60, pp. 258 – 264.

Abdelrahman, M., ElBatanouny, M., Ziehl, P., Fasl, J., Larosche, C., and Fraczek, J. (2015). Classification of Alkali–Silica Reaction Damage using Acoustic Emission: A Proof-of-Concept Study. Construction and Building Materials, Vol. 95, pp. 406-413.

Abdelrahman, M., ElBatanouny, M., Serrato, M., Dixon, K., Larosche, C., and Ziehl, P. (2016). Classification of Alkali-Silica Reaction and Corrosion Distress Using Acoustic Emission. In 42nd Annual Review of Progress in Quantitative Nondestructive Evaluation: Incorporating the 6th European-American Workshop on Reliability of NDE (Vol. 1706, p. 140001). AIP Publishing.

Aggelis, D.G., Shiotani, T., Momoki, S., and Hirama, A. (2009). Acoustic Emission and Ultrasound for Damage Characterization of Concrete Elements. ACI Materials Journal, 106(6), 509.

American Association of State Highway and Transportation Officials (AASHTO). (2012). Standard Practice for Determining the Reactivity of Concrete Aggregates and Selecting Appropriate Measures for Preventing Deleterious Expansion in New Concrete Construction. AASHTO PP 65-11, AASHTO, pp. 24.

Anastasopoulos, A,A,, Tsimogiannis, A.N., and Kouroussis, D.A. (2002). Pressure Vessel Evaluation with Pattern Recognition Acoustic Emission Data Analysis. Proc. EWGAE 2002, Vol. I, pp. 29.

Anastasopoulos, A. (2005). Pattern Recognition Techniques for Acoustic Emission Based Condition Assessment of Unfired Pressure Vessels. Journal of Acoustic Emission, 23, pp. 318-331.

Anay, R., Cortez, T., Jáuregui, D., ElBatanouny, M., Ziehl, P. (2015). On-Site Acoustic Emission Monitoring for Assessment of a Prestressed Concrete Double-Tee Beam Bridge without Plans. ASCE Journal of Performance of Constructed Facilities, 04015062, pp. 9.

Andrade, C., Alonso, M.C., Gonzalez, J.A. (1990). An Initial Effort to Use Corrosion Rate Measurements for Estimating Rebar Durability Corrosion Rates of Steel in Concrete. ASTM STP 1065, N.S. Berke et al. editors. ASTM, Philadelphia 1990, pp. 29-37.

Appalla, A., ElBatanouny, M., Velez, W., and Ziehl, P. (2015). Assessing Corrosion Damage in Post-Tensioned Concrete Structures using Acoustic Emission. Journal of Materials in Civil Engineering, 04015128, pp. 10.

Arumugam, V., Kumar, C.S., Santulli, C., Sarasini, F., and Stanley, A.J. (2013). Identification of Failure Modes in Composites from Clustered Acoustic Emission Data Using Pattern Recognition and Wavelet Transformation. Arabian Journal for Science and Engineering, 38(5), pp. 1087-1102.

Assouli, B., Simescu, F., Debicki, G., and Idrissi, H. (2005). Detection and Identification of Concrete Cracking during Corrosion of Reinforced Concrete by Acoustic Emission Coupled to the Electrochemical Techniques. NDT & E International, 38, pp. 682-9.

ASTM C1293-08b. (2008). Standard Test Method for Determination of Length Change of Concrete Due to Alkali-Silica Reaction. ASTM International, West Conshohocken, PA, pp. 1-7.

ASTM C876-09. (2009). Standard Test Method for Half-Cell Potentials of Uncoated Reinforcing Steel in Concrete. ASTM International, West Conshohocken, PA, pp. 1-8.

ASTM E976-10. (2010). Standard Guide for Determining the Reproducibility of Acoustic Emission Sensor Response, ASTM International, West Conshohocken, PA, pp. 1-7.

ASTM E1067/E1067M-11. (2011). Standard Practice for Acoustic Emission Examination of Fiberglass Reinforced Plastic Resin (FRP) Tanks/Vessels. ASTM International, West Conshohocken, PA, pp.1-15.

ASTM E1316-13c. (2013). Standard Terminology for Nondestructive Examinations. ASTM International, West Conshohocken, PA, pp.1-38.

ASTM E1316-16a. (2016). Standard Terminology for Nondestructive Examinations. ASTM International, West Conshohocken, PA, pp.1-38.

ASTM E2374-15. (2015). Standard Guide for Acoustic Emission System Performance Verification. ASTM International, West Conshohocken, PA, pp. 1-5.

ASTM E2075/E2075M-15. (2015). Standard Practice for Verifying the Consistency of AE-Sensor Response Using an Acrylic Rod. ASTM International, West Conshohocken, PA, pp. 1-5.

ASTM G59. (1997-Reapproved 2014). Standard Test Method for Conducting Potentiodynamic Polarization Resistance Measurements. ASTM International, West Conshohocken, PA, pp. 1-4.

Beattie, A. G. (2013). Acoustic Emission Non-Destructive Testing of Structures using Source Location Techniques. Sandia National Laboratories, Livemore, California.

Braverman, J.I., Xu, J., Ellingwood, B.R., Costantino, C.J., Morante, R.J., and Hofmayer, C.H. (2007). Evaluation of the Seismic Design Criteria in ASCE/SEI Standard 43-05 for Application to Nuclear Power Plants. U.S. Nuclear Regulatory Commission, Job Code N6112, pp. 1-73.

Broomfield, J.P., Rodriguez, J., Ortega, L.M. and Garcia, A.M. (1994). Corrosion Rate Measurements in Reinforced Concrete Structures by a Linear Polarization Device, In: R.E. Weyers (ed.) Symposium on Corrosion of Steel in Concrete, Special Publication: SP 151-9, pp.163.

Calabrese, L., Campanella, G., and Proverbio, E. (2010). Use of Cluster Analysis of Acoustic Emission Signals in Evaluating Damage Severity in Concrete Structures. J. Acoustic Emission, 28, pp. 129-141.

Calabrese, L., Campanella, G., and Proverbio, E. (2013). Identification of Corrosion Mechanisms by Univariate and Multivariate Statistical Analysis during Long Term Acoustic Emission Monitoring On a Pre-Stressed Concrete Beam. Corrosion Science, 73, pp. 161-171.

Chang, P.C., and Liu, S.C. (2003). Recent Research in Nondestructive Evaluation of Civil Infrastructures. ASCE Journal of Materials in Civil Engineering, 15(3), pp. 298-304.

Clifton, J. F. (1991). Predicting the remaining service life of concrete. No. NISTIR--4712. National Inst. of Standards and Technology, Gaithersburg, Maryland (United States), Center for Atomic, Molecular and Optical Physics.

Colombo, S., Main, I.G., and Forde, M.C. (2003). Assessing Damage of Reinforced Concrete Beam Using "b-value" Analysis of Acoustic Emission Signals. ASCE Journal of Materials in Civil Engineering; 15(3), pp. 280-286.

Daubechies, I. (1988). Orthonormal Bases of Compactly Supported Wavelets. Communications on pure and applied mathematics, 41(7), pp. 909-996.

Daubechies, I. (1992). Ten Lectures on Wavelets. Philadelphia: Society for Industrial and Applied Mathematics, Vol. 61, pp. 198-202.

Daubechies, I., Landau, H. J., & Landau, Z. (1994). Gabor Time-Frequency Lattices and the Wexler-Raz Identity. Journal of Fourier Analysis and Applications, 1(4), 437-478.

Deroo, F., Kim, J. Y., Qu, J., Sabra, K., & Jacobs, L. J. (2010). Detection of Damage in Concrete Using Diffuse Ultrasound. The Journal of the Acoustical Society of America, 127(6), 3315-3318.

Di Benedetti, M., Loreto, G., Matta, F., and Nanni, A. (2013). Acoustic Emission Monitoring of Reinforced Concrete under Accelerated Corrosion. Journal of Materials in Civil Engineering, 10.1061/(ASCE)MT.19435533.0000647, pp. 1022-1029.

Di Benedetti, M., Loreto, G., Matta, F., and Nanni, A. (2014). Acoustic Emission Historic Index and Frequency Spectrum of Reinforced Concrete under Accelerated Corrosion. Journal Materials in Civil Engineering, 10.1061/(ASCE)MT.1943-5533.0000954, 04014059.

Doan, D.D., Ramasso, E., Placet, V., Zhang, S., Boubakar, L., and Zerhouni, N. (2015). An Unsupervised Pattern Recognition Approach for AE Data Originating From Fatigue Tests on Polymer–Composite Materials. Mechanical Systems and Signal Processing, 64, pp. 465-478.

Donnell, K. M., Zoughi, R., & Kurtis, K. E. (2013). Demonstration of Microwave Method for Detection of Alkali–Silica Reaction (ASR) Gel in Cement-Based Materials. Cement and Concrete Research, 44, pp. 1-7.

Dunn, S. E., Young, J. D., Hartt, W. H., and Brown, R. P. (1984). Acoustic Emission Characterization of Corrosion Induced Damage in Reinforced Concrete. Corrosion, 40(7), pp. 339-343.

ElBatanouny, M., Mangual, J., Vélez, W., Ziehl, P., Matta, F., and Gonzalez-Nunez, M. (2012). Monitoring Corrosion in Prestressed Concrete Beams using Acoustic Emission Technique. SPIE Smart Structures/NDE, San Diego, California, March 11-15.

ElBatanouny, M., Mangual, J., Ziehl, P., and Matta, F. (2014a). Early Corrosion Detection in Prestressed Concrete Girders Using Acoustic Emission. Journal of Materials in Civil Engineering, 26(3), pp. 504– 511.

ElBatanouny, M., Ziehl, P., Larosche, A., Mangual, J., Matta, F., and Nanni, A. (2014b). Acoustic Emission Monitoring for Assessment of Prestressed Concrete Beams. Construction and Building Materials, Vol. 58, pp. 46-53.

ElBatanouny, M., Jones, M., and Ziehl, P. (2014c). Assessment of Alkali-Silica-Reaction using Acoustic Emission. 2014 International Congress on Advances in Nuclear Power Plants (ICAPP), Charlotte, North Carolina, April 6-9, pp.5.

ElBatanouny, M., Larosche, A., Mazzoleni, P., Ziehl, P. H., Matta, F., and Zappa, E. (2014d). Identification of Cracking Mechanisms in Scaled FRP Reinforced Concrete Beams using Acoustic Emission. Experimental Mechanics, V. 54, No. 1, pp. 69-82.

Ercolino, M., Farhidzadeh, A., Salamone, S., & Magliulo, G. (2015). Detection of Onset of Failure in Prestressed Strands by Cluster Analysis of Acoustic Emissions. Structural Monitoring and Maintenance, 2(4), pp. 339-355.

Eskridge, A.E., Klahorst, J.T., Klingner, R.E., and Kreger, M.E. (2005). Mitigation Techniques for In-Service Structures with Premature Concrete Deterioration: Synthesis Report. FHWA/TX-05/0-4069-3.

Flis, J., Sehgal, A., Li, D., KHO, Y.T., Sabotl, S., Pickering, H., Osseo-Assare, K., and Cady, P.D. (1992). Condition Evaluation of Concrete Bridges Relative to Reinforcement Corrosion, vol.2, method for measuring the corrosion rate of reinforcing steel, Natural Research Council, Washington, DC, SHRP-S/FR-92-104.

Fournier, B., Berube, M. A., Folliard, K. J., and Thomas, M. (2010). Report on the Diagnosis, Prognosis, and Mitigation of Alkali-Silica Reaction (ASR) in Transportation Structures (No. FHWA-HIF-09-001).

Fowler, T., Blessing, J., Conlisk, P., Swanson, T.L. (1989). The MONPAC system. Journal of Acoustic Emission, V.8, No. 3, pp.1–8.

Gallego, A., Gil, J.F., Castro, E., and Piotrkowski, R. (2007). Identification of Coating Damage Processes in Corroded Galvanized Steel by Acoustic Emission Wavelet Analysis. Surface and Coatings Technology, 201(8), pp. 4743-4756.

Ganesan, R., Das, T. K., and Venkataraman, V. (2004). Wavelet-based multiscale statistical process monitoring: A literature review. IIE transactions, 36(9), 787-806.

Ghorbanpoor, A., Borchelt, R., Edwards, M., and Abdel Salam, E. (2000). Magnetic-Based NDE of Prestressed and Post-Tensioned Concrete Members—The MFL System. Final Rep. No. FHWA-RD-00-026, Federal Highway Administration, Washington, DC.

Giannini, E. R., Folliard, K. J., Zhu, J., Bayrak, O., Kreitman, K., Webb, Z., and Hanson, B. (2013). Non-Destructive Evaluation of In-Service Concrete Structures Affected by Alkali-Silica Reaction (ASR) or Delayed Ettringite Formation (DEF)—Final Report, Part I (No. FHWA/TX-13/0-6491-1).

Godin, N., Huguet, S., Gaertner, R. and Salmon, L. (2004). Clustering of Acoustic Emission Signals Collected during Tensile Tests on Unidirectional Glass/Polyester Composite Using Supervised and Unsupervised Classifiers. NDT &E Int., 37(4), 253-264. DOI 10.1016/j.ndteint.2003.09.010

Golaski, L, Gebski, P., and Ono, K. (2002). Diagnostics of Concrete Bridges by Acoustic Emission. Journal of Acoustic Emission, Vol. 20, pp. 83-98.

Golaski, L., Swit, G., Kalicka, M., and Ono, K. (2006). Acoustic Emission Behavior of Prestressed Concrete Girder during Proof Loading. Journal of Acoustic Emission, 24, 187-196.

Gong, P., Patton, M. E., Greve, D. W., Harley, J. B., Liu, C., and Oppenheim, I. J. (2014a). Alkali-Silica Reaction (ASR) Detection in Concrete from Frequency Dependent Ultrasonic Attenuation. In 40th Annual Review of Progress in Quantitative Nondestructive Evaluation: Incorporating the 10th International Conference on Barkhausen Noise and Micromagnetic Testing (Vol. 1581, No. 1, pp. 909-916). AIP Publishing.

Gong, P., Patton, M. E., Greve, D. W., Harley, J. B., Junker, W. R., Liu, C., and Oppenheim, I. J. (2014b). ASR Damage Detection in Concrete from Ultrasonic Methods. In SPIE Smart Structures and Materials+ Nondestructive Evaluation and Health Monitoring (pp. 90610E-90610E). International Society for Optics and Photonics.

Grattan-Bellew, P.E., and Danay, A. (1992). Comparison of Laboratory and Field Evaluation of AAR in Large Dams, International Conference on Concrete AAR in Hydroelectric Plants and Dams. Canadian Electrical Association & Canadian National Committee of the Int. Commission on Large Dams, September 28 – October 2 1992, Fredericton, New Brunswick, (Canada), pp. 23.

Grattan-Bellew, P. E. (1995). Laboratory Evaluation of Alkali-silica Reaction in Concrete from Saunders Generating Station. ACI Material Journal, Vol. 92, No. 2, pp. 1–9.

Grosse, C. U., Finck, F., Kurz, J. H., and Reinhardt, H.W. (2004). Improvements of AE Technique Using Wavelet Algorithms, Coherence Functions and Automatic Data Analysis. Construction and building Materials, 18(3), pp. 203-213.

Grossmann, A., and Morlet, J. (1984). Decomposition of Hardy Functions into Square Integrable Wavelets of Constant Shape. SIAM journal on mathematical analysis, 15(4), pp. 723-736.

Gutkin, R., Green, C.J., Vangrattanachai, S., Pinho, S.T., Robinson, P., and Curtis, P.T. (2011). On Acoustic Emission for Failure Investigation in CFRP: Pattern Recognition and Peak Frequency Analyses. Mechanical Systems and Signal Processing, 25(4), pp. 1393-1407.

Hamdi, S.E., Le Duff, A., Simon, L., Plantier, G., Sourice, A., and Feuilloy, M. (2013). Acoustic Emission Pattern Recognition Approach Based on Hilbert–Huang Transform for Structural Health Monitoring in Polymer-Composite Materials. Applied Acoustics, 74(5), pp. 746-757.

Hashemi, A., Hatfield, S., Donnell, K.M., Kurtis, K.E., and Zoughi, R. (2014). Microwave NDE Method for Health-Monitoring Of Concrete Structures Containing Alkali-Silica Reaction (ASR) Gel. In Proc. 40th Annu. Rev. Prog. Quant. Nondestruct. Eval. Conf., Amer. Inst. Phys (Vol. 33, pp. 787-792).

Hinton, Y.L. (1999). Problems Associated with Statistical Pattern Recognition of Acoustic Emission Signals in a Compact Tension Fatigue Specimen.

Hossain, M.M. (2013). Acoustic Emission Source Characterization of Fatigue Crack Extension in Steel Bridge Material. (Doctoral dissertation). Retrieved from http://scholarcommons.sc.edu/etd/243.

Idrissi, H., and Limam, A. (2003). Study and characterization by acoustic emission and electrochemical measurements of concrete deterioration caused by reinforcement steel corrosion. NDT & E International, 36(8), 563-569.

Iliopoulos, S., Aggelis, D.G., Pyl, L., Vantomme, J., Van Marcke, P., Coppens, E., and Areias, L. (2015). Detection and Evaluation of Cracks in the Concrete Buffer of the Belgian Nuclear Waste Container Using Combined NDT Techniques. Construction and Building Materials, V. 78, pp. 369-378.

Jagasivamani, V. (2014). Investigation of Corrosion and Other Deterioration Effects in Highway Bridge Components Using Nondestructive Testing Technology of Acoustic Emission.

Jolliffe, I.T. (2002). Principal component analysis (2nd Edition), Springer, New York, NY.

Kaphle, M. R. (2012). Analysis of acoustic emission data for accurate damage assessment for structural health monitoring applications.

Kappatos, V., and Dermatas, E. (2009). Feature Selection for Robust Classification of Crack and Drop Signals. Structural health monitoring,8, 59-70.

Kawasaki, Y., Wakuda, T., Kobarai, T., and Ohtsu, M. (2013). Corrosion Mechanisms in Reinforced Concrete by Acoustic Emission. Construction and Building Materials, V. 48, pp. 1240-1247.

Kharrat, M., Ramasso, E., Placet, V., and Boubakar, L. (2014). Acoustic Emission in Composite Materials under Fatigue Tests: Effect of Signal-Denoising Input Parameters on the Hits Detection and Data Clustering. In 31st Conference of the European Working Group on Acoustic Emission (EWGAE).

Kharrat, M., Ramasso, E., Placet, V., and Boubakar, M. L. (2016). A signal processing approach for enhanced Acoustic Emission data analysis in high activity systems: Application to organic matrix composites. Mechanical Systems and Signal Processing, 70, 1038-1055.

Kojima, F. (2009). Structural Health Monitoring of Nuclear Power Plants using Inverse Analysis in Measurements. MFPT.

Komlos, K., Popovics, S., Nürnbergerova, T., Babal, B., and Popovics, J.S. (1996). Ultrasonic Pulse Velocity Test of Concrete Properties as Specified in Various Standards. Cement and Concrete Composites, 18(5), pp. 357-364.

Larosche, A., Ziehl, P., Mangual, J., and ElBatanouny, M. (2015). Damage Evaluation of Prestressed Piles to Cast in Place Bent Cap Connections with Acoustic Emission. Engineering Structures, V. 84, pp. 184–194.

Li, Z., Zudnek, A., Landis, E., and Shah, S., (1998). Application of Acoustic Emission Technique to Detection of Reinforcing Steel Corrosion in Concrete. ACI Materials Journal, 95(1), pp. 68-76.

Likas, A., Vlassis, N., and Verbeek, J. J. (2003). The global k-means clustering algorithm. Pattern recognition, 36(2), 451-461.

Loutas, T.H., Kostopoulos, V., Ramirez-Jimenez, C., and Pharaoh, M. (2006). Damage Evolution in Center-Holed Glass/Polyester Composites under Quasi-Static Loading using Time/Frequency Analysis of Acoustic Emission Monitored Waveforms. Composites science and technology, 66(10), pp. 1366-1375.

Lovejoy S. (2008). Acoustic Emission Testing of Beams to Simulate SHM of Vintage Reinforced Concrete Deck Girder Highway Bridges. Structural Health Monitoring 2008, Vol. 7, pp. 327-346.

Lu, C., Ding, P., and Chen, Z. (2011). Time-frequency analysis of acoustic emission signals generated by tension damage in CFRP. Procedia Engineering, 23, 210-215.

Ma, S., and Chen, X. (2015). The Acoustic Emission Signal Recognition based on Wavelet Transform and RBF Neural Network. International Journal of Grid and Distributed Computing, 8(2), 167-176.

Maaddawy, T., and Soudki, K. (2007). A Model for Prediction of Time from Corrosion Initiation to Corrosion Cracking. Cement and Concrete Composites, 29(3), pp.168-175.

Mallat, S.G. (1989). Multifrequency Channel Decompositions of Images and Wavelet Models. IEEE Transactions on Acoustics, Speech, and Signal Processing, 37(12), pp. 2091-2110.

Mallat, S.G. (1989). Multiresolution Approximations and Wavelet Orthonormal Bases of $L^2(R)$. Transactions of the American mathematical society, 315(1), pp. 69-87.

Mangual, J., ElBatanouny, M., Ziehl, P., and Matta, F. (2013a). Acoustic-Emission-Based Characterization of Corrosion Damage in Cracked Concrete with Prestressing Strand. ACI Materials Journal, V. 110, No. 1, pp. 89-98.

Mangual, J., ElBatanouny, M., Ziehl, P., and Matta, F. (2013b). Corrosion Damage Quantification of Prestressing Strands Using Acoustic Emission. Journal of Materials in Civil Engineering, 25(9), pp. 1326–1334.

Marec, A., Thomas, J. H., and El Guerjouma, R. (2008). Damage Characterization of Polymer-Based Composite Materials: Multivariable Analysis and Wavelet

Transform for Clustering Acoustic Emission Data. Mechanical Systems and Signal Processing, 22(6), pp. 1441-1464.

Martinez-Gonzalez, E., Picas, I., Romeu, J., and Casellas, D. (2013). Filtering of acoustic emission signals for the accurate identification of fracture mechanisms in bending tests. Materials Transactions, 54(7), 1087-1094.

McCrory, J. P., Al-Jumaili, S. K., Crivelli, D., Pearson, M. R., Eaton, M. J., Featherston, C. A., ... and Pullin, R. (2015). Damage classification in carbon fibre composites using acoustic emission: A comparison of three techniques. Composites Part B: Engineering, 68, 424-430.

Meyer, Y. (1986). Ondelettes Et Functions Splines, Séminaire Sur Les Équations Aux Dérivées Partielles. Exp. No. VI, École Polytechnique, Palaiseau.

Nair, A., and Cai, C.S., (2010). Acoustic Emission Monitoring of Bridges: Review and Case Studies. Engineering Structures, 32(6), pp. 1704-1714.

Nemati, N., Metrovich, B., and Nanni, A. (2015). Acoustic emission assessment of through-thickness fatigue crack growth in steel members. Advances in Structural Engineering, 18(2), 269-282.

Ni, Q. Q., and Iwamoto, M. (2002). Wavelet Transform of Acoustic Emission Signals in Failure of Model Composites. Engineering Fracture Mechanics, 69(6), pp. 717-728.

Nilsson, L.O., Sandberg, P., Poulsen, E., Tang, L., Andersen, A., Frederiksen, J.M. (2011). HETEK, a System for Estimation of Chloride Ingress into Concrete, Theoretical Background. Danish Technological Institute. Niri, E. D., Farhidzadeh, A., and Salamone, S. (2014). Nonlinear Kalman Filtering for acoustic emission source localization in anisotropic panels. Ultrasonics, 54(2), 486-501.

NRC IN 2011-20. (2011). Concrete Degradation by Alkali-Silica Reaction. Nuclear Regulatory Commission (NRC), Washington, DC, November 18.

Ohno, K., and Ohtsu, M. (2010). Crack Classification in Concrete Based On Acoustic Emission. Construction and Building Materials, 24(12), pp. 2339-2346.

Ohtsu, M. (1996). The History and Development of Acoustic Emission in Concrete Engineering. Magazine of concrete research, 48 (177), pp. 321-330.

Ohtsu, M., Uchida, M., Okamoto, T., & Yuyama, S. (2002). Damage Assessment of Reinforced Concrete Beams Qualified by Acoustic Emission. ACI Structural Journal, 99(4), pp. 411-417.

Ohtsu, M., and Tomoda, Y. (2008). Phenomenological Model of Corrosion on Process in Reinforced Concrete Identified by Acoustic Emission. ACI Materials Journal, 105, 194-199.

Ono, K., and Huang, Q. (1997). Pattern recognition analysis of acoustic emission signals. NDT and E International, 2(30), 109.

Ono, K. (2010). Application of Acoustic Emission for Structure Diagnosis. Konferencja Naukowa, pp. 317-341.

Pollock, A.A. (1986). Classical Wave Theory in Practical AE Testing. Progress in AE III, Proceedings of the 8th International AE Symposium, Japanese Society for Nondestructive Testing, pp. 708-721.

Pour-Ghaz, M., Spragg, R., Castro, J., and Weiss, J. (2012). Can Acoustic Emission be used to Detect Alkali Silica Reaction Earlier than Length Change Tests? 14th International Conference On Alkali Aggregate Reaction in Concrete, May 20-25, Austin, TX.

Qu, J., Bazant, Z., Jacobs, L., and Guimaraes, M. (2015). Nonlinear Ultrasonic Diagnosis and Prognosis of ASR Damage in Dry Cask Storage (No. 12--3736). Northwestern Univ., Evanston, IL (United States).

Ramadan, S., Gaillet, L., Tessier, C., and Idrissi, H. (2008). Detection of stress corrosion cracking of high-strength steel used in prestressed concrete structures by acoustic emission technique. Applied surface science, 254(8), 2255-2261.

Rioul O and Vetterli M. Wavelets and Signal Processing. IEEE Signal Proc Mag, 8 LCAV-article-1991-005, pp. 14-38.

Rivard, P., Fournier, B., and Ballivy, G. (2000). Quantitative Petrographic Technique for Concrete Damage Due to ASR: experimental and application. Cement, Concrete, and Aggregates, Vol. 22, No. 1, pp.63–72.

Rivard, P., Fournier, B. and Ballivy, G. (2002). The Damage Rating Index Method for ASR Affected Concrete – A Critical review of Petrographic Features of Deterioration and Evaluation Criteria. Cement, Concrete & Aggregates, Vol. 24, No. 2, pp. 1-11.

Sagasta, F. A., Torné, J. L., Sánchez-Parejo, A., and Gallego, A. (2013). Discrimination of Acoustic Emission Signals for Damage Assessment in a Reinforced Concrete Slab Subjected to Seismic Simulations. Archives of Acoustics, 38(3), pp. 303-310.

Sagasta, F., Benavent-Climent, A., Fernández-Quirante, T., and Gallego, A. (2014). Modified Gutenberg–Richter Coefficient for Damage Evaluation in Reinforced Concrete Structures Subjected to Seismic Simulations on a Shaking Table. Journal of Nondestructive Evaluation, 33(4), pp. 616-631.

Sansalone, M., and Street, W. (1995). Use of the Impact-Echo Method and Field Instrument for Non-Destructive Testing Of Concrete Structures. In International Symposium ND-Testing in Civil Engineering, Berlin, pp. 495-502.

Saouma, V.E., Perotti, L., and Shimpo, T. (2007). Stress Analysis of Concrete Structures Subjected to Alkali-Aggregate Reactions. ACI Structural Journal, V. 104, No. 5, pp. 532-541.

Sause, M. G. (2011). Investigation of Pencil-Lead Breaks as Acoustic Emission Sources. Journal of Acoustic Emission, 29, pp. 184-196.

Shrimer, F.H. (2000). Application and Use of Damage Rating Index in Assessment of AAR-Affected Concrete - Selected Case Studies. Proceedings of the 11thInternational Conference on Alkali-Aggregate Reaction in Concrete, Quebec City, Canada, Editors: M.A. Bérubé, B. Fournier and B. Durand, pp. 899-908.

Shrimer, F.H. (2006). Development of the Damage Rating Index method as a tool in the assessment of alkali–aggregate reaction in concrete: a critical review, Proc. MarcAndré Bérubé Symposium on AAR in Concrete, CANMET/ACI Advances in Concrete Technology Seminar, Montréal, Canada, pp. 391–411.

Stark, D., Morgan, B., and Okamoto, P. (1993). Eliminating or Minimizing Alkali-Silica Reactivity. Report No. SHRP-C-343.

Tabatabai H, Mehrabi AB and Yen W P. (1998). Bridge Stay Cable Condition Assessment using Vibration Measurement Techniques. SPIE 3400, Structural Materials Technology III: An NDT Conference, San Antonio, TX, pp.194–204.

Thomas, M.D.A., Fournier, B. and Folliard, K.J. (2009). Report on Determining the Reactivity of Concrete Aggregates and Selecting Appropriate Measures for Preventing Deleterious Expansion in New Concrete Construction. FHWA-HIF-09-001, Federal Highway Administration.

Thomas, M. D., Folliard, K. J., Fournier, B., Rivard, P., and Drimalas, T. (2013a). Methods for Evaluating and Treating ASR-Affected Structures: Results of Field Application and Demonstration Projects–Volume I: Summary of Findings and Recommendations (No. FHWA-HIF-14-0002).

Thomas, M. D., Folliard, K. J., Fournier, B., Rivard, P., Drimalas, T., and Garber, S. I. (2013b). Methods for Evaluating and Treating ASR-Affected Structures: Results of Field Application and Demonstration Projects–Volume II: Details of Field Applications and Analysis (No. FHWA-HIF-14-0003).

Tinkey, B.V., Fowler, T.J., and Klingner, R.E. (2002). Nondestructive Testing of Prestressed Bridge Girders with Distributed Damage. Research Report 1857-2, pp. 106.

Tuutti, K. (1982). Corrosion of Steel in Concrete. Swedish Cement and Concrete Institute, Stockholm.

Vélez, W., ElBatanouny, M., Matta, F., and Ziehl, P. H. (2012). Assessment of Corrosion In Prestressed Concrete Piles In Marine Environment With Acoustic Emission. NACE International.

Vélez, W., Matta, F. and Ziehl, P. (2015). Acoustic Emission Monitoring of Early Corrosion in Prestressed Concrete Piles. Structural Control and Health Monitoring, 22: 873–887. doi: 10.1002/stc.1723.

Videm, K. (1997). Instrumentation and Condition Assessment Performed on Gimsoystraumen Bridge" In: Aage Blankvoll (ed.), Proceedings of International Conference-Repair Of Concrete Structures, From Theory To Practice In A MarineEnviroment, pp.375 (Norway).

Weng, M.S., Dunn, S.E., Hartt, W. H., and Brown, R.P. (1982). Application of Acoustic Emission to Detection of Reinforcing Steel Corrosion in Concrete. Corrosion, 38(1), pp. 9-14.

Wijaya, I.G.P.S., and Kencanawati, N.N. Denoising Acoustic Emission Signal using Wavelet Transforms for Determining The Micro Crack Location Inside of Concrete. International Journal of Technology 5(3), pp. 259-268. ·

Williams, M., Choudhuri, D., and Perez, M. (2009). Managing Premature Concrete Deterioration in Bridges. In Structures Congress 2009: Don't Mess with Structural Engineers: Expanding Our Role, ASCE, pp. 1-6.

Yoon, D.J., Weiss, W.J., and Shah, S.P. (2000). Assessing Damage in Corroded Reinforced Concrete Using Acoustic Emission. Journal of engineering mechanics, 126(3), pp. 273-283.

Yu, Z., Ziehl, P., Zarate, B., and Caicedo, J. (2011). Prediction of Fatigue Crack Growth in Steel Bridge Components Using Acoustic Emission. Journal of Constructional Steel Research, 67, pp. 1254-1260.

Yu, J., Ziehl, P., Matta, F., and Pollock, A. (2013). Acoustic Emission Detection of Fatigue Damage in Cruciform Welded Joints. Journal of Constructional Steel Research, 86, 85-91.

Zdunek, A.D., Prine, D.W., Li, Z., Landis, E., and Shah, S. (1995). Early Detection of Steel Rebar Corrosion by Acoustic Emission Monitoring. No.16, Northwestern University Infrastructure Technology Institute.

Ziehl, P. (2008). Applications of Acoustic Emission Evaluation for Civil Infrastructure. SPIE Smart Structures and Materials and Nondestructive Evaluation and Health Monitoring, San Diego, CA, 9-13 March 2008, pp. 9.

Ziehl, P., Engelhardt, M., Fowler, T., Ulloa, F., Medlock, R., and Schell, E. (2009). Design and Live Load Evaluation of a Hybrid FRP/RC Bridge Superstructure System. ASCE Journal of Bridge Engineering, V. 14, No. 5, pp. 309-318.

Ziehl, P., and Pollock, A. (2012). Acoustic Emission, Chapter 1: Acoustic Emission for Civil Infrastructure, Intech (ISBN 979-953-307-372-8).

Ziehl, P. and ElBatanouny, M. 2015. Chapter 11: Low –Level Acoustic Emission (AE) in the Long Term Monitoring of Concrete. In: Ohtsu, M. ed. Acoustic Emission and Related Non-destructive Evaluation Techniques in the Fracture Mechanics of Concrete: Fundamentals and Applications, Woodhead Publishing, PP. 217- 236.

Zitto, M. E., Piotrkowski, R., Gallego, A., and Sagasta, F. (2012). AE Wavelet Processing In Dynamical Tests of a Reinforced Concrete Slab. J. Acoust. Emiss, 30, pp. 64-75.

Zitto, M. E., Piotrkowski, R., Gallego, A., Sagasta, F., and Benavent-Climent, A. (2015). Damage Assessed By Wavelet Scale Bands and b-Value in Dynamical Tests of a Reinforced Concrete Slab Monitored With Acoustic Emission. Mechanical Systems and Signal Processing, 60, pp. 75-89.

APPENDIX A – DISCRIMINATION BETWEEN LEAKAGE AND CORROSION DATA

This work was performed as part of the accelerated corrosion testing of the reactor concrete block discussed in Chapter 5. To investigate the potential of utilizing acoustic emission data to assess leakage through reinforced concrete structural systems such as those found in spent fuel pools, data was plotted for the 1 in. cover location over two separate 12 hour periods. This location is known to have leakage as demonstrated by drainage of the sodium chloride solution. The first 12 hour period investigated was early in the testing program, prior to the initiation of corrosion activity. The second 12 hour period investigated was during a dry period when leakage could not have occurred, but corrosion activity was still ongoing.

The first investigation of the data was focused on the evaluation of acoustic emission parameters. Typical parameters associated with acoustic emission waveforms include amplitude, duration, rise time, counts, average frequency, energy, signal strength, and others (acoustic emission terminology is defined in ASTM E1316). Data was plotted over each of the 12 hour periods mentioned above to enable direct comparisons.

Figure A.1 demonstrates the correlation between rise time and amplitude for the leakage and corrosion periods. From these plots it is clear that some overlap in rise time is present. However, rise time events exceeding 370 µ-seconds and amplitude less than 50 dB are associated with leakage only.

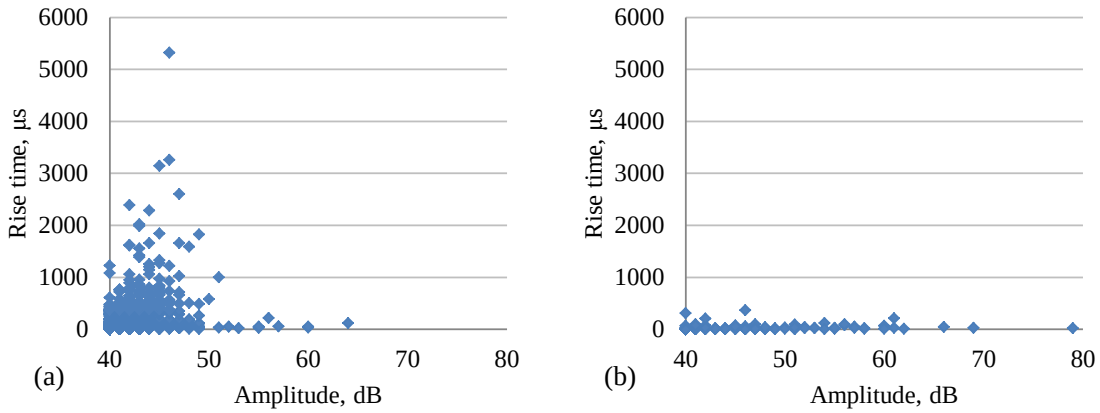

Figure A.1 Rise time versus amplitude: (a) due to leakage, and (b) due to corrosion.

Figure A.2 demonstrates the correlation between duration and amplitude for the leakage and corrosion periods. From these plots it is clear that duration associated with leakage is generally longer than that associated with corrosion. Also, hits with duration exceeding 1,300 µ-seconds and amplitude less than 50 dB are associated with leakage rather than corrosion.

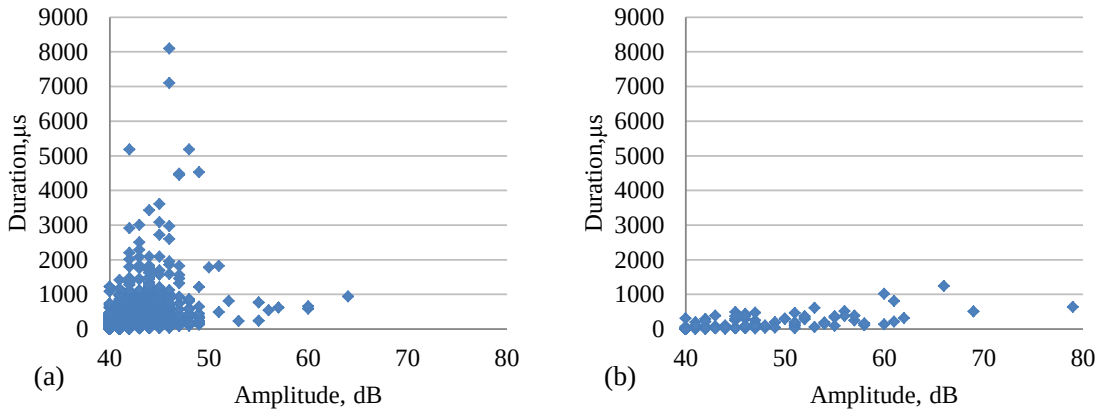

Figure A.2 Duration versus amplitude: (a) due to leakage, and (b) due to corrosion.

Figure A.3 demonstrates the correlation between energy and amplitude for the leakage and corrosion periods. From these plots it is clear that energy associated with leakage data is generally higher than that associated with corrosion data. This is to be

expected based on the previous finding that the duration of the signals is generally longer for the leakage data. The contrast between energy associated with leakage data and energy associated with corrosion data is not as stark as was the case for either rise time or duration associated with these two different datasets. This is in keeping with the general expectation that both of these mechanisms are of relatively low amplitude and, therefore, are not generally energetic, with the majority of the data occurring below 50 dB. This is to be expected as leakage will not result in crack formation and corrosion is expected to result in formation of micro-cracks at this early stage (nonvisible and located at the level of the steel reinforcement due to volumetric expansion). From this data set it is possible to state that energy exceeding 60 Joules is associated only with leakage, however the overlap in the data sets is very significant in the case of energy and therefore this conclusion is not as strongly supported as for the cases of rise time and duration.

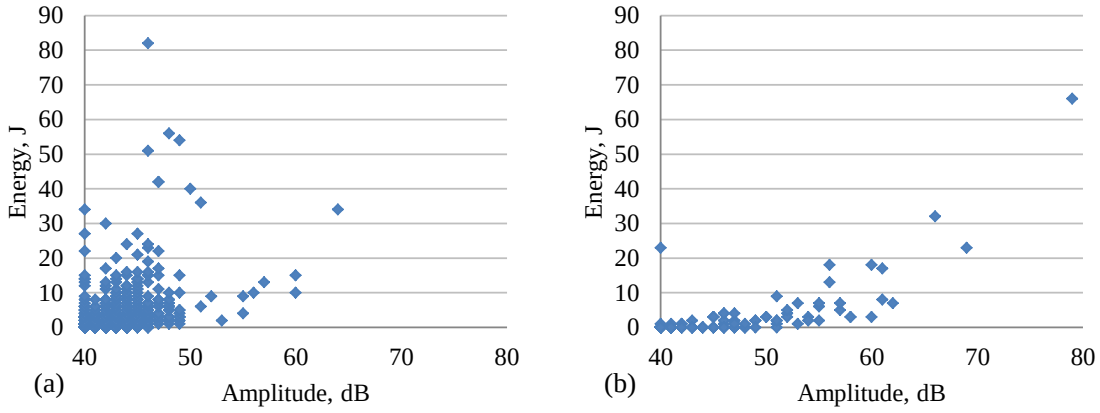

Figure A.3 Energy versus amplitude: (a) due to leakage and (b) due to corrosion.

Figure A.4 demonstrates the correlation between signal strength and time for the leakage and corrosion periods. Because these plots involve time, differences in the rate of acoustic emission data associated with leakage and corrosion become clear. It is observed from these plots that the rate of hits is much higher when leakage is ongoing. During the

two different 12 hour periods investigated, the leakage data had an average rate of 373 hits per hour compared to the corrosion data which had an average rate of 15 hits per hour. It can also be observed that the rate of acoustic emission activity associated with leakage decayed as the hydraulic head was diminished.

Because signal strength is closely related to energy in the sense that both parameters are related to measures of area under the signal envelope, it is to be expected that signal strength would likewise not serve as a particularly useful discriminator between leakage and corrosion data. This is in fact the case, as can be seen from Figure A.4, where significant overlap in the signal strength data sets is present.

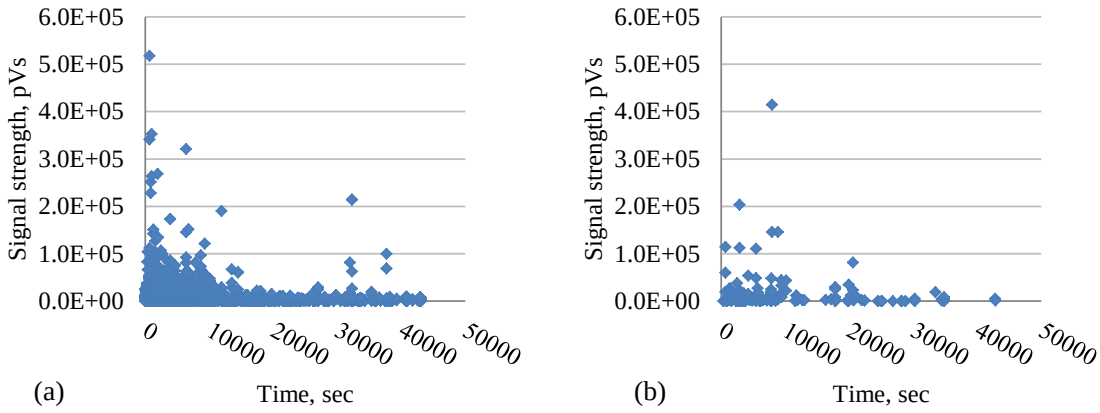

Figure A.4 Signal strength (pVs) versus time (seconds): (a) due to leakage, and (b) due to corrosion.

If rise time is used as a discriminator, considering values exceeding 370 µ-seconds are related to leakage, Figures A.2 through A.4 can be re-plotted as shown in Figures A.5 through A.7. Data points plotted in red represents hits with rise time values exceeding 370 µ-seconds.

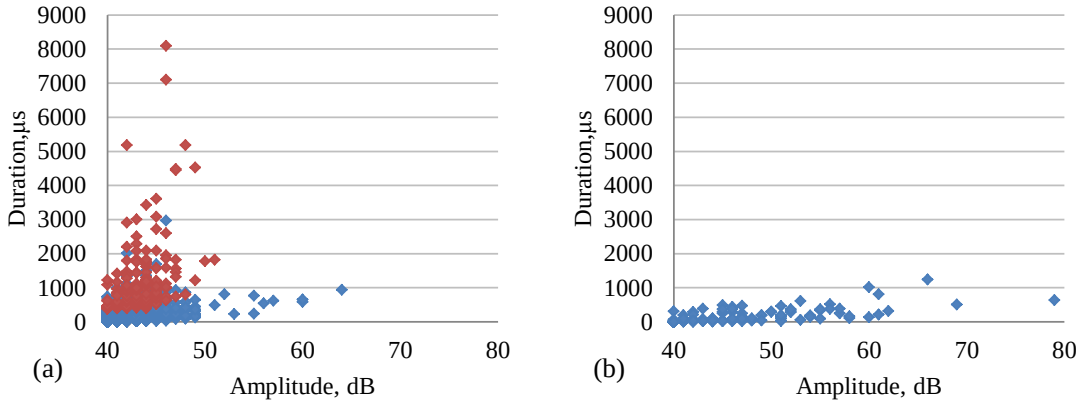

Figure A.5 Duration versus amplitude (hits with rise time higher than 370 µ-seconds plotted in red): (a) due to leakage, and (b) due to corrosion.

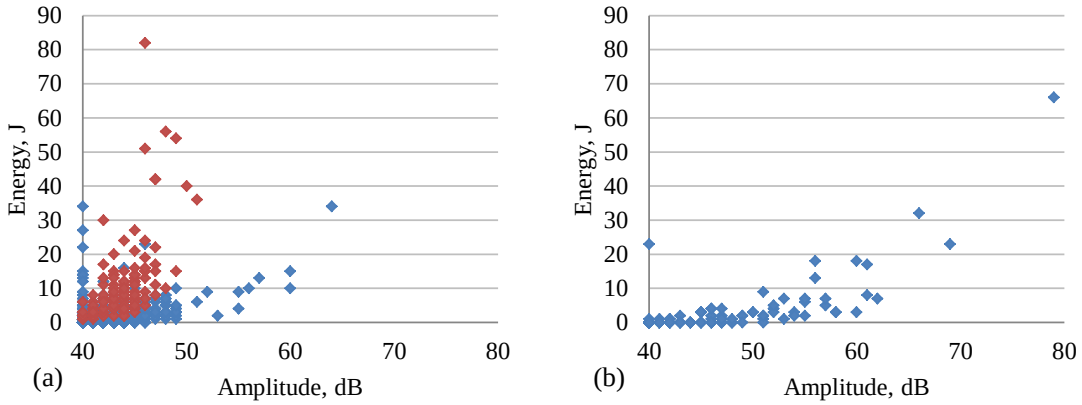

Figure A.6 Energy versus amplitude (hits with rise time higher than 370 µ-seconds plotted in red): (a) due to leakage, and (b) due to corrosion.

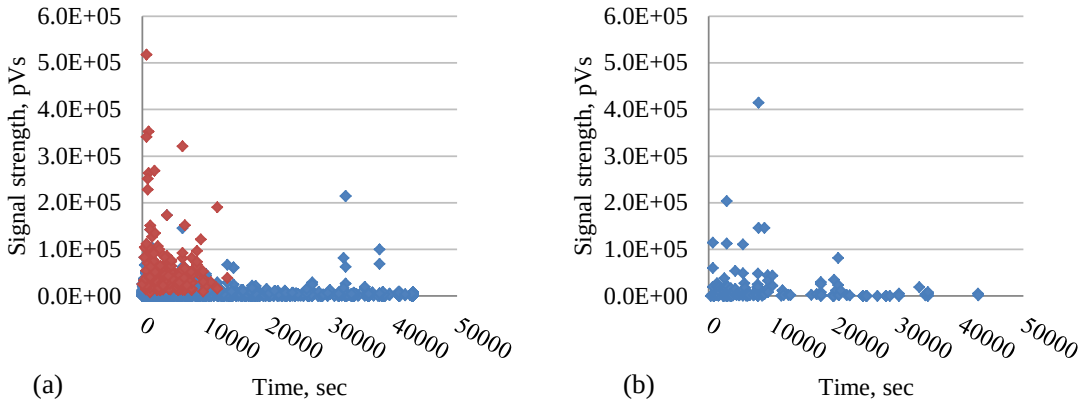

Figure A.7 Signal strength (pVs) versus time (seconds), (hits with rise time higher than 370 µ-seconds plotted in red): (a) due to leakage, and (b) due to corrosion.

A signal processing described in Chapter 3 was used to further investigate the data. Figure A.8 shows an example of a wavelet transform performed on a signal from each of the two data sets. The x-axis on the figure represents time within the signal duration, and the y-axis is inversely related to frequency. The energy distribution is plotted as contours in the time-frequency domain. Criterion C4 that was developed to separate controlled source signals from reflections was investigated. This criterion is based on the spatial distribution of energy within the wavelet transform. To calculate C4, the values of wavelet coefficients lower than 10% of the max coefficient value are set to equal zero. The remaining non-zero coefficients are considered high energy nodes and their center of mass in the x-y plane is determined. C4 is then calculated as the summation of each high energy coefficient value multiplied by its distance to the center of mass of the high energy zone and the resulting value is divided by the summation of values at the high energy nodes. For example, if we considered the circled nodes in Figure A.8a, with the values at each of the four nodes assumed equal to a, b, c and d respectively and the distance from each node to the center of mass is d_a, d_b, d_c and d_d respectively, C4 related to this portion of the grid is $(a*d_a+b*d_b+c*d_c+d*d_d)/(a+b+c+d)$.

The values of C4 were plotted for signals from both data sets as seen in Figure A.9. In this figure the data sets associated with leakage are plotted to the left while the data sets associated with corrosion are plotted to the right. As seen in the figure there are similarities in criterion values from leakage data and corrosion related signals, suggesting that the energy distribution in the two different data sets are not significantly different. However, there are visually observable differences between Figure A.8a and Figure A.8b. If a filtering limit of 4452 is used for C4 such that hits related to lower values are related to

corrosion dataset, the percentage of corrosion data remained is 61% and percentage of leakage data remained is 9%. Thus, the wavelet based approach does show clear differences in the majority of the dataset and the general wavelet based approach is promising. The wavelet coefficients may benefit from further development that is specifically tailored to this data set.

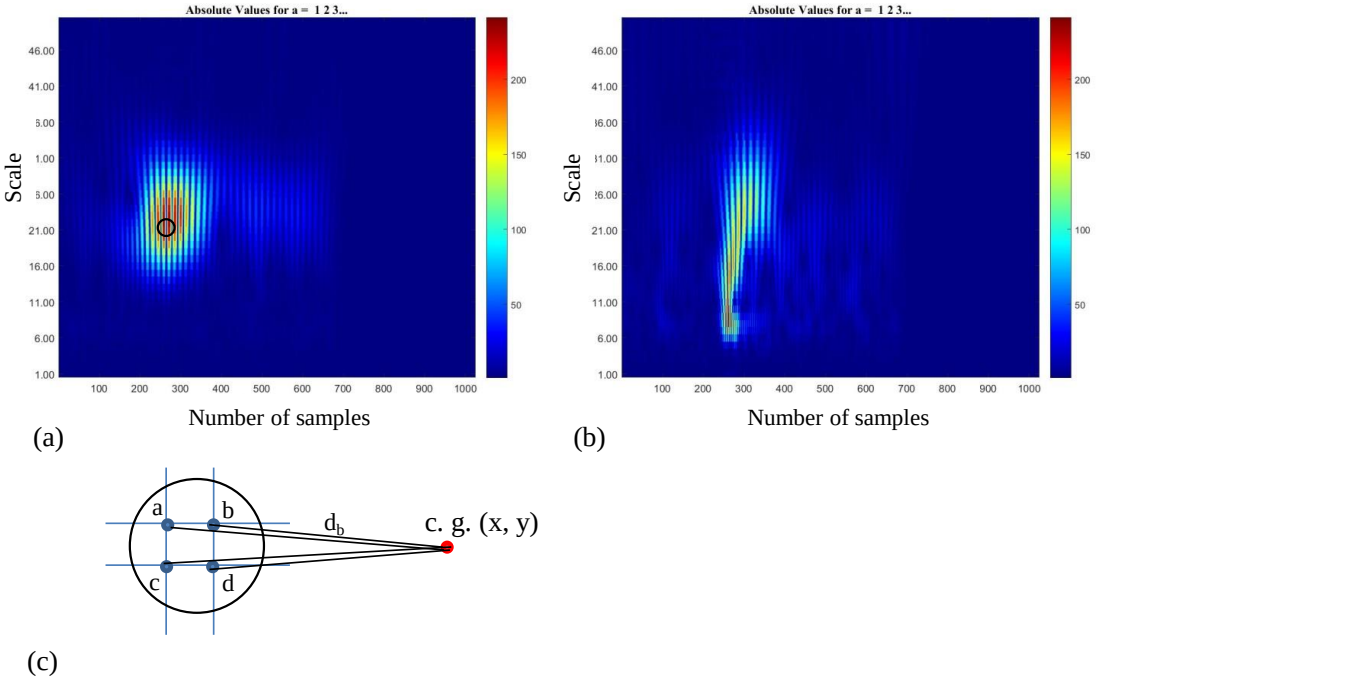

Figure A.8 Example of wavelet transform for: (a) leakage signal, (b) corrosion signal and (c) a schematic for describing criterion C4.

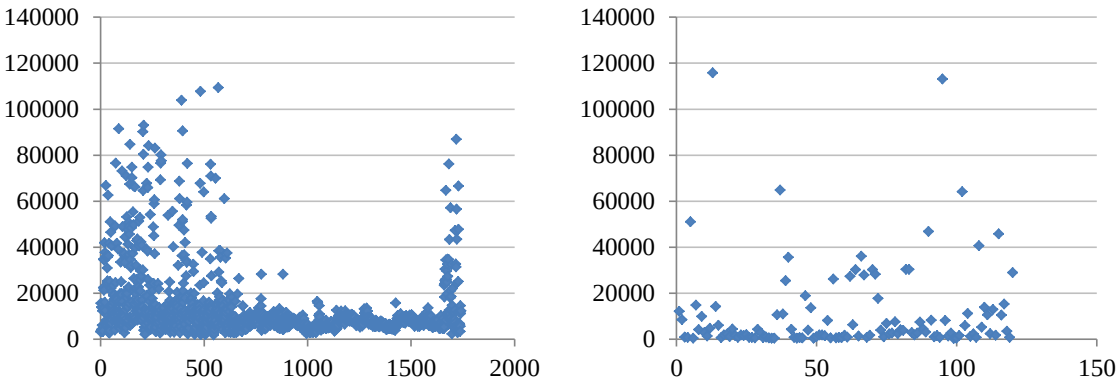

Figure A.9 Values of wavelet based criterion C4 for leakage dataset (left) and corrosion dataset (right).

To summarize the findings related to discrimination between acoustic emission data from the leakage and corrosion data sets:

- Rise time and duration of the acoustic emission waveforms are promising for discrimination between leakage and corrosion mechanisms.
- Both rise time and duration has higher values for leakage in comparison to corrosion. As expected, some overlap does exist in the data sets for these parameters.
- Acoustic emission hits exceeding 370 µ-seconds in rise time were always associated with leakage. Acoustic emission hits exceeding 1,300 µ-seconds were likewise always associated with leakage. This finding provides clear threshold values for determination of leakage in a data set.
- When averaged over a 12 hour period, the rate of acoustic emission activity was significantly higher (25 times higher) for the case of leakage in comparison to corrosion. This finding may be utilized as an alarm mechanism for determination of leakage. As an illustrative example, if the rate of acoustic emission activity increases by more the 10 times the baseline rate then leakage would be suspected.
- The wavelet based approach showed differences in criterion C4 values. However, this approach may benefit from further development for this particular data set.

The findings from this study are promising. However, these findings are based on relatively small, yet highly relevant, data sets. Further studies should be conducted and the findings verified through both laboratory and field studies.

APPENDIX B – MONITORING ASR DAMAGE IN CONCRETE BLOCKS (STORED AT WJE, AUSTIN)

A feasibility study was conducted by the University of South Carolina, Wiss, Janney, Elstner Associates, Austin office (WJE, Austin), and Texas Department of Transportation (TxDOT) to extend and verify the controlled laboratory test results for alkali-silica reaction (ASR) damage evaluation using acoustic emission (AE). In this study, TxDOT provided four specimens; three specimens were cast in August 2014 while the fourth specimen was cast in 2012. The specimens were unreinforced concrete blocks with dimensions 14 x 14 x 14 inches and had different mix designs to promote ASR damage as follows:

- Non-reactive (TxDOT Block Designation 939) – Cast August 2014
- ASR 1293 mix reactive (TxDOT Block Designation 940) – Cast August 2014
- ASR/DEF block (TxDOT Block Designation 941) – Cast August 2014
- Low alkali mix with reactive aggregate (TxDOT Block Designation 409) – Cast 2012

All specimens were placed in an outdoor setting at WJE-Austin. The specimens were instrumented using DEMEC points to measure length change. Wireless AE sensors, PK6I resonant sensors (55 kHz resonant frequency), were also used to monitor the progression of ASR damage in the specimens. The monitoring results between August 2014 and July 2015 are presented in this appendix.

As typical for monitoring of material degradation mechanisms using AE (also known as low-level AE), proper filters must be used to reduce the data. In this study a combination of parameter based filters was implemented including Duration-Amplitude filters and Rise time-Amplitude filters, similar to the filters presented in Chapter 4 of this dissertation. An additional filtering challenge in this study is the presence of AE activity from rain events in the collected data. To filter data from rain, cross-examining of the data from all channels was conducted and if a significant amount of data was collected on all channels at the same time the data was rejected. After applying the above filters, it was found that the control specimen still contained a large amount of data. Therefore, a RMS based filter was developed based on the control data to delete all signals with RMS value between 0.00039 and 0.00041. The number of hits for unfiltered data (amplitude threshold exceeding 40 dB) and filtered data are shown in Figure B.1. As seen in the figure, the applied filters reduced the data significantly which indicates the importance of applying filters for low-level AE data.

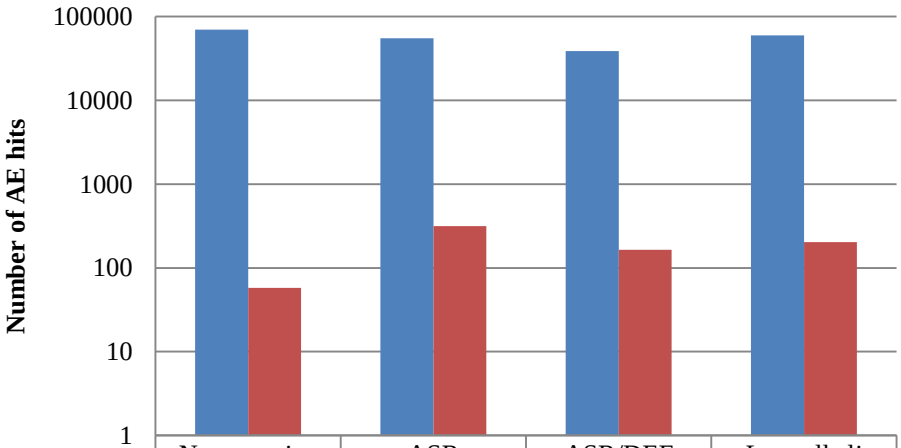

	Non-reactive	ASR	ASR/DEF	Low-alkali
Unfiltered	70233	55114	38932	59801
Filtered	58	316	165	203

Figure B.1 Number of hits for unfiltered and filtered data.

Data from length change measurements is shown in Figure B.2 and indicate that the ASR specimen had the most expansion through all the specimens by an order of magnitude. It is noted that a different y-axis scale was used in the figure to allow for better visualization.

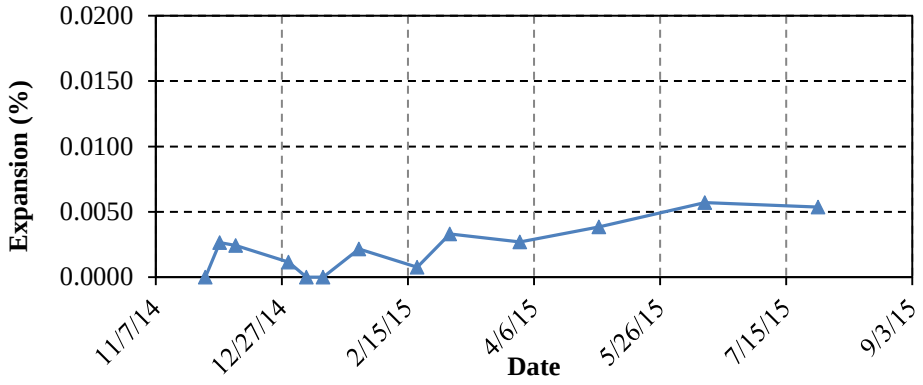

(a)

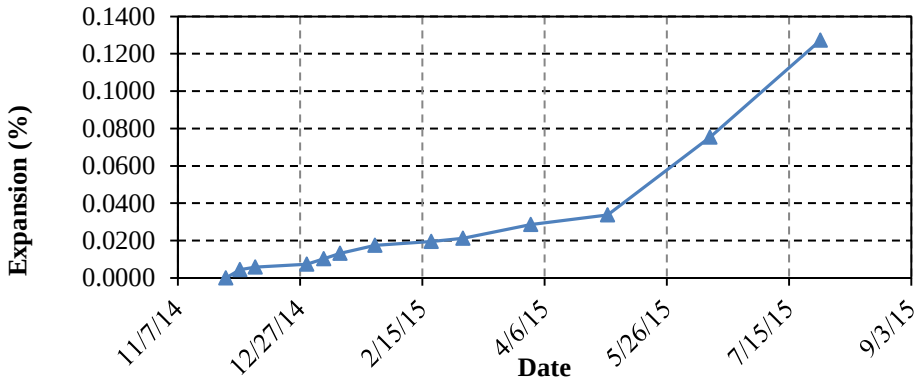

(b)

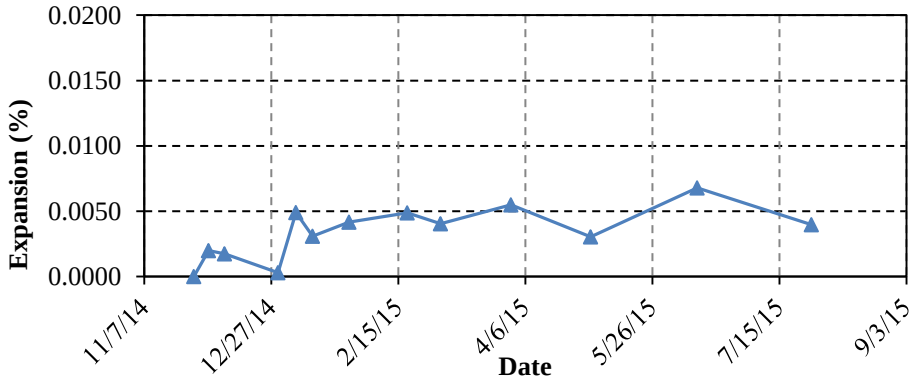

(c)

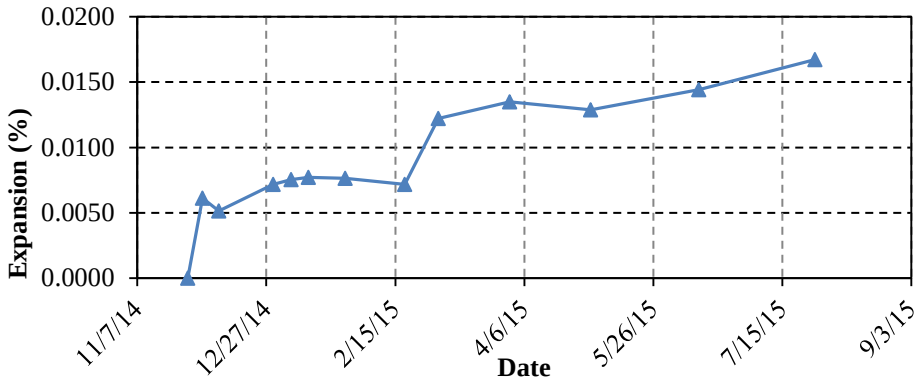

(d)

Figure B.2 Length change measurements: (a) non-reactive block, (b) ASR specimen, (c) ASR/DEF specimen, and (d) low alkali mix specimen.

AE data was collected starting on August 9, 2014. The system collected data for approximately one month then the system was inactive until late December 2014. Data was collected afterwards until April 18, 2015. The amplitude versus time plots of the unfiltered and filtered AE data for the four specimens are shown in Figure B.4 and B.4, respectively.

The cumulative signal strength (CSS) results of filtered AE data collected during the first month of monitoring are shown in Figure B.5. As seen in the figure, the ASR specimen had a higher AE activity during the first month compared to the other specimens. This agrees with the length change measurements which indicated a higher rate of expansion in the ASR specimen.

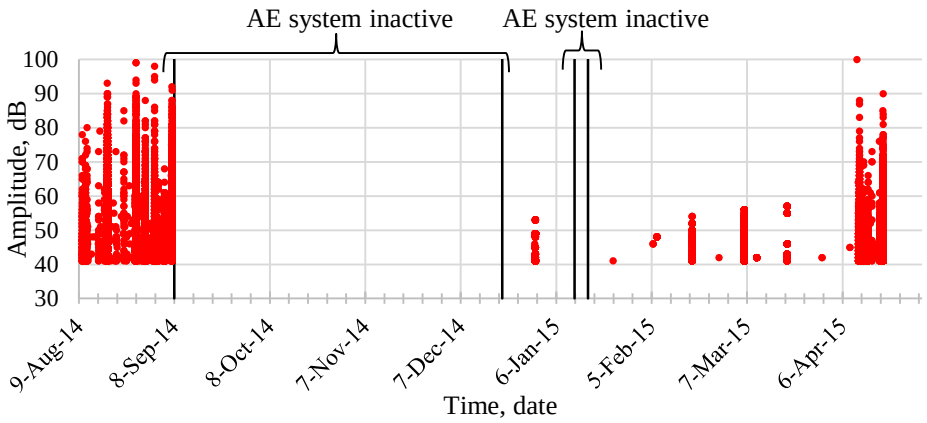
AE system inactive
AE system inactive
Amplitude, dB
100
90
80
70
60
50
40
30
9-Aug-14
8-Sep-14
8-Oct-14
7-Nov-14
7-Dec-14
6-Jan-15
5-Feb-15
7-Mar-15
6-Apr-15
Time, date

(a)

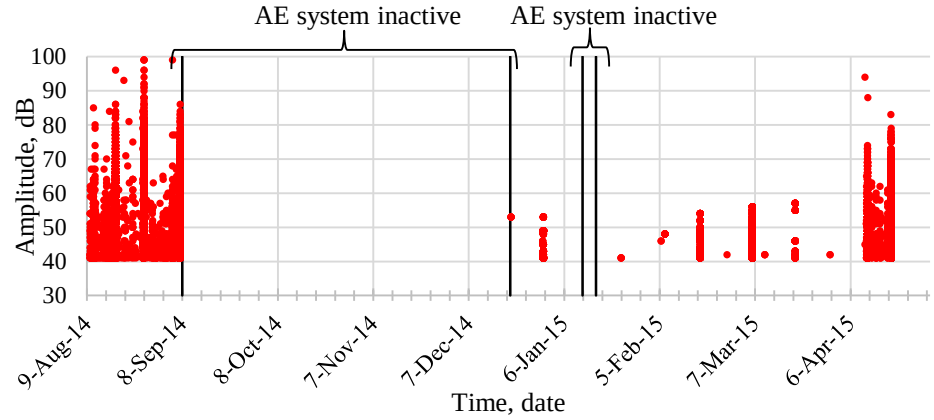
AE system inactive
AE system inactive
Amplitude, dB
100
90
80
70
60
50
40
30
9-Aug-14
8-Sep-14
8-Oct-14
7-Nov-14
7-Dec-14
6-Jan-15
5-Feb-15
7-Mar-15
6-Apr-15
Time, date

(b)

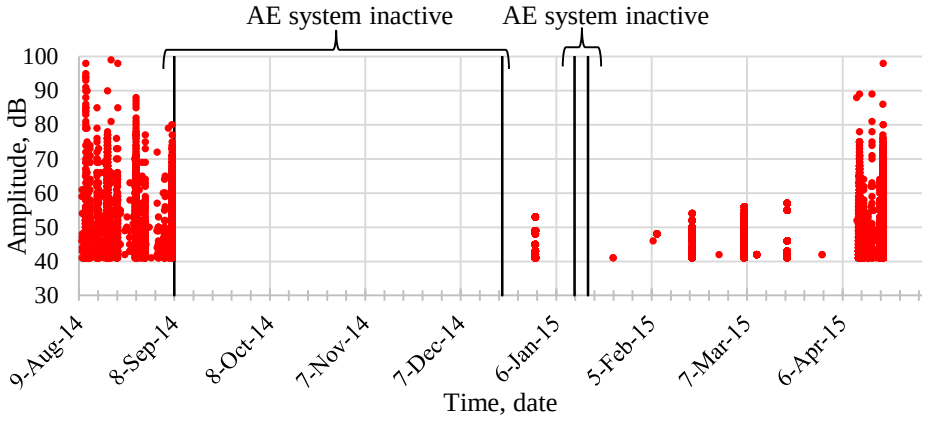
AE system inactive
AE system inactive
Amplitude, dB
100
90
80
70
60
50
40
30
9-Aug-14
8-Sep-14
8-Oct-14
7-Nov-14
7-Dec-14
6-Jan-15
5-Feb-15
7-Mar-15
6-Apr-15
Time, date

(c)

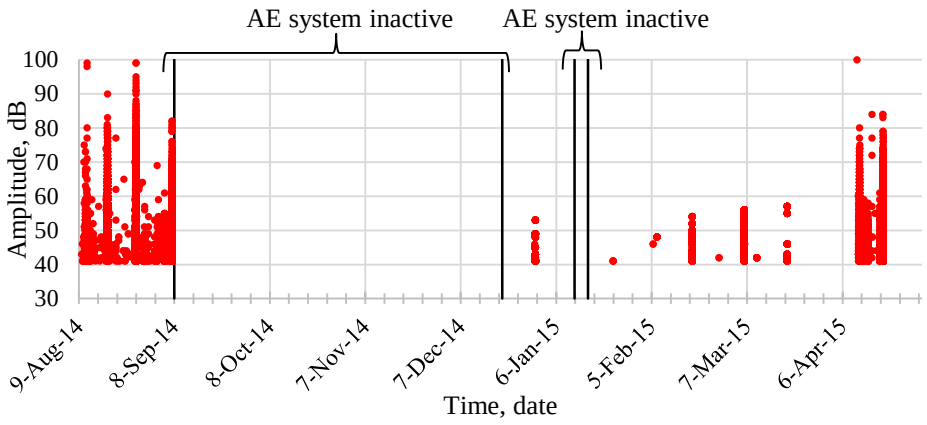

(d)

Figure B.3 Unfiltered AE data, amplitude versus time: (a) non-reactive block, (b) ASR specimen, (c) ASR/DEF specimen, and (d) low alkali mix specimen.

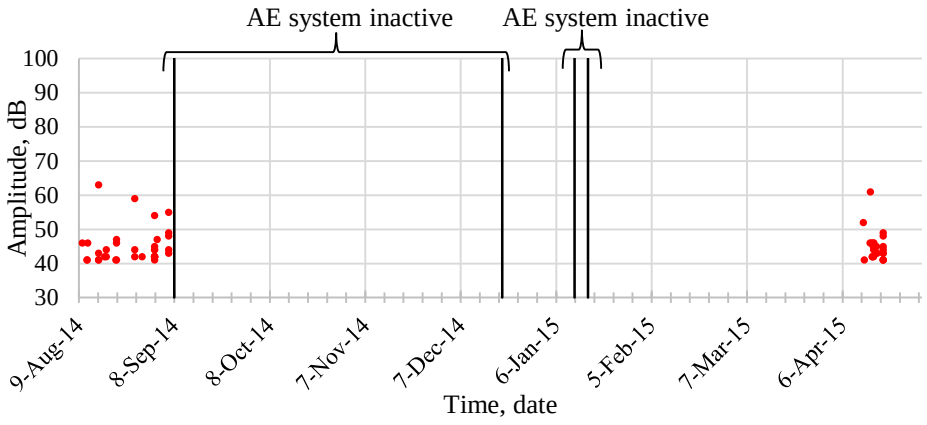

(a)

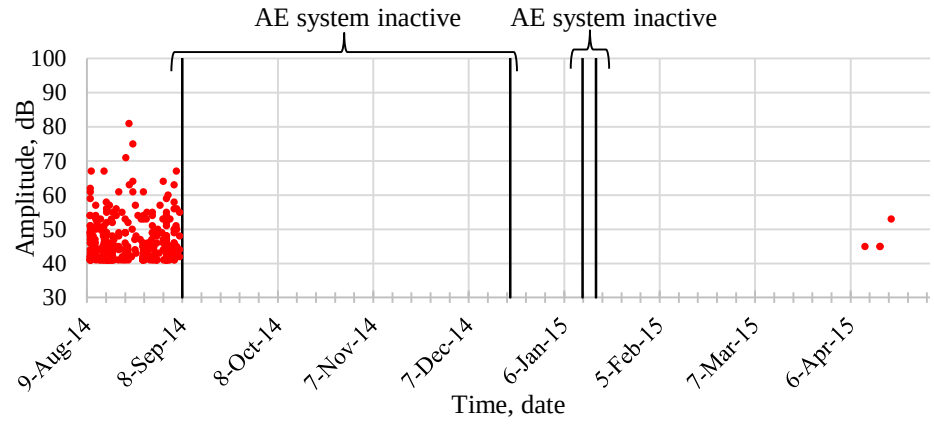

(b)

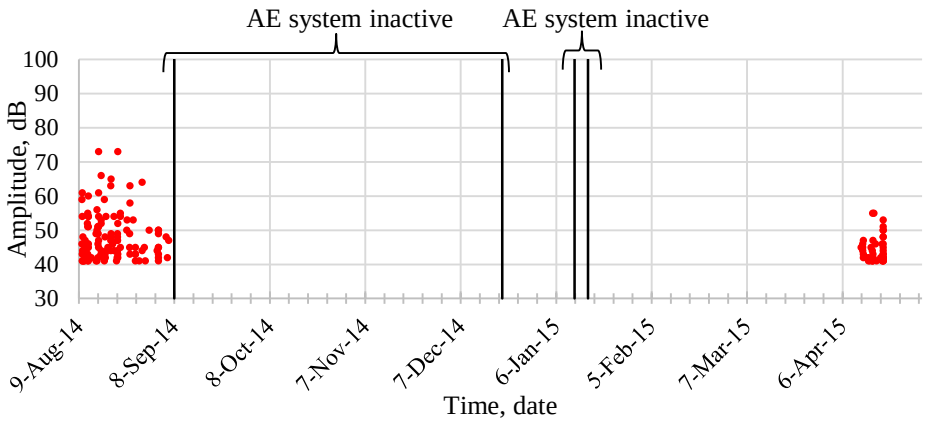

(c)

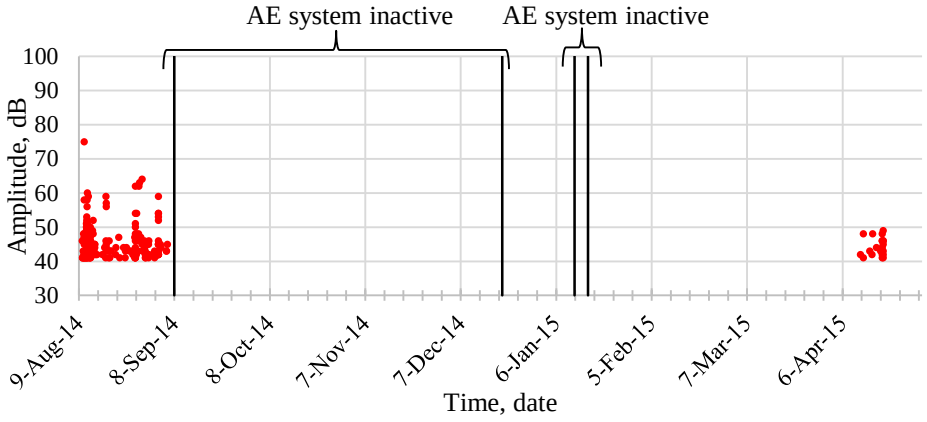

(d)

Figure B.4 Filtered AE data, amplitude versus time: (a) non-reactive block, (b) ASR specimen, (c) ASR/DEF specimen, and (d) low alkali mix specimen.

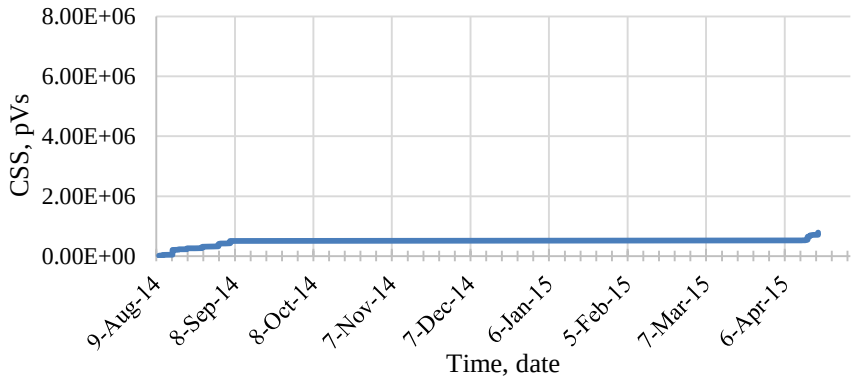

(a)

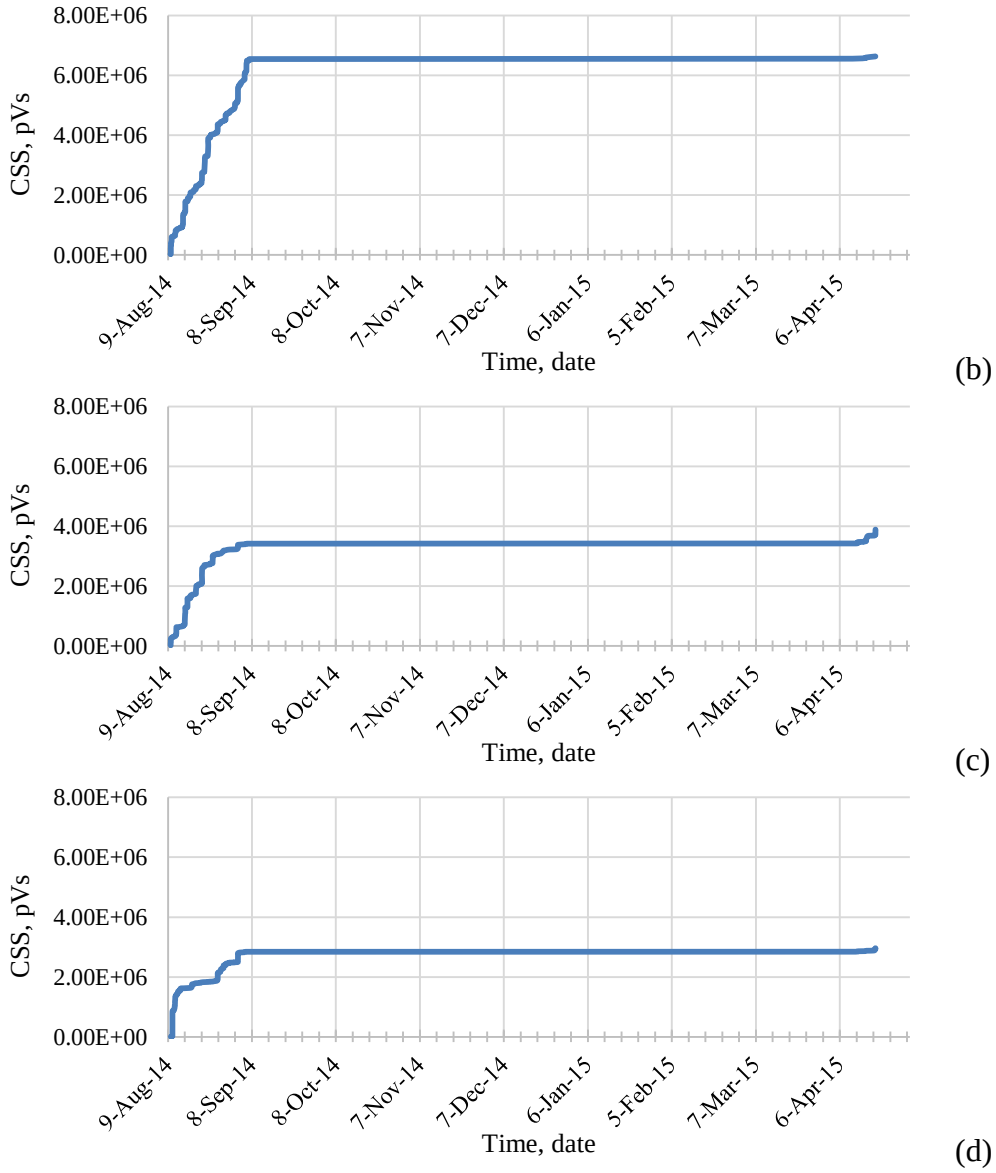

Figure B.5 AE CSS versus time: (a) non-reactive block, (b) ASR specimen, (c) ASR/DEF specimen, and (d) low alkali mix specimen.

Intensity Analysis method was used to analyze data from all the specimens and the same limits proposed in Chapter 4 were used to classify damage. Data collected only during the first month of testing, before system malfunction, was used. As seen in Figure B.6, the highest damage was detected in the ASR specimen followed by the ASR/DEF specimen. This agrees with the expected results during the first month of monitoring. It is noted that the non-reactive specimen plotted in the 'Minor damage' zone. The data collected from

this specimen during the first month may be attributed to early age shrinkage cracking. Therefore, it is recommended that this effect is studied in future research.

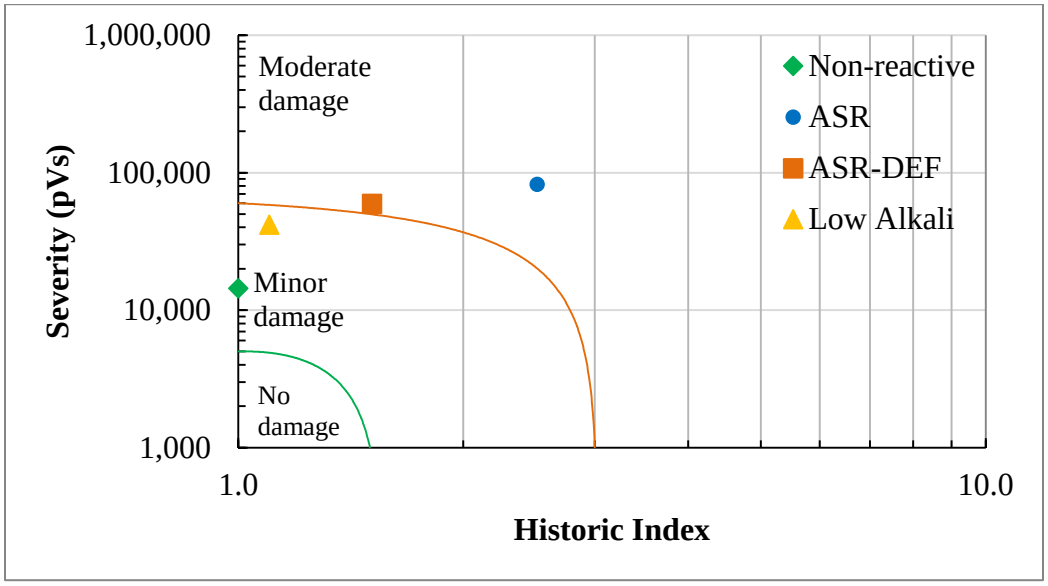

Figure B.6 Intensity Analysis ASR damage classification chart.

APPENDIX C – PERMISSION TO REPRINT

Copyright Clearance Center RightsLink®

Home | Account Info | Help

Title: Classification of alkali–silica reaction damage using acoustic emission: A proof-of-concept study

Author: Marwa Abdelrahman,Mohamed K. ElBatanouny,Paul Ziehl,Jeremiah Fasl,Carl J. Larosche,John Fraczek

Publication: Construction and Building Materials

Publisher: Elsevier

Date: 1 October 2015

Logged in as:
Marwa Abdelrahman
Account #:
3000649111

LOGOUT

Order Completed

Thank you for your order.

This Agreement between Marwa Abdelrahman ("You") and Elsevier ("Elsevier") consists of your license details and the terms and conditions provided by Elsevier and Copyright Clearance Center.

Your confirmation email will contain your order number for future reference.

Printable details.

License Number	3992900862374
License date	Nov 20, 2016
Licensed Content Publisher	Elsevier
Licensed Content Publication	Construction and Building Materials
Licensed Content Title	Classification of alkali–silica reaction damage using acoustic emission: A proof-of-concept study
Licensed Content Author	Marwa Abdelrahman,Mohamed K. ElBatanouny,Paul Ziehl,Jeremiah Fasl,Carl J. Larosche,John Fraczek
Licensed Content Date	1 October 2015
Licensed Content Volume	95
Licensed Content Issue	n/a
Licensed Content Pages	8
Type of Use	reuse in a thesis/dissertation
Portion	full article
Format	both print and electronic
Are you the author of this Elsevier article?	Yes
Will you be translating?	No
Order reference number	
Title of your thesis/dissertation	EVALUATION OF CONCRETE DEGRADATION USING ACOUSTIC EMISSION: DATA FILTERING AND DAMAGE DETECTION
Expected completion date	Dec 2016
Estimated size (number of pages)	204
Elsevier VAT number	GB 494 6272 12
Requestor Location	Marwa Abdelrahman 300 Main st Columbia, SC 29208 United States Attn: Marwa Abdelrahman

Total 0.00 USD

ORDER MORE CLOSE WINDOW